PROCESSING AND ASSESSMENT OF ALUMINUM CERAMIC FIBER REINFORCED METAL MATRIX COMPOSITE PARTS FOR AUTOMOTIVE AND DEFENSE APPLICATIONS

A THESIS SUBMITTED TO
THE GRADUATE SCHOOL OF NATURAL AND APPLIED SCIENCES
OF
MIDDLE EAST TECHNICAL UNIVERSITY

BY

GÖKHAN TÜRKYILMAZ

IN PARTIAL FULFILLMENT OF THE REQUIREMENTS
FOR
THE DEGREE OF MASTER OF SCIENCE
IN
METALLURGICAL AND MATERIALS ENGINEERING

JULY 2009

Approval of the thesis:

PROCESSING AND ASSESSMENT OF ALUMINUM CERAMIC FIBER REINFORCED METAL MATRIX COMPOSITE PARTS FOR AUTOMOTIVE AND DEFENSE APPLICATIONS

submitted by **GÖKHAN TÜRKYILMAZ** in partial fulfillment of the requirements for the degree of **Master of Science in Metallurgical and Materials Engineering Department, Middle East Technical University** by,

Prof. Dr. Canan Özgen _____
Dean, Graduate School of **Natural and Applied Sciences**

Prof. Dr. Tayfur Öztürk _____
Head of Department, **Metallurgical and Materials Engineering**

Prof. Dr. Ali Kalkanlı _____
Supervisor, **Metallurgical and Materials Engineering Dept., METU**

Examining Committee Members:

Prof. Dr. Ekrem Selçuk _____
Metallurgical and Materials Engineering Dept., METU

Prof. Dr. Ali Kalkanlı _____
Metallurgical and Materials Engineering Dept., METU

Prof. Dr. Cevdet Kaynak _____
Metallurgical and Materials Engineering Dept., METU

Assoc. Prof. Dr. Nuri Durlu _____
Mechanical Engineering Dept., TOBB ETU

Dr. Nurşen Koç _____
Metallurgical and Materials Engineering Dept., METU

Date: 24.07.2009

I hereby declare that all information in this document has been obtained and presented accordance with the academic rules and ethical conduct. I also declare that, as required by these rules and conduct, I have fully cited and referenced all material and results that are not original to this work.

Name, Last name : Gökhan Türkyılmaz

Signature :

ABSTRACT

PROCESSING AND ASSESSMENT OF ALUMINUM CERAMIC FIBER REINFORCED ALUMINUM METAL MATRIX COMPOSITE PARTS FOR AUTOMOTIVE AND DEFENSE APPLICATIONS

Türkyılmaz, Gökhan

M.S., Department of Metallurgical and Materials Engineering

Supervisor: Prof. Dr. Ali Kalkanlı

July 2009, 158 pages

The aim of this study was to produce partially reinforced aluminum metal matrix composite components by insertion casting technique and to determine the effects of silicon content, fiber vol% and infiltration temperature on the mechanical properties of inserts, which were the local reinforcement parts of the components. Silicon content of alloys was selected as 7 wt% and 10 wt%. The reinforcement material, i.e. Saffil fiber preforms, had three different fiber vol% of 20, 25 and 30 vol% respectively. The infiltration temperatures of composite specimens were fixed as 750 °C and 800 °C.

In the first part of the thesis, physical and mechanical properties of composite specimens were determined according to the parameters of silicon content of the matrix alloy, infiltration temperature and vol% of the reinforcement phase. X-ray diffraction examination of fibers resulted as the fibers mainly composed of delta-alumina fibers and scanning electron microscopy analyses showed that fibers had

planar isotropic condition for infiltration. Microstructural examination of composite specimens showed that appropriate fiber/matrix interface was created together with small amount of micro-porosities. Bending tests of the composites showed that as fiber vol% increases flexural strength of the composite increases. The highest strength obtained was 880.52 MPa from AlSi10Mg0.8 matrix alloy reinforced with 30 vol% Saffil fibers and infiltrated at 750 °C. Hardness values were also increased by addition of Saffil fibers and the highest value was obtained as 191 HB from vertical to the fiber orientation of AlSi10Mg0.8 matrix alloy reinforced with 30 vol% Saffil fibers. Density measurement revealed that micro-porosities existed in the microstructure and the highest difference between the theoretical values and experimental values were observed in the composites of 30 vol% Saffil fiber reinforced ones for both AlSi7Mg0.8 and AlSi10Mg0.8 matrix alloys.

In the second part of the experiments, insertion casting operation was performed. At casting temperature of 750 °C, a good interface/component interface was obtained. Image analyses were also showed that there had been no significant fiber damage between the insert and the component.

Keywords: Metal matrix composites, insertion casting, alumina fiber, squeeze casting

ÖZ

OTOMOTİV VE SAVUNMA UYGULAMALARI İÇİN SERAMİK FİBER TAKVİYELİ ALÜMİNYUM METAL MATRİS KOMPOZİT PARÇALARININ ÜRETİMİ VE DEĞERLENDİRİLMELERİ

Türkyılmaz, Gökhan

Yüksek Lisans, Metalürji ve Malzeme Mühendisliği Bölümü

Tez Yöneticisi: Prof. Dr. Ali Kalkanlı

Temmuz 2009, 158 sayfa

Bu tez çalışmasının amacı ekleme döküm yöntemi ile yerel olarak güçlendirilmiş alüminyum metal matris kompozit parçalarının üretilmesi ve silisyum içeriğinin, fiberlerin hacimsel yüzdesinin ve süzdürme sıcaklığının yerel takviye parçaları olan insertlerin mekanik ve fiziksel özellikleri üzerindeki etkilerinin belirlenmesidir. Alaşımların silisyum içeriği kütlece %7 ve %10 olarak belirlenmiştir. Takviye malzemesi olan Saffil fiberler, sırasıyla %20, %25 ve %30 olan üç farklı hacimsel yüzdeye sahiptir. Kompozit numunelerin süzdürme sıcaklıkları 750 °C ve 800 °C olarak belirlenmiştir.

Tezin birinci bölümünde, kompozit numunelerin mekanik ve fiziksel özellikleri matris alaşımın silisyum içeriği, süzdürme sıcaklığı ve fiberlerin hacimsel yüzdesi parametrelerine göre belirlenmiştir. Fiberlerin x-ışınları incelemesi fiberlerin genel olarak delta-alümina evresinden oluşmuş olduğu sonucunu vermiş olup, fiberlerin tarama elektron mikroskobu incelemesi de fiberlerin süzdürme işlemi için düzlemsel eş-yönlülük özelliğine sahip olduğu sonucunu vermiştir. Kompozit

numunelerin içyapı incelemeleri küçük bir miktar mikro-gözenekle beraber uygun fiber/matris arayüzeyinin oluşturulduğunu göstermiştir. Kompozitlerin bükme testleri, fiberlerin hacimsel yüzdelerinin artmasıyla kompozitlerin bükme dayançlarının arttığını göstermiştir. En yüksek dayanç değeri AlSi10Mg0.8 matrisli, hacimce %30 fiber takviyeli ve 750 °C sıcaklıkta süzdürülmüş kompozit numuneden 880,52 MPa olarak elde edildiğini göstermiştir. Yine sertlik değerleri de Saffil fiberlerin eklenmesiyle artış göstermiş olup, en yüksek sertlik değeri fiber yönelimine paralel olan yerden AlSi10Mg0.8 matrisli, hacimce %30 fiber takviyeli ve 750 °C sıcaklıkta süzdürülmüş kompozit numuneden 191 HB olarak ölçülmüştür. Özkütle ölçümleri içyapıdaki mikro-gözenekleri ve teorik ve deneysel değerler arasında en büyük farka sahip olan numunelerin her iki matris alaşımı AlSi7Mg0.8, AlSi10Mg0.8 için hacimsel olarak %30 Saffil fiber takviye edilmiş kompozitler olduğunu açığa çıkarmıştır.

Tezin ikinci bölümünde, ekleme döküm işlemi uygulanmıştır. 750 °C döküm sıcaklığında, iyi bir insert/parça arayüzeyi elde edilmiştir. Görüntü analizleri de insert ve parça arasında önemli bir fiber hasarının meydana gelmediğini göstermiştir.

Anahtar kelimeler: Metal matris kompozitler, ekleme döküm, alümina fiber, sıkıştırma döküm

To My Family,

ACKNOWLEDGEMENTS

I would like to express my deepest gratitude to my supervisor Prof. Dr. Ali Kalkanlı for his guidance, continuous support and encouragement throughout this study.

I am also thankful to Seda Sayılgan and Özgür Keleş for their valuable supports, motivation and invaluable friendship in all part of the study.

My special thanks go to the technical staff of the Department of Metallurgical and Materials Engineering, METU, especially Salih Türe for their contributions to this study.

I would also like to thank to Arda Çetin, Turgut Kırma, Yankı Başaran, Betül Pelin Maradit, Çağla Özgit, Gülhan Çakmak, Güher Kotan, Evren Tan, Serdar Tan, Emre Ergül and Onur Rauf Bingöl for their helps and supports.

Thanks are also extended to Zafer Pesen from Mechanical and Chemical Industry Corporation and Deniz Taşkesen from RUTAŞ Aluminum.

I would like to express my sincere thanks to Mustafa Emre Yücetürk, Şevket Reha Soysal and Tuğba Uyar for always being supportive in my life.

Finally, I want to express my greatest thanks to my family for supporting, encouraging, and loving me all through my life.

This study was supported by The Ministry of Industry & Commerce of Turkey and Mechanical & Chemical Industry Corporation, Project No: 00023.STZ.2006-1.

TABLE OF CONTENTS

ABSTRACT iv

ÖZ vi

ACKNOWLEDGEMENTS ix

TABLE OF CONTENTS x

LIST OF TABLES xiii

LIST OF FIGURES xvii

CHAPTERS

1. INTRODUCTION 1

2. LITERATURE REVIEW 3

2.1 Composites 3

2.1.1 Matrix Phase 4

2.1.2 Reinforcement Phase 6

2.1.3 Interface 8

2.2 Metal Matrix Composites (MMCs) 10

2.2.1 Types of MMCs 10

2.2.2 Processing Techniques of MMCs 12

2.2.2.1 Liquid State Processing 12

2.2.2.2 Solid State Processing 12

2.2.2.3 Infiltration 13

2.2.3 Aluminum Metal Matrix Composites (Al-MMCs) 14

2.2.3.1 Matrix Alloys 15

2.2.3.2 Reinforcement Material 18
2.2.3.2.1 Physical and Chemical Properties of Saffil Fibers 18
2.2.3.2.2 Processing Technique of Saffil Preforms 20
2.3 Component Production 22
2.4 Mechanism of Fiber Reinforcement 26
2.4.1 Long Fiber Reinforcement 26
2.4.2 Short Fiber Reinforcement 27
3. EXPERIMENTAL PROCEDURE 29
3.1 Matrix Alloy Preparation 29
3.2 XRD and SEM Analysis of Preforms 32
3.3 Squeeze Casting 34
3.4 Mechanical Tests and Test Apparatus 38
3.5 Microscopy and Microstructural Analysis 39
3.5.1 Sample Preparation 39
3.5.2 Scanning Electron Microscopy Analysis 40
3.5.3 Optical Microscopy Analysis 40
3.6 Density Measurement 40
4. RESULTS AND DISCUSSION 42
4.1 Microscopy and Microstructural Analysis 42
4.1.1 Scanning Electron Microscopy Results 42
4.1.2 Optical Microscopy Results 84
4.2 XRD Analyses Results 89
4.2.1 XRD Analyses of the Preforms 90
4.2.2 XRD Analyses of the Composite Specimens 91
4.3 Mechanical Test Results 96

4.3.1 Three Point Bending Test Results 97
4.3.2 Hardness Test Results 100
4.4 Density Measurement 102
4.5 Insertion Casting 106
5. CONCLUSION 109
REFERENCES 112
APPENDICES
Appendix A: Spectral Analyses of the Matrix Alloys 117
Appendix B: Details of the Squeeze Casting Operation 121
Appendix C: Reports of the Image Analyses 123
Appendix D: X-Ray Diffraction Cards of Present Phases 149
Appendix E: Detailed Tabulation of Three Point Bending Test Results 151
Appendix F: Detailed Tabulation of Hardness Test Results 155
Appendix G: Detailed Results of Density Measurement 158

LIST OF TABLES

TABLES

Table 2.1 Mechanical properties of some metals used as matrices in composites 4

Table 2.2 Mechanical properties of some polymers used as matrices in composites 5

Table 2.3 Mechanical properties of some ceramics used as matrices in composites..... 5

Table 2.4 Surface tensions of selected metal-ceramic systems at different temperatures 9

Table 2.5 Typical reinforcements used in MMCs..... 11

Table 2.6 Synthesis of selected cast aluminum-matrix composites of interest to automotive industries 15

Table 2.7 Standard chemical composition of Al-7wt%Si alloy..... 16

Table 2.8 Standard chemical composition of Al-10wt%Si alloy..... 17

Table 2.9 Typical physical properties of A356.0 alloy..... 17

Table 2.10 Typical physical properties of 361.0 alloy..... 17

Table 2.11 Mechanical properties of alloys A356.0 and 361.0 18

Table 2.12 Physical properties of Saffil fibers..... 19

Table 3.1 Chemical composition of alloys used in the experiments..... 29

Table 3.2 Chemical composition of pure aluminum used in the experiments... 31

Table 3.3 Chemical composition of AlTi5B master alloy 31

Table 3.4 Chemical composition of AlSr10 master alloy..... 31

Table 3.5 Chemical composition of Saffil RF grade fibers 32

Table 3.6 Properties of Saffil RF grade fibers 32

Table 3.7 Arrangement of specimens used in the experiments..... 38

Table 4.1 Image analysis result of AlSi7Mg0.8/30vol%Saffil composite infiltrated at 750 °C from vertical to the fiber orientation..... 85

Table 4.2 Image analyses results of the composite specimens 86
Table 4.3 Deviations of the image analyzing results compared to the theoretical values 86
Table 4.4 Average flexural strength values of the composite specimens 97
Table 4.5 Effect of Si on the flexural strength of the matrix 98
Table 4.6 Fiber efficiencies and the specific surface areas of 10^6 fibers 99
Table A.1 Spectrometer analyses of AlSi7Mg0.8 matrix composites infiltrated at 800 °C 117
Table A.2 Spectrometer analyses of AlSi7Mg0.8 matrix composites infiltrated at 750 °C 118
Table A.3 Spectrometer analyses of AlSi10Mg0.8 matrix composites infiltrated at 750 °C 119
Table A.4 Spectrometer analyses of AlSi10Mg0.8 matrix composites infiltrated at 750 °C 120
Table B.1 Squeeze casting parameters of AlSi7Mg0.8 alloy matrix inserts 121
Table B.2 Squeeze casting parameters of AlSi7Mg0.8 alloy matrix three point bending test specimens 121
Table B.3 Squeeze casting parameters of AlSi10Mg0.8 alloy matrix three point bending test specimens 122
Table B.4 Squeeze casting parameters of AlSi10Mg0.8 alloy matrix inserts .. 122
Table C.1 Image analysis result of AlSi7Mg0.8/20 vol% Saffil composite infiltrated at 750 °C from parallel to the fiber orientation 123
Table C.2 Image analysis result of AlSi7Mg0.8/20vol%Saffil composite infiltrated at 750 °C from vertical to the fiber orientation 124
Table C.3 Image analysis result of AlSi7Mg0.8/25vol%Saffil composite infiltrated at 750 °C from parallel to the fiber orientation 125
Table C.4 Image analysis result of AlSi7Mg0.8/25vol%Saffil composite infiltrated at 750 °C from vertical to the fiber orientation 126
Table C.5 Image analysis result of AlSi7Mg0.8/30 vol% Saffil composite infiltrated at 750 °C from parallel to the fiber orientation 127

Table C.6 Image analysis result of AlSi7Mg0.8/30vol%Saffil composite infiltrated at 750 °C from vertical to the fiber orientation 128
Table C.7 Image analysis result of AlSi7Mg0.8/20 vol% Saffil composite infiltrated at 800 °C from parallel to the fiber orientation 129
Table C.8 Image analysis result of AlSi7Mg0.8/20 vol% Saffil composite infiltrated at 800 °C from vertical to the fiber orientation 130
Table C.9 Image analysis result of AlSi7Mg0.8/25vol%Saffil composite infiltrated at 800 °C from parallel to the fiber orientation 131
Table C.10 Image analysis result of AlSi7Mg0.8/25vol%Saffil composite infiltrated at 800 °C from vertical to the fiber orientation 132
Table C.11 Image analysis result of AlSi7Mg0.8/30vol%Saffil composite infiltrated at 800 °C from parallel to the fiber orientation 133
Table C.12 Image analysis result of AlSi7Mg0.8/30 vol% Saffil composite infiltrated at 800 °C from vertical to the fiber orientation 134
Table C.13 Image analysis result of AlSi10Mg0.8/20vol%Saffil composite infiltrated at 750 °C from parallel to the fiber orientation 135
Table C.14 Image analysis result of AlSi10Mg0.8/20vol%Saffil composite infiltrated at 750 °C from vertical to the fiber orientation 136
Table C.15 Image analysis result of AlSi10Mg0.8/25vol%Saffil composite infiltrated at 750 °C from parallel to the fiber orientation 137
Table C.16 Image analysis result of AlSi10Mg0.8/25vol%Saffil composite infiltrated at 750 °C from vertical to the fiber orientation 138
Table C.17 Image analysis result of AlSi10Mg0.8/30vol%Saffil composite infiltrated at 750 °C from parallel to the fiber orientation 139
Table C.18 Image analysis result of AlSi10Mg0.8/30vol%Saffil composite infiltrated at 750 °C from vertical to the fiber orientation 140
Table C.19 Image analysis result of AlSi10Mg0.8/20vol%Saffil composite infiltrated at 800 °C from parallel to the fiber orientation 141
Table C.20 Image analysis result of AlSi10Mg0.8/20vol%Saffil composite infiltrated at 800 °C from vertical to the fiber orientation 142

Table C.21 Image analysis result of AlSi10Mg0.8/25vol%Saffil composite infiltrated at 800 °C from parallel to the fiber orientation 143
Table C.22 Image analysis result of AlSi10Mg0.8/25vol%Saffil composite infiltrated at 800 °C from vertical to the fiber orientation 144
Table C.23 Image analysis result of AlSi10Mg0.8/30vol%Saffil composite infiltrated at 800 °C from parallel to the fiber orientation 145
Table C.24 Image analysis result of AlSi10Mg0.8/30vol%Saffil composite infiltrated at 800 °C from vertical to the fiber orientation 146
Table C.25 Image analysis result of AlSi10Mg0.8/30vol%Saffil composite insert-component alloy interface at X400 magnification insertion casted at 800 °C 147
Table C.26 Image analysis result of AlSi10Mg0.8/30vol%Saffil composite insert-component alloy interface at X400 magnification insertion casted at 800 °C 148
Table E.1 Three point bending test results of AlSi7Mg0.8 matrix composite specimens 151
Table E.2 Three point bending test results of AlSi10Mg0.8 matrix composite specimens 153
Table F.1 Hardness test results of AlSi7Mg0.8 matrix composite specimens obtained from vertical to the fiber orientation 155
Table F.2 Hardness test results of AlSi7Mg0.8 matrix composite specimens obtained from parallel to the fiber orientation 156
Table F.3 Hardness test results of AlSi10Mg0.8 matrix composite specimens obtained from vertical to the fiber orientation 156
Table F.4 Hardness test results of AlSi10Mg0.8 matrix composite specimens obtained from parallel to the fiber orientation 157
Table F.1 Density measurement results of AlSi7Mg0.8 alloy matrix composite specimens 158
Table F.2 Density measurement results of AlSi10Mg0.8 alloy matrix composite specimens 159

LIST OF FIGURES

FIGURES

Figure 2.1 Specific properties of some selected reinforcing fibers 7

Figure 2.2 Geometric representation of contact angle, θ. (a) wetting condition, (b) non-wetting condition. 9

Figure 2.3 Different types of MMCs 11

Figure 2.4 Aluminum-silicon phase diagram 16

Figure 2.5 Al_2O_3-SiO_2 phase diagram 20

Figure 2.6 a) Direct and b) Indirect squeeze casting 23

Figure 2.7 Start condition of an adiabatic unidirectional infiltration process 24

Figure 2.8 Schematic view of an adiabatic unidirectional infiltration process ... 25

Figure 2.9 Schematic view of tensile stress distribution on fibers of different lengths ($\sigma_{f,\,av} = \sigma_{F,\,eff}$) 27

Figure 3.1 Flow chart of the experimental procedure 30

Figure 3.2 The steel mold used to produce three point bending test specimens . 35

Figure 3.3 The steel mold used to infiltrate the inserts 36

Figure 3.4 Details of the insertion casting mold 1 37

Figure 3.5 Details of the insertion casting mold 2 37

Figure 4.1 SEM image of 20 vol% Saffil fibers parallel to the fiber orientation 43

Figure 4.2 SEM image of 25 vol% Saffil fibers parallel to the fiber orientation 44

Figure 4.3 SEM image of 30 vol% Saffil fibers parallel to the fiber orientation 44

Figure 4.4 SEM image of 20 vol% Saffil fibers vertical to the fiber orientation 45

Figure 4.5 SEM image of 25 vol% Saffil fibers vertical to the fiber orientation 45

Figure 4.6 SEM image of 30 vol% Saffil fibers vertical to the fiber orientation 46

Figure 4.7 Fracture surface of AlSi7Mg0.8 alloy squeeze cast at 750 °C 47

Figure 4.8 Fracture surface of AlSi7Mg0.8/20vol%Al_2O_3 reinforced composite squeeze cast at 750 °C..... 47

Figure 4.9 Fracture surface of AlSi7Mg0.8/25vol%Al_2O_3 reinforced composite squeeze cast at 750 °C..... 48
Figure 4.10 Fracture surface of AlSi7Mg0.8/30vol%Al_2O_3 reinforced composite squeeze cast at 750 °C..... 48
Figure 4.11 Fracture surface of AlSi7Mg0.8 alloy squeeze cast at 800 °C 49
Figure 4.12 Fracture surface of AlSi7Mg0.8/20vol%Al_2O_3 reinforced composite squeeze cast at 800 °C..... 49
Figure 4.13 Fracture surface of AlSi7Mg0.8/25vol%Al_2O_3 reinforced composite squeeze cast at 800 °C..... 50
Figure 4.14 Fracture surface of AlSi7Mg0.8/30vol%Al_2O_3 reinforced composite squeeze cast at 800 °C..... 50
Figure 4.15 Fracture surface of AlSi10Mg0.8 alloy squeeze cast at 750 °C 51
Figure 4.16 Fracture surface of AlSi10Mg0.8/20vol%Al_2O_3 reinforced composite squeeze cast at 750 °C..... 51
Figure 4.17 Fracture surface of AlSi10Mg0.8/25vol%Al_2O_3 reinforced composite squeeze cast at 750 °C..... 52
Figure 4.18 Fracture surface of AlSi10Mg0.8/30vol%Al_2O_3 reinforced composite squeeze cast at 750 °C..... 52
Figure 4.19 Fracture surface of AlSi10Mg0.8 alloy squeeze cast at 800 °C 53
Figure 4.20 Fracture surface of AlSi10Mg0.8/20vol%Al_2O_3 reinforced composite squeeze cast at 800 °C..... 53
Figure 4.21 Fracture surface of AlSi10Mg0.8/25vol%Al_2O_3 reinforced composite squeeze cast at 800 °C..... 54
Figure 4.22 Fracture surface of AlSi10Mg0.8/25vol%Al_2O_3 reinforced composite squeeze cast at 800 °C..... 54
Figure 4.23 SEM image of AlSi7Mg0.8 alloy matrix squeeze cast at 750 °C at X1000 magnification 56
Figure 4.24 SEM image of AlSi7Mg0.8 alloy matrix squeeze cast at 750 °C at X5000 magnification, reveals fibrous eutectic 56

Figure 4.25 Back scattered SEM image of AlSi7Mg0.8/20vol%Al_2O_3 reinforced composite squeeze cast at 750 °C parallel to the fiber orientation at X250 magnification 57
Figure 4.26 Back scattered SEM image of AlSi7Mg0.8/20vol%Al_2O_3 reinforced composite squeeze cast at 750 °C parallel to the fiber orientation at X1000 magnification 57
Figure 4.27 Back scattered SEM image of AlSi7Mg0.8/20vol%Al_2O_3 reinforced composite squeeze cast at 750 °C vertical to the fiber orientation at X250 magnification 58
Figure 4.28 Back scattered SEM image of AlSi7Mg0.8/20vol%Al_2O_3 reinforced composite squeeze cast at 750 °C vertical to the fiber orientation at X1000 magnification 58
Figure 4.29 Back scattered SEM image of AlSi7Mg0.8/25vol%Al_2O_3 reinforced composite squeeze cast at 750 °C parallel to the fiber orientation at X250 magnification 59
Figure 4.30 Back scattered SEM image of AlSi7Mg0.8/25vol%Al_2O_3 reinforced composite squeeze cast at 750 °C parallel to the fiber orientation at X1000 magnification 59
Figure 4.31 Back scattered SEM image of AlSi7Mg0.8/25vol%Al_2O_3 reinforced composite squeeze cast at 750 °C vertical to the fiber orientation at X250 magnification 60
Figure 4.32 Back scattered SEM image of AlSi7Mg0.8/25vol%Al_2O_3 reinforced composite squeeze cast at 750 °C vertical to the fiber orientation at X1000 magnification 60
Figure 4.33 Back scattered SEM image of AlSi7Mg0.8/30vol%Al_2O_3 reinforced composite squeeze cast at 750 °C parallel to the fiber orientation at X250 magnification 61
Figure 4.34 Back scattered SEM image of AlSi7Mg0.8/30vol%Al_2O_3 reinforced composite squeeze cast at 750 °C parallel to the fiber orientation at X1000 magnification 61

Figure 4.35 Back scattered SEM image of AlSi7Mg0.8/30vol%Al_2O_3 reinforced composite squeeze cast at 750 °C vertical to the fiber orientation at X250 magnification 62
Figure 4.36 Back scattered SEM image of AlSi7Mg0.8/30vol%Al_2O_3 reinforced composite squeeze cast at 750 °C vertical to the fiber orientation at X1000 magnification 62
Figure 4.37 SEM image of AlSi7Mg0.8 alloy matrix squeeze cast at 800 °C at X1000 magnification 63
Figure 4.38 SEM image of AlSi7Mg0.8 alloy matrix squeeze cast at 800 °C at X5000 magnification, reveals fibrous eutectic 63
Figure 4.39 Back scattered SEM image of AlSi7Mg0.8/20vol%Al_2O_3 reinforced composite squeeze cast at 800 °C parallel to the fiber orientation at X250 magnification 64
Figure 4.40 Back scattered SEM image of AlSi7Mg0.8/20vol%Al_2O_3 reinforced composite squeeze cast at 800 °C parallel to the fiber orientation at X1000 magnification 64
Figure 4.41 Back scattered SEM image of AlSi7Mg0.8/20vol%Al_2O_3 reinforced composite squeeze cast at 800 °C vertical to the fiber orientation at X250 magnification 65
Figure 4.42 Back scattered SEM image of AlSi7Mg0.8/20vol%Al_2O_3 reinforced composite squeeze cast at 800 °C vertical to the fiber orientation at X1000 magnification 65
Figure 4.43 Back scattered SEM image of AlSi7Mg0.8/25vol%Al_2O_3 reinforced composite squeeze cast at 800 °C parallel to the fiber orientation at X250 magnification 66
Figure 4.44 Back scattered SEM image of AlSi7Mg0.8/25vol%Al_2O_3 reinforced composite squeeze cast at 800 °C parallel to the fiber orientation at X1000 magnification 66
Figure 4.45 Back scattered SEM image of AlSi7Mg0.8/25vol%Al_2O_3 reinforced composite squeeze cast at 800 °C vertical to the fiber orientation at X250 magnification 67

Figure 4.46 Back scattered SEM image of AlSi7Mg0.8/25vol%Al_2O_3 reinforced composite squeeze cast at 800 °C vertical to the fiber orientation at X1000 magnification 67
Figure 4.47 Back scattered SEM image of AlSi7Mg0.8/30vol%Al_2O_3 reinforced composite squeeze cast at 800 °C parallel to the fiber orientation at X250 magnification 68
Figure 4.48 Back scattered SEM image of AlSi7Mg0.8/25vol%Al_2O_3 reinforced composite squeeze cast at 800 °C parallel to the fiber orientation at X1000 magnification 68
Figure 4.49 SEM image of AlSi10Mg0.8 alloy matrix squeeze cast at 750 °C at X1000 magnification 69
Figure 4.50 SEM image of AlSi10Mg0.8/ alloy matrix squeeze cast at 750 °C at X5000 magnification, reveals fibrous eutectic 69
Figure 4.51 Back scattered SEM image of AlSi10Mg0.8/20vol%Al_2O_3 reinforced composite squeeze cast at 750 °C parallel to the fiber orientation at X250 magnification 70
Figure 4.52 Back scattered SEM image of AlSi10Mg0.8/20vol%Al_2O_3 reinforced composite squeeze cast at 750 °C parallel to the fiber orientation at X1000 magnification 70
Figure 4.53 Back scattered SEM image of AlSi10Mg0.8/20vol%Al_2O_3 reinforced composite squeeze cast at 750 °C vertical to the fiber orientation at X250 magnification 71
Figure 4.54 Back scattered SEM image of AlSi10Mg0.8/20vol%Al_2O_3 reinforced composite squeeze cast at 750 °C vertical to the fiber orientation at X1000 magnification 71
Figure 4.55 Back scattered SEM image of AlSi10Mg0.8/25vol%Al_2O_3 reinforced composite squeeze cast at 750 °C parallel to the fiber orientation at X250 magnification 72
Figure 4.56 Back scattered SEM image of AlSi10Mg0.8/25vol%Al_2O_3 reinforced composite squeeze cast at 750 °C parallel to the fiber orientation at X1000 magnification 72

Figure 4.57 Back scattered SEM image of AlSi10Mg0.8/25vol%Al_2O_3 reinforced composite squeeze cast at 750 °C vertical to the fiber orientation at X250 magnification 73
Figure 4.58 Back scattered SEM image of AlSi10Mg0.8/25vol%Al_2O_3 reinforced composite squeeze cast at 750 °C vertical to the fiber orientation at X1000 magnification 73
Figure 4.59 Back scattered SEM image of AlSi10Mg0.8/30vol%Al_2O_3 reinforced composite squeeze cast at 750 °C parallel to the fiber orientation at X250 magnification 74
Figure 4.60 Back scattered SEM image of AlSi10Mg0.8/30vol%Al_2O_3 reinforced composite squeeze cast at 750 °C parallel to the fiber orientation at X1000 magnification 74
Figure 4.61 Back scattered SEM image of AlSi10Mg0.8/30vol%Al_2O_3 reinforced composite squeeze cast at 750 °C vertical to the fiber orientation at X250 magnification 75
Figure 4.62 Back scattered SEM image of AlSi10Mg0.8/30vol%Al_2O_3 reinforced composite squeeze cast at 750 °C vertical to the fiber orientation at X1000 magnification 75
Figure 4.63 SEM image of AlSi10Mg0.8 alloy matrix squeeze cast at 800 °C at X1000 magnification 76
Figure 4.64 SEM image of AlSi10Mg0.8 alloy matrix squeeze cast at 800 °C at X5000 magnification, reveals fibrous eutectic 76
Figure 4.65 Back scattered SEM image of AlSi10Mg0.8/20vol%Al_2O_3 reinforced composite squeeze cast at 800 °C parallel to the fiber orientation at X250 magnification 77
Figure 4.66 Back scattered SEM image of AlSi10Mg0.8/20vol%Al_2O_3 reinforced composite squeeze cast at 800 °C parallel to the fiber orientation at X1000 magnification 77
Figure 4.67 Back scattered SEM image of AlSi10Mg0.8/20vol%Al_2O_3 reinforced composite squeeze cast at 800 °C vertical to the fiber orientation at X250 magnification 78

Figure 4.68 Back scattered SEM image of AlSi10Mg0.8/20vol%Al_2O_3 reinforced composite squeeze cast at 800 °C vertical to the fiber orientation at X1000 magnification 78
Figure 4.69 Back scattered SEM image of AlSi10Mg0.8/25vol%Al_2O_3 reinforced composite squeeze cast at 800 °C parallel to the fiber orientation at X250 magnification 79
Figure 4.70 Back scattered SEM image of AlSi10Mg0.8/25vol%Al_2O_3 reinforced composite squeeze cast at 800 °C parallel to the fiber orientation at X1000 magnification 79
Figure 4.71 Back scattered SEM image of AlSi10Mg0.8/25vol%Al_2O_3 reinforced composite squeeze cast at 800 °C vertical to the fiber orientation at X250 magnification 80
Figure 4.72 Back scattered SEM image of AlSi10Mg0.8/25vol%Al_2O_3 reinforced composite squeeze cast at 800 °C vertical to the fiber orientation at X1000 magnification 80
Figure 4.73 Back scattered SEM image of AlSi10Mg0.8/30vol%Al_2O_3 reinforced composite squeeze cast at 800 °C parallel to the fiber orientation at X250 magnification 81
Figure 4.74 Back scattered SEM image of AlSi10Mg0.8/30vol%Al_2O_3 reinforced composite squeeze cast at 800 °C parallel to the fiber orientation at X1000 magnification 81
Figure 4.75 Back scattered SEM image of AlSi10Mg0.8/30vol%Al_2O_3 reinforced composite squeeze cast at 800 °C vertical to the fiber orientation at X250 magnification 82
Figure 4.76 Back scattered SEM image of AlSi10Mg0.8/30vol%Al_2O_3 reinforced composite squeeze cast at 800 °C vertical to the fiber orientation at X1000 magnification 82
Figure 4.77 SEM image of AlSi10Mg0.8/30vol%Al_2O_3 reinforced composite squeeze cast at 800 °C parallel to the fiber orientation at X250 magnification 83
Figure 4.78 The sample image after image analyzing at 100X magnification..... 84

Figure 4.79 Optical microscopy image of insert/backing alloy interface at X100 magnification 87
Figure 4.80 Optical microscopy image of insert/backing alloy interface at X400 magnification 88
Figure 4.81 Connecting rod obtained from the insertion casting operation 89
Figure 4.82 XRD analyses of the preforms (a) 20vol%, (b) 25 vol% and (c) 30 vol% Saffil fibers 91
Figure 4.83 XRD analysis of AlSi7Mg0.8 matrix composite infiltrated at 750 °C (a) 0 vol% fiber reinforced, (b) 20 vol% fiber reinforced, (c) 25 vol% fiber reinforced and (d) 30 vol% fiber reinforced..... 93
Figure 4.85 XRD analysis of AlSi7Mg0.8 matrix composite infiltrated at 800 °C (a) 0 vol% fiber reinforced, (b) 20 vol% fiber reinforced, (c) 25 vol% fiber reinforced and (d) 30 vol% fiber reinforced..... 94
Figure 4.86 XRD analysis of AlSi10Mg0.8 matrix composite infiltrated at 750 °C (a) 0 vol% fiber reinforced, (b) 20 vol% fiber reinforced, (c) 25 vol% fiber reinforced and (d) 30 vol% fiber reinforced..... 95
Figure 4.87 XRD analysis of AlSi10Mg0.8 matrix composite infiltrated at 800 °C (a) 0 vol% fiber reinforced, (b) 20 vol% fiber reinforced, (c) 25 vol% fiber reinforced and (d) 30 vol% fiber reinforced..... 96
Figure 4.88 Three point bending test results of the composite specimens..... 100
Figure 4.89 Hardness results of the composite specimens taken from the parallel to the fiber orientation..... 101
Figure 4.90 Hardness results of the composite specimens taken from the vertical to the fiber orientation..... 102
Figure 4.91 Theoretical and experimental densities of AlSi7Mg0.8 matrix composite cast at 750 °C and reinforced by Saffil fibers..... 103
Figure 4.92 Theoretical and experimental densities of AlSi7Mg0.8 matrix composite cast at 800 °C and reinforced by Saffil fibers..... 104
Figure 4.93 Theoretical and experimental densities of AlSi10Mg0.8 matrix composite cast at 750 °C and reinforced by Saffil fibers..... 104

Figure 4.94 Theoretical and experimental densities of AlSi10Mg0.8 matrix composite cast at 800 °C and reinforced by Saffil fibers..... 105
Figure 4.95 Components obtained from insertion casting for automotive applications 106
Figure 4.96 Components obtained from insertion casting for defense applications 107
Figure 4.97 Sample drawing of the more suitable inserts for the defense application parts 108
Figure D.1 X-ray details of aluminum 149
Figure D.2 X-ray details of silicon..... 149
Figure D.3 X-ray details of delta aluminum oxide..... 150

CHAPTER 1

INTRODUCTION

Composite materials are artificially made materials which have two or more physically distinct phases containing an interface separating them and of which characteristics cannot be attained by conventional materials [1, 2].

The reason why composite materials are used in engineering field is due to their characteristics, custom-made and dependent on application. From this point, metal matrix composites (MMCs) becomes interesting both as constructional and functional materials. In property profile of MMCs, there exists the possibility of various system combinations (metal–ceramic–nonmetal) together with a reasonable cost/performance relationship. Therefore this property profile offers the engineer to have a large chance to solve the specific demands or the solution of the problem of the component [3].

Importance of MMCs can be divided into two main groups. In the first group advantages with respect to unreinforced metals/alloys and in the second group advantages with respect to other composites such as polymer matrix composites (PMCs). With respect to metals/alloys; weight savings (due to high strength/weight ratio), remarkable dimensional stability, higher elevated temperature stability (i.e. creep resistance) and exceptionally improved cyclic fatigue behavior can be stated as advantages of MMCs. With respect to PMCs, higher service temperatures together with strength and stiffness, improved transverse properties, higher electrical conductivity (grounding and space charging), higher thermal conductivity, little or no contamination (i.e. no out-gassing or moisture absorption

problems) and radiation survivability (laser, UV, nuclear etc.) can be stated as advantages [4].

General applications of MMCs can be grouped in terms of ground vehicle, aerospace and industrial applications. Some of the examples of ground vehicle applications are cylinder liners, diesel pistons, connecting rods, valve lifters and piston pins (engine applications), drive shafts, disc rotors, calipers (chassis and drive trains). Similarly for aerospace applications, the examples are exhaust nozzles, links, blades, cases, shafts and vanes. Finally, cutting tools, drill bits, valves and gates can be the examples of the structural applications [5]. Moreover to these general application fields, the common usage fields of Al/Al_2O_3 composites are cylinder liners, piston (lighter material for cold start), rings and connecting rods (fuel conservation, improved efficiency, tribological application) [6].

The problem with the limited commercial use of discontinuous reinforced aluminum matrix composites not only related to the cost but also complexity of the production routes. Some of the consequential obstacles during alumina short fiber reinforced aluminum matrix composites are simply efficiency of fiber/matrix adhesion, appropriate microstructure and high temperature required for the infiltration of the reinforcement.

The main objective of the present thesis work was to conduct research on fiber/matrix adhesion together with insert/component adhesion in the entire composite product. During the experiments different volume percentages of reinforcement for three different Al-Si foundry alloys (mainly hypo-eutectic, eutectic and hyper-eutectic) were produced. Casting temperatures were selected as 750 °C and 800 °C and mold temperature was fixed at 200 °C.

CHAPTER 2

LITERATURE REVIEW

2.1 Composites

Composite materials are defined as macroscopic combination of two or more distinct materials, having a recognizable interface between them. Modern composites are generally manufactured to achieve a particular balance of properties for a given range of applications [7].

Classification of composites can be done into two ways. The first classification is based on type of the matrix used in composite and the second one is based on the reinforcement used in the composite [7]. For simplification, classification based on the matrix material is used throughout the text. According to this classification, composites are divided into four main groups, which are:

- Metal matrix composites (MMC),
- Ceramic matrix composites (CMC),
- Polymer matrix composites (PMC),
- Carbon-carbon composites (CCC) [2].

Composite materials consist of two or more physically and/or chemically distinct phases, which can be suitable arranged or distributed, with an interface separating them. These two phases are named as matrix phase and reinforcement phase [1].

2.1.1 Matrix Phase

Matrix is the continuous and generally the soft phase of the composites. Properties of the matrix phase can be stated as:

- To bind the reinforcements together by a virtue of its cohesive and adhesive characteristics,
- To transfer load to the reinforcements and to protect them from the environment and handling,
- To control transverse properties, interlaminar strength and elevated-temperature strength,
- To hold the reinforcement material in a in the proper orientation and position,
- To provide an inelastic response (stress concentrations are reduced dramatically and internal stresses are redistributed from broken reinforcements) [7].

In the Table 2.1, Table 2.2 and Table 2.3, a few examples of matrix materials used in the composites can be seen together with some of their mechanical properties.

Table 2.1 Mechanical properties of some metals used as matrices in composites [8]

Material (Metal Alloys)	Ultimate tensile strength, σ_{UTS} (MPa)	Elastic modulus, E (GPa)	Density, ρ (g/cm^3)
Steel	400–2200	180–210	7.8–7.85
Aluminum	140–700	69–72	2.7–2.85
Titanium	420–1200	110	4.5
Magnesium	220–320	40	1.8
Beryllium	620	320	1.85
Nickel	400–500	200	8.9

Table 2.2 Mechanical properties of some polymers used as matrices in composites [8]

Material (Polymers)		Ultimate tensile strength, σ_{UTS} (MPa)	Elastic modulus, E (GPa)	Density, ρ (g/cm^3)
Thermoset polymeric resins	Epoxy	60–90	2.4–4.2	1.2–1.3
	Polyester	30–70	2.8–3.8	1.2–1.35
	Phenol-formaldehyde	40–70	7–11	1.2–1.3
	Organosilicone	25–50	6.8–10	1.35–1.4
	Polyimide	55–110	3.2	1.3–1.43
	Bismaleimide	80	4.2	1.2
Thermoplastic polymers	Polyethylene	25–45	6–8.5	0.95
	Polystyrene	35–45	30	1.05
	Teflon	15–35	3.5	2.3
	Nylon	80	2.8	1.14
	Polyester (PC)	60	2.5	1.32
	Polysulfone (PSU)	70	2.7	1.24

Table 2.3 Mechanical properties of some ceramics used as matrices in composites [9]

Material (Ceramics)	Melting/sublimation temperature, °C	Elastic modulus, (GPa)	Density, ρ (g/cm^3)
TaC	4255	550	14.3
HfC	3890	450	12.6
NbC	3615	500	7.56
TiC	3260	490	4.92
TaB_2	3040	690	11.70
α-BN	3000	86	2.29
TiB_2	2850	540	4.45
MgO	2825	290	3.65
SiC	2600	460	3.2
B_4C	2470	450	2.5
B	2300	400	2.7
Al_2O_3	2050	400	3.97
$MoSi_2$	2020	440	6.1
Si_3N_4	1877	485	3.2

General matrix systems have shown in the above tables. Moreover to those matrices stated in the tables, some of the metal matrix systems used in composite component production can be grouped as *conventional cast alloys* (G-AlSi12CuMgNi, G-AlSi9Mg, G-AlSi7 (A356), AZ91, AE42), *conventional wrought alloys* (AlMgSiCu (6061), AlCuSiMn (2014), AlZnMgCu1.5 (7075), TiAl6V4) and *special alloys* (Al–Cu–Mg–Ni–Fe-alloy (2618), Al–Cu–Mg–Li-alloy (8090), AZ91Ca) [3].

2.1.2 Reinforcement Phase

The purpose of reinforcement phase can be stated as follows:

- To provide superior levels of strength and stiffness to the composite (principle purpose),
- To provide thermal and electrical conductivity, controlled thermal expansion and wear resistance in addition to structural properties [7].

Reinforcements can be in the form of particles, flakes, whiskers, short fibers, continuous fibers or sheets. Although reinforcements can be in different forms, most of them are used fibrous form (generally called advanced fibers). The important characteristics of these advanced fibers are:

- Small diameter with respect to its grain size, which allows higher fraction of theoretical strength to be attained compared to the bulk form,
- High aspect ratio (*l/d*), which allows very large applied load transfer to the matrix,
- Very high degree of plasticity, which is the result of very high modulus and small diameter [1].

Specific properties of some selected reinforcing fibers are given in Figure 2.1.

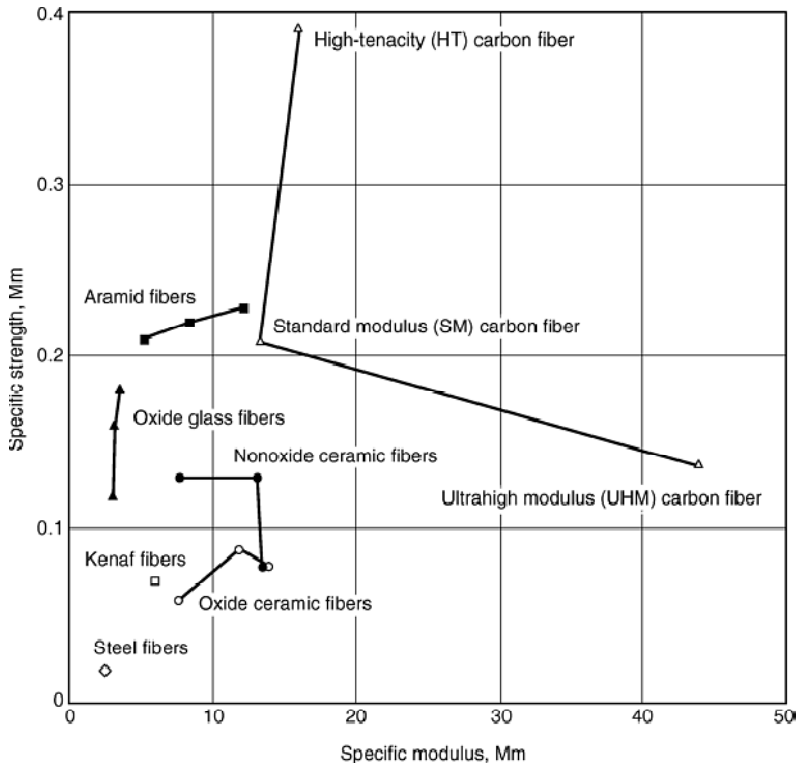

Figure 2.1 Specific properties of some selected reinforcing fibers [7]

In the above figure, given fibers are used for all composites. However, for MMCs, generally the following reinforcements are used:

- Continuous fibers (e.g. Al_2O_3, Al_2O_3+SiO_2, B, C, SiC, Si_3N_4, Nb-Ti, Nb_3Sn),
- Discontinuous fibers,
    - Whiskers (SiC, TiB, Al_2O_3),
    - Short fibers (Al_2O_3, SiC, Al_2O_3+SiO_2, vapor grown carbon fibers),
- Particles (SiC, Al_2O_3, TiC, B_4C, WC) [4].

2.1.3 Interface

An interface is defined as the bonding surface between a reinforcement and a matrix. The requirement of an ideal interface is protection of the reinforcement and allowing the load transfer from the (soft) matrix to the (strong) reinforcement [1, 4].

To understand the ability of interface forming in a composite, *wettability* term is used. Wettability can simply be defined as the ability of a liquid to spread on a solid surface. The degree of wettability is shown in Figure 2.2 by the edge angle adjustment of a molten on a solid base, where γ_{LV} represents the surface energy of the liquid phase, γ_{SV} represents the surface energy of solid phase and γ_{SL} represents the surface energy of the liquid/solid interface [3, 4]. Mathematically formulization can be written as:

$$\gamma_{SV} - \gamma_{SL} = \gamma_{LV} \cdot \cos\theta \tag{2.1}$$

For metal-ceramic systems, some numerical values of surface tensions at certain temperatures are given in Table 2.4.

Table 2.4 Surface tensions of selected metal-ceramic systems at different temperatures [3]

Alloy, Ceramic, Systems	Temperature (K)	γ_{LV} (mJ/m^2)	γ_{SL} (mJ/m^2)	γ_{SV} (mJ/m^2)
Al	953	1050	-	-
Mg	943	560	-	-
Al_2O_3	0	-	930	-
MgO	0	-	1150	-
Cu/Al_2O_3	1370	1308	1485	2541
	1450	1292	1422	2284
Ni/Al_2O_3	1843	1751	1114	2204
	2003	1676	988	1598
Al/SiC	973	851	2469	2949
	1073	840	2414	2773
	1173	830	2350	2684

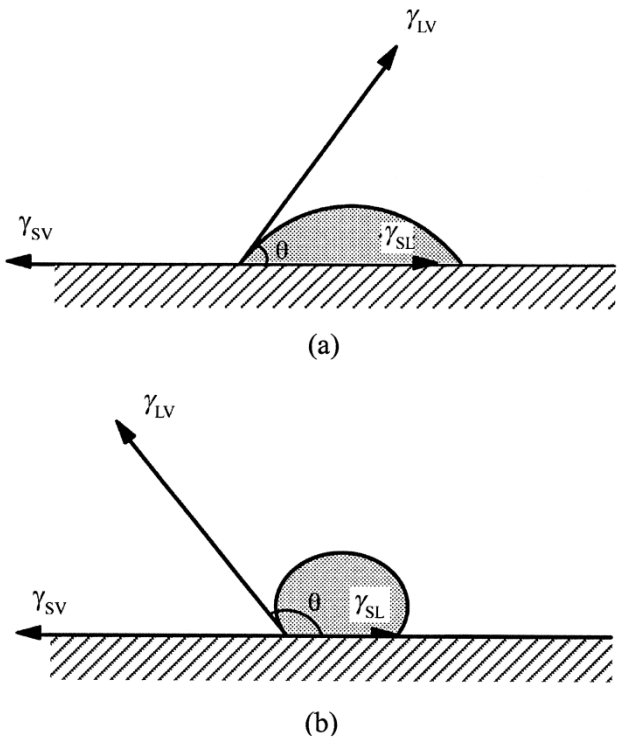

Figure 2.2 Geometric representation of contact angle, θ. (a) wetting condition, (b) non-wetting condition [4].

The reason why the interface has great importance in the composite is due to its ability of having a large internal surface area occupied by the interface. It is possible to have a 3000 cm^2/cm^3 surface area [1].

2.2 Metal Matrix Composites (MMCs)

Metal matrix composites consist of at least two chemically and physically distinct phases, like all composites. The fibrous or particulate phase is suitable distributed in the matrix phase to provide properties which are not attainable with either of the individual phases [3, 4, 6].

2.2.1 Types of MMCs

Types of MMCs are named according to their reinforcement types. In general, there are three kinds of MMCs, which are:

(a) Particle reinforced MMCs,
(b) Short fiber or whisker reinforced MMCs,
(c) Continuous fiber or sheet reinforced MMCs [4].

To have a consistent understanding, it is important to visualize what a particle, short fiber/whisker or continuous fiber means. In Table 2.5, together with their dimensions, common reinforcements used in MMCs are given.

Table 2.5 Typical reinforcements used in MMCs [4]

Type	Aspect ratio	Diameter, μm	Examples
Particle	1–4	1–25	SiC, Al_2O_3, BN, B_4C, WC
Short fiber or whisker	10–10000	1–5	C, SiC, Al_2O_3, Al_2O_3+SiO_2
Continuous fiber	>1000	3–150	SiC, Al_2O_3, C, B, W, Nb-Ti, Nb_3Sn

In the Figure 2.3, three types of MMCs can be seen schematically.

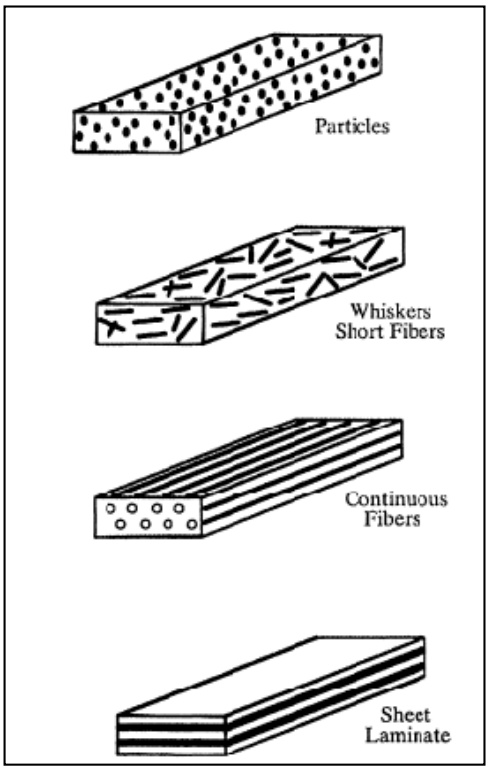

Figure 2.3 Different types of MMCs [4]

2.2.2 Processing Techniques of MMCs

The main processing techniques for MMCs can be grouped into two parts, mainly liquid state processes and liquid state processes [5]. In the following parts, details of these processing techniques are given.

2.2.2.1 Liquid State Processing

A great number of practical applications are produced by the liquid state processes because of their inherent advantages which are the lower cost and better handling ability of the liquid metal compared to powders and ability of production of these composite parts by the conventional casting methods. There are four major processing techniques in liquid state processes [10]:

- Infiltration
- Dispersion
- Spraying
- In-situ fabrication.

2.2.2.2 Solid State Processing

Solid state processing techniques generally necessitate the matrix material to be in the form of powder. Using the matrix material in the powder form provides some advantages as given:

- Homogeneously distributed particles
- Homogeneous distribution of elements
- Super-saturation at alloying elements also in the manufacturing powder
- Isotropic material properties
- Higher cooling rates (10^{-2} – 10^{-4} K/s)

- Large quantity production
- High economic efficiency [3].

In discontinuous MMCs, solid state processes are used to obtain the highest mechanical properties. Solid state processing techniques can be separated into three main groups [5]:

- Powder metallurgy
- Diffusion bonding
- Deposition techniques.

2.2.2.3 Infiltration

Infiltration is basically infiltrating the porous preform (reinforcement phase) by the molten metal that flows through the interstices to produce the composite. Classification of the infiltration process is done according to type of the force(s) exist(s) in the infiltration process. Types of infiltration are stated as [5]:

- No external force [11],
- Vacuum-assisted infiltration [12],
- Pressure driven infiltration
    - Gas pressure-assisted infiltration [13, 14],
    - Mechanical pressure-driven infiltration [15, 16],
- Other forces
    - Low pressures with the assistance of vibrations [17, 18],
    - Centrifugal casting [19],
    - Electromagnetic body forces [5].

2.2.3 Aluminum Metal Matrix Composites (Al-MMCs)

Aluminum, as the matrix material, provides the basis of the most of the commercial and academic researches on MMCs. Aluminum has well suited properties for use a matrix material, which are:

- Light weight,
- Environment resistance,
- Useful mechanical properties.

In addition to the properties stated above, one of the most important properties of aluminum for its use as the most popular matrix material is its melting point. Its melting point is high enough to satisfy many application requirements and, yet low enough to provide the reasonably convenient composite processing [20].

Aluminum matrix composites have a large range of applications especially in the automotive industry due to its applicability for the mass production. In Table 2.6, some of the interests of the automotive industries up to the 90s are given.

Table 2.6 Synthesis of selected cast aluminum-matrix composites of interest to automotive industries [6]

Period	Location	Composite System	Technique Used
1965	Inca	Al/Gr	Gas injection and stir casting
1968	IITK, India	Al/Al_2O_3	Stir casting
1974	IISc., India	Al/SiC, Al_2O_3, Al/Mica	Stir casting
1975	MIT	Al/ Al_2O_3 (and other particles)	Compocasting
1979	RRL, India	Al/Silicate, Al/TiO_2, ZrO_2,	Stir casting
1979	USSR	Al/Gr	Stir casting
1980	Dural	Al/SiC	Stir casting
1981	Hitachi, Japan	Al/Gr	Pressure casting
1982	DuPont	Al/Al_2O_3	Pressure casting
1983	Toyota, Japan	Al/Saffil	Squeeze casting
1984	RRL, India	Al/Microballoons	Stir casting
1984	Norsk Hydro, Norway	Al/SiC	Stir casting
1985	Martin Marietta	Al/TiC	XD Process
1986	MIT	Al/SiC	Pressure infiltration
1987	U of WI-Milwaukee	Al/Hybrids	Pressure, stir casting
1987	Comalco, Australia	Al/ Al_2O_3	Stir casting
1988	Grenoble France	Al/SiC	Stir casting
1989	Honda, Japan	Al/ Al_2O_3-C	Pressure casting
1989	Lanxide	Al/Al_2O_3, Al/SiC	Pressureless infiltration

2.2.3.1 Matrix Alloys

Among the matrix materials used in MMC components, aluminum is the most frequently used matrix metal due to its low density, good casting ability together with superior mechanical properties [21]. Due to the addition of Si to Al, which increases the melting range and imparts fluidity together with low shrinkage during cooling and high hardness, Al-Si alloys are the most popular casting alloys [22]. In Figure 2.4, Al-Si phase diagram can be seen.

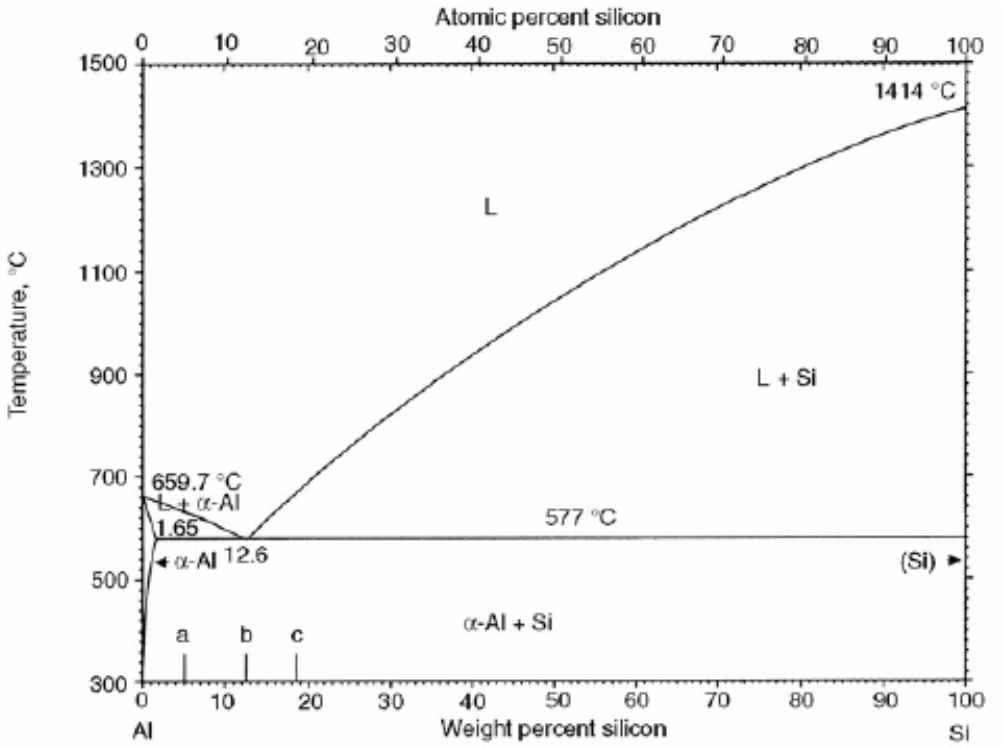

Figure 2.4 Aluminum-silicon phase diagram [23]

To make a comparison between the mechanical properties and infiltration parameters, two different Al-Si alloys were tried to investigate. Those matrix alloys are Al-7wt%Si and Al-10wt%Si. Detailed properties of those alloys were given in the following subtitles.

Table 2.7 Standard chemical composition of Al-7wt%Si alloy [20]

Alloy	Products	Si	Fe	Cu	Mn	Mg	Zn	Ti
A356.0	S,P	6.5–7.5	0.20	0.20	0.10	0.25–0.45	0.10	0.20

Table 2.8 Standard chemical composition of Al-10wt%Si alloy [20]

Alloy	Products	Si	Fe	Cu	Mn	Mg	Zn	Ti
361.0	D	9.5–10.5	1.1	0.6	0.35	0.40–0.60	0.50	0.20
		Ni	Cr	Sn				
		0.20–0.30	0.20–0.30	0.10				

In Table 2.7 and Table 2.8, S, P and D corresponds to the terms *sand casting*, *permanent mold casting* and *die casting* respectively.

Some of the physical properties of alloys (as cast condition) A356.0 and 361.0 are given in the following tables.

Table 2.9 Typical physical properties of A356.0 alloy

Temper and product form	Specific gravity	Density (kg/m^3)	Approximate melting range (°C)	Electrical conduct. (%IACS)	Thermal conduct. at 25 °C (cal/cm·s·°C)	Coeff. of thermal expansion ($°C \times 10^{-6}$)	
T6(S)	2.69	2713	560-610	40	0.36	21.4	23.4

Table 2.10 Typical physical properties of 361.0 alloy

Temper and product form	Specific gravity	Density (kg/m^3)	Approximate melting range (°C)	Electrical conduct. (%IACS)	Thermal conduct. at 25 °C (cal/cm·s·°C)	Coeff. of thermal expansion ($°C \times 10^{-6}$)	
F(D)	2.68	2685	570-590	37	0.35	20.9	22.9

In Table 2.9 and Table 2.10, T6 and F represent the thermal conditions of the cast specimen, i.e. T6 is heat treatment condition and F means as cast condition.

In the case of some mechanical properties, details of the alloys are given in the Table 2.11.

Table 2.11 Mechanical properties of alloys A356.0 and 361.0 [20]

Alloy	Temper	σ_{UTS}	$\sigma_{Y(0.2\%)}$	HB
A356.0 (S)	F	159	83	
	T51	179	124	60
	T6	278	207	70
	T71	207	138	60
A356.0 (P)	T61	255	207	90
361.0 (D)	F	324	175	75

Generally, A356.0 alloy is used in the applications of structural parts requiring high strength such as machine parts and truck chassis parts. Also 361.0 alloy is used in outboard motor parts, instrument cases, cover plates, marine and aircraft cases [20].

2.2.3.2 Reinforcement Material

As the reinforcement material, alumina is commonly used in MMCs production. Alumina (Al_2O_3) is an appropriate reinforcing material for aluminum matrix composites, since it has a good compatibility with aluminum even at the projected temperatures [20]. Commercial name of selected reinforcement material is Saffil fiber, Fibralloy Preform®. Details of the reinforcement material are given below.

2.2.3.2.1 Physical and Chemical Properties of Saffil Fibers

High alumina (Saffil) type of preforms was used as the matrix material. By using the term “high alumina” 96-97 wt% Al_2O_3 together with 3-4 wt% SiO_2 is

emphasized in the chemical composition. Physical properties of the material are given in Table 2.12.

Table 2.12 Physical properties of Saffil fibers [24]

Specific gravity	3.3 – 3.5
Tensile strength (MPa)	100 – 2000
Young's modulus (GPa)	300 – 330
Mean fiber diameter (μm)	3.0

In addition to the physical properties of the material, to understand the chemical nature of Saffil fibers, alumina silica phase diagram, as given in Figure 2.5, can be used to investigate the material. In Al_2O_3-SiO_2 phase diagram, term "mullite" is the name of a mineral and its chemical formula is $3Al_2O_3 \cdot 2SiO_2$ [25].

From the phase diagram given in Figure 2.5, it is seen that mullite + alumina region starts from room temperature and lasts until the temperature of 1890 °C above where liquid + alumina region starts at composition level of 96-97 wt% Al_2O_3 + 3-4 wt% SiO_2. This indicates that Saffil fibers show no chemical transformation up to the temperature of 1890 °C.

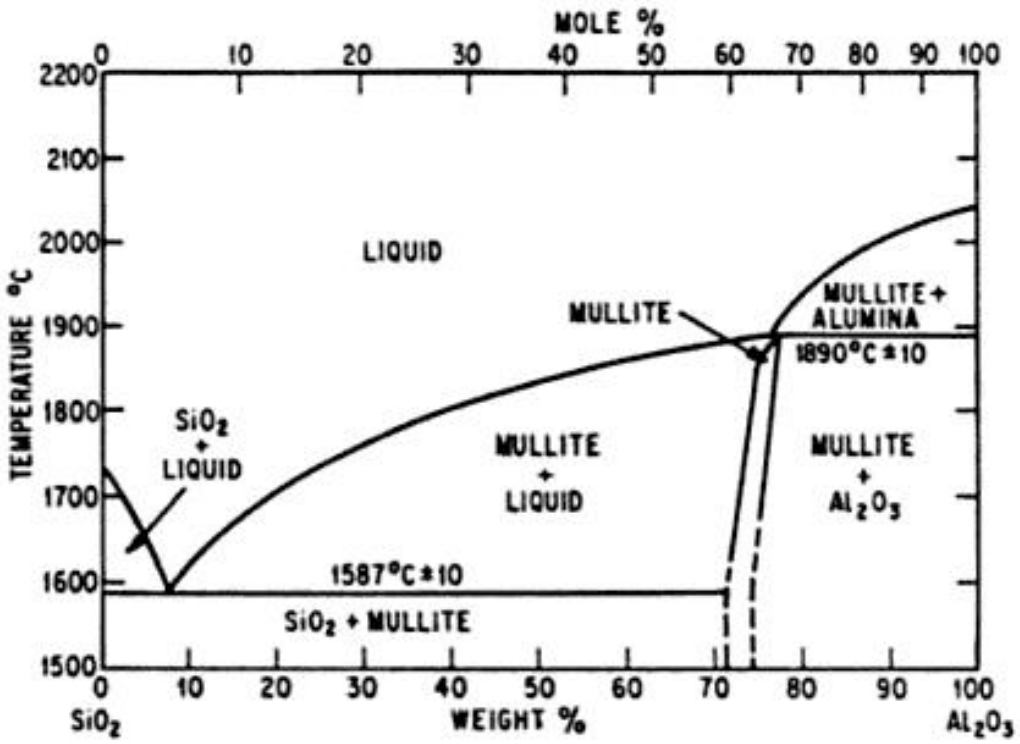

Figure 2.5 Al_2O_3-SiO_2 phase diagram [26]

Manufacturing technique of preforms is strongly dependent on the chemical composition of the fibers. Details of the manufacturing process are given in the following subtitle.

2.2.3.2.2 Processing Technique of Saffil Preforms

Saffil preforms are mainly composed of alumina fibers (96-97 wt% Al_2O_3 + 3-4 wt% SiO_2) as stated in the previous part of this chapter. As historical information, both continuous and discontinuous ceramic oxide fibers have been commercially available since the 1970s. Among all the oxide fibers, alumina is one of the most widely used reinforcement material. There exist different allotropic forms of

alumina fibers which are γ, δ, η and α. Among them α-alumina is the thermodynamically stable phase [4].

Preform preparation stage is the most important and grueling step of the locally reinforced short fiber MMCs. To have an efficient reinforcement, a preform must:

- Be extremely clean,
- Have homogeneous fiber distribution together with homogeneous fiber orientation,
- Have minimum and homogeneously distributed fiber content,
- Have sufficient strength with high aspect ratio [3].

There are two main routes to produce alumina silicate fibers which are [3]:

1. Melt spun process
2. Spin sinter process

Melt spun process is the process suitable for alumina silicate fibers up to alumina content approximately 60 wt%. Melt spun process involves melting of the raw material by electrodes above 2000 °C, firstly. Secondly the melt is run out through an orifice at the bottom of the furnace. Finally, by the rotating rollers or blowing by high pressure air, fibers are formed [3].

Spin sinter process is the process for alumina silicate fibers up to alumina content higher than 60 wt%. Spin sinter process starts with preparation of an aqueous phase containing an oxide sol, aluminum oxychloride [$Al_2(OH)_5Cl$], and an organic polymer, medium molecular weight such as 2 wt% polyvinyl alcohol. This solution is then slowly evaporated in a rotary evaporator until 80 Pa·s viscosity is attained. After this step, it is extruded through a spinneret. Fibers are wound in a drum and fired to about 800 °C yielding a microstructure of fine-grained alumina fiber having 5-10 % porosity and a diameter of 3-5 μm. At this stage, fibers are suitable

for filter applications because of their high porosity. Finally, heating them to 1400-1500 °C causes a linear shrinkage, which provides a suitable material for reinforcement purposes to the manufacturer [4].

2.3 Component Production

Manufacturing possibilities of MMCs have quite different routes as stated in the previous part. Among them, one of the most suitable method to produce both particulate and fiber reinforced aluminum metal matrix composites is mechanical pressure driven infiltration, i.e. squeeze casting. One of the most important advantages of this process is the short contact time between the reinforcement and the matrix to improve wettability by avoiding interface reactions [14-16].

Squeeze casting can be described as the combination of casting and forging. During the process, the mold is filled by the molten metal. After filling of the mold, high pressure is applied and solidification starts. Pressure is present during the solidification to prevent pore formation, which causes plastic deformation. The mechanical properties of the casting are improved by this method compared to conventional casting operations.

There are two different types of squeeze casting process [27].

1. Direct squeeze casting
2. Indirect squeeze casting

In Figure 2.6, types of squeeze casting process are shown.

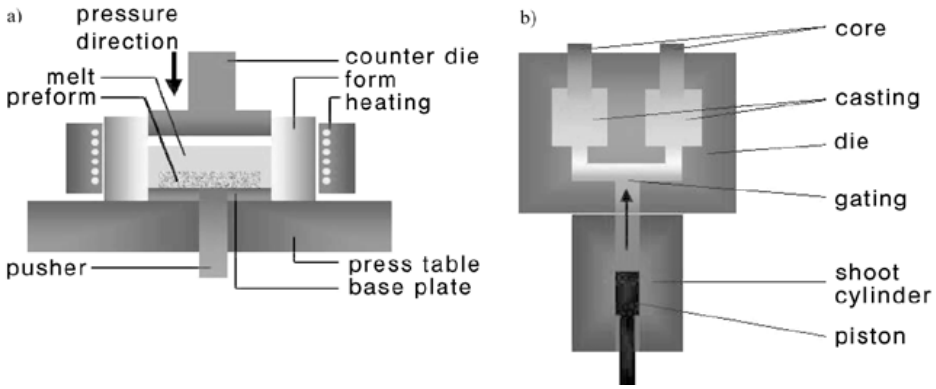

Figure 2.6 a) Direct and b) Indirect squeeze casting [3]

During squeeze casting, it is seen that, the increase in pressure alters the equilibrium phase diagram. In general, most metals experience an increase in phase diagram which obeys Clausius-Clapeyron equation [28]:

$$\frac{\Delta T}{\Delta P} = \frac{T_m(V_2 - V_1)}{Q} \tag{2.2}$$

Where ΔT = increase in melting temperature

ΔP = increase in pressure from atmospheric pressure

Q = latent heat of fusion

V_2 = specific volume of liquid phase

V_1 = specific volume of solid phase

T_m = melting temperature at atmospheric pressure

From the above equation, it is expected that binary Al-Si alloys, eutectic point is shifted upward in the direction of the higher melting point constituent, in this case towards increasing silicon content. For Al-Si alloys, a rise in the liquidus temperature of approximately 6 K is expected for every 100 MPa of pressure applied [28].

In the case of short fiber reinforced aluminum MMC production, preforms are placed into the mold and molten metal is poured on it followed by application of high pressure until the solidification is completed [15].

Squeeze casting technique, in composite production, has some parameters as given below [29]:

- Preform pre-heat temperature
- Inter-fiber spacing (fiber volume content)
- Pressure of infiltration
- Speed of infiltration
- Melt super-heat temperature.

To start the infiltration, a threshold pressure should be attained. Threshold pressure is the minimum pressure to be overcome to start the infiltration. In Figure 2.7 and Figure 2.8, schematic view of infiltration process at the start and an arbitrary condition.

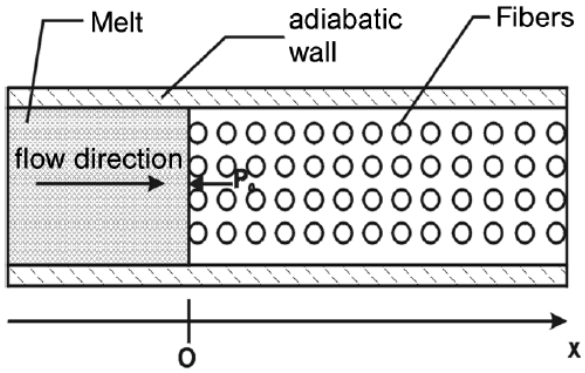

Figure 2.7 Start condition of an adiabatic unidirectional infiltration process [30]

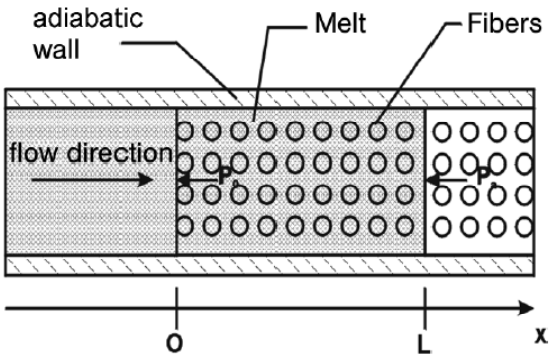

Figure 2.8 Schematic view of an adiabatic unidirectional infiltration process [30]

In the above figures, P_0 is pressure in the melt entering the preform and P_a is the pressure in the melt at the infiltration front. Assuming that the resultant pressure is ΔP and the pressure drop due to the wetting of the surfaces yield [30]:

$$\Delta P = P_0 - P_a - \Delta P_\gamma \tag{2.3}$$

When P_0 equals to P_a, the threshold pressure (P_{th}) can be found as follows [3]:

$$P_{th} = \Delta P_\gamma = S_f(\gamma_{SL} - \gamma_{SV}) \tag{2.4}$$

Where S_f is the surface interface per unit area and is defined for short fiber preforms as [5]:

$$S_f = \frac{4V_f}{d_f(1-V_f)} \tag{2.5}$$

Where d_f is the fiber diameter and V_f is the fiber volume fraction.

The main requirement in for squeeze casting of Al-Al_2O_3 system is wetting of the fibers by the molten aluminum. The wetting condition, stated by equation (2.1), is

determined by the wetting angle. To increase the wetting ability, following parameters should be controlled during the processing [31]:

- Contact time of matrix and the reinforcement [32],
- Temperature of the molten metal and the preform [33]
- Interface reactions [34]
- Surrounding atmosphere of the matrix and the reinforcement [35].

2.4 Mechanism of Fiber Reinforcement

Mechanism of fiber reinforcement is divided into two parts, which are long fiber reinforcement and short fiber reinforcement. Reinforcement materials show different levels of strengthening in the composite structures according to their geometries [1, 4, 5]. Details of this topic are given in the following subtitles.

2.4.1 Long Fiber Reinforcement

The Rule of Mixtures can be used to determine the strength of a long fiber reinforced composite material. However, only reinforcement type is not important in determining the strength values. Together with the geometry, important assumptions, which are having no fiber contact and optimum interface formation of the composite, should also be considered [1, 3, 4]. The rule of mixtures can be stated as:

$$\sigma_C = \varphi_F \cdot \sigma_F + (1 - \varphi_F) \cdot \sigma_M^* \qquad (2.6)$$

Where σ represents the strength and φ represents the volume fraction of the constituents. Subscripts C, F and M denote composite, fiber (i.e. reinforcement) and matrix. Moreover σ_M^* denotes the matrix yield strength.

2.4.2 Short Fiber Reinforcement

Strength prediction of the short fiber composites is somewhat different from the long fiber reinforced composites. The main difference originates from the fiber geometry. In the long fiber reinforced composites, load is carried along the entire length of the fibers. However, in short fiber reinforced composites; interfacial shear through the matrix transfers the load from the matrix to the fiber as shown in the Figure 2.9.

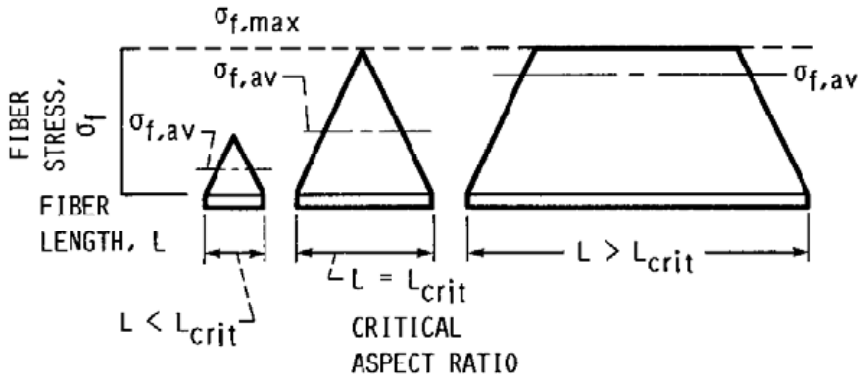

Figure 2.9 Schematic view of tensile stress distribution on fibers of different lengths ($\sigma_{f,\,av} = \sigma_{F,\,eff}$)

Where $\sigma_{f,\,av}$ is the average fiber strength and $\sigma_{F,\,eff}$ is the effective fiber strength.

The ends of the fibers carry high shear stress together with low tensile stress. To be able to provide the fiber to carry its maximum tensile strength, a balance between the shear strength and tensile strength should be generated i.e. fiber length should be longer than a critical length l_c. Defining d_F and τ_{FM} as the fiber diameter and fiber/matrix shear strength respectively, calculation of l_c is written as shown below [36]:

$$l_c = \frac{\sigma_F \cdot d_F}{2\tau_{FM}} \quad (2.7)$$

Where τ_{FM} can be written as [3]:

$$\tau_{FM} = 0.5 \cdot \sigma_{M*} \quad (2.8)$$

Starting from the above equations, effective fiber strength ($\sigma_{F,\,eff}$) for a composites having a mean fiber length l_m and fiber efficiency η can be calculated as in the following [3]:

$$\sigma_{F,eff} = \eta \cdot \sigma_F \cdot \left[1 - \left(\frac{l_c}{2 \cdot l_m}\right)\right] \quad (2.9)$$

To sum up, strength prediction of short fiber reinforced composites having longer fibers than the critical fiber length (i.e. $l_m > l_c$) and having an orientation factor C can be done as [3]:

$$\sigma_C = \eta \cdot C \cdot \varphi_F \cdot \left[1 - d_F \cdot \left(\frac{\sigma_F}{2 \cdot l_m \cdot \sigma_M^*}\right)\right] + (1 - \varphi_F) \cdot \sigma_M^* \quad (2.10)$$

Where C = 1 for aligned fibers, C = 0.2 for irregular fibers and C = 0.375 for planar isotropic fibers [37].

CHAPTER 3

EXPERIMENTAL PROCEDURE

The experimental procedure consists of composite fabrication which involves the infiltration by the squeeze casting. Characterization part includes density measurement followed by mechanical tests and microscopy. The steps of the experimental procedure are shown schematically in the Figure3.1.

3.1 Matrix Alloy Preparation

Matrix alloys used in the experiments were two different aluminum-silicon alloys, of which silicon concentrations were 7 wt% and 10 wt%. Silicon affects the solubility range of the matrix alloys. In Table 3.1, actual compositions of the matrix alloys used in the experiments are given according to the wt% of constituent elements.

Table 3.1 Chemical composition of alloys used in the experiments

Alloy	Si	Mg	Fe	Ti	Sr	Cu	Al	Other
Al-7wt%Si (AlSi7Mg0.8)	6.9	0.85	0.195	0.21	0.014	0.004	91.8	0.001
Al-10wt%Si (AlSi10Mg0.8)	10.4	0.81	0.178	0.15	0.012	0.003	88.4	0.001

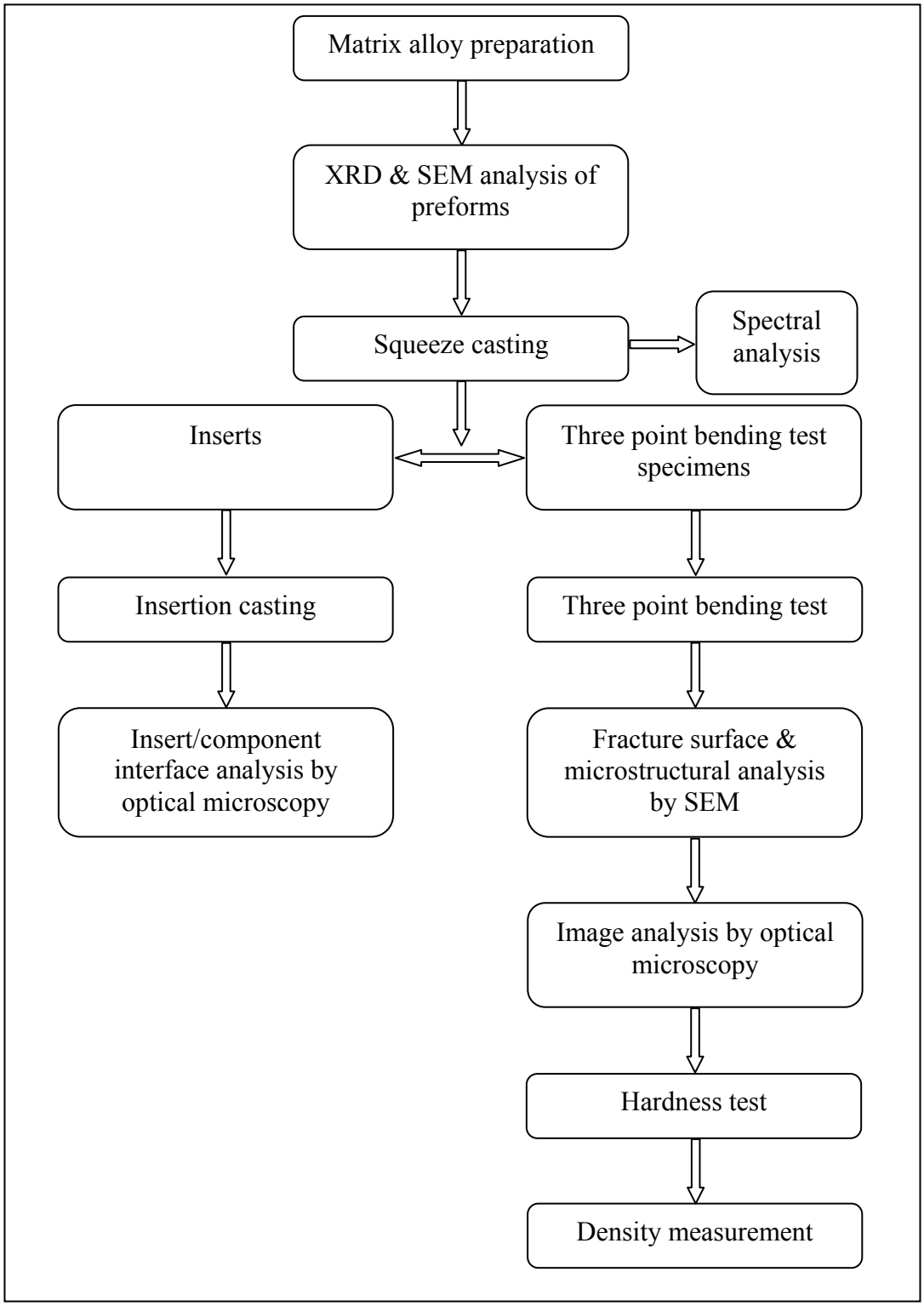

Figure 3.1 Flow chart of the experimental procedure

Spectrometer analyses of the alloys used during the experiments are given in Appendix A.

The matrix alloys were composed of pure aluminum, pure silicon, aluminum-titanium-boron master alloy (AlTi5B) and aluminum-strontium master alloy (AlSr10). In the Table 3.2, Table 3.3 and Table 3.4, average chemical compositions of the constituents (in wt%) of the matrix alloys are given.

Table 3.2 Chemical composition of pure aluminum used in the experiments

Si	Mg	Fe	Ti	Sr	Cu	Al	Other
0.12	<0.0010	0.20	0.002	<0.0001	0.008	99.6	0.001

Table 3.3 Chemical composition of AlTi5B master alloy

Ti	B	Al
5.0	1.0	94.0

Table 3.4 Chemical composition of AlSr10 master alloy

Sr	Al
10.0	90.0

Matrix alloys were prepared by the Ajax Magnethermic 59 kW induction furnace. Firstly, pure aluminum was melted. Then pure silicon was added into the melt. At this point, the melt is solidified. Rests of the constituents were added into the alloy prior to the composite fabrication. Pure magnesium and AlTi5B and AlSr10 master alloys were added into the melt to control the chemical composition.

3.2 XRD and SEM Analysis of Preforms

Preforms used in the experiments were purchased from Thermal Ceramics Co. Preforms used in the experiments belong to the family of Fibralloy Preforms. Fibrally preforms are two types. Composite grade preforms are Saffil^{TM} RF grade fibers. Fibers having volume percentages of 20, 25 and 30 vol%'s were purchased from thermal ceramics. In Table 3.5 and Table 3.6, chemical composition (in wt%) and properties of Saffil RF grade fibers are given.

Table 3.5 Chemical composition of Saffil RF grade fibers [24]

Al_2O_3	SiO_2	Other Oxides
96-97	3-4	Trace

Table 3.6 Properties of Saffil RF grade fibers [24]

Elastic Modulus (GPa)	270-330
Ultimate Tensile Strength (MPa)	2000
Average Fiber Diameter (μm)	3.0-3.5
Density (g/cm^3)	3.3
Mohs Hardness	7.0
Maximum Service Temperature	1600

Fibers of the preform consist of polycrystalline δ-Al_2O_3 phase having an average grain size of 50 nm. Presence of 3-4 wt% SiO_2 stabilizes the δ-Al_2O_3 phase and hinders grain coarsening at high temperatures [24].

The reason why fibers having volume percentages of 20, 25 and 30 had been purchased was due to the critical fiber content needed to have an effective strengthening for these types of Al-Si alloys. It was seen that fibers having fiber content above at least 16 vol percents are needed to have an efficient strengthening

in AlSi10MgX ($0.3 \leq X \leq 1.0$) type alloys [31]. Since manufacturer of the preforms had preforms having volume percentages of 10, 15, 20, 25 and 30; 20, 25 and 30 vol% preforms purchased.

The fibers should have planar isotropy, in which fiber orientation is perpendicular to the flow direction according to Darcy's Law. Note that equation (2.3) necessitates a pressure drop of molten metal due to infiltrating the ceramic preform. For the minimum pressure drop, contact between fibers and the molten metal must be as short as possible [30]. In the case of parallel conditions of molten metal and the fibers, molten metal contacts with the fiber along the fiber length. However, in the case of vertical condition of the molten metal and the fibers, molten metal contacts with the fibers along the half of the circumference of the fibers. Technical data shows that Saffil fibers have mean diameters of 3 μm and average lengths of 150 μm. Using the technical information, parallel conditions of the fibers necessitates a 150 μm molten metal/fiber contact and vertical conditions of the fibers necessitates a 4.71 μm molten metal/fiber contact. Details of Darcy Law (assume liquid metal is an incompressible fluid and metal flow in the preform is laminar) is given below [38]:

$$U = \frac{k \cdot \rho}{n \cdot \mu} \cdot \frac{\Delta P}{X} \tag{3.1}$$

Where U is the penetrating velocity of the molten metal, ΔP is the pressure drop due to molten metal/fiber contact, X is the infiltration depth, k is the permeability of the of the preform, n is the porosity of the preform, ρ is the density of the molten metal and μ is the viscosity of the liquid metal.

It is seen in equation (3.1) that for the complete infiltration of the same preforms with the same molten metal, all parameters except ΔP values are the same. Since pressure drop, i.e. ΔP, is related to the fiber/molten metal contact; perpendicular

condition of the fibers and the molten metal stands for the highest infiltration ability.

XRD analyses of the preforms were performed by Rigaku X-Ray Diffractometer Model: D/MAX2200/PC at 2°/min continuous scan speed to determine the chemical composition of the preforms.

SEM analyses of the preforms were performed by JEOL JSM-6400 Scanning Microscope to determine the fiber orientation of the preforms. Au coating was employed to the specimens to determine the fiber characteristics of the preforms due to their dielectric characteristics. Therefore Au peaks were seen in EDS analysis.

3.3 Squeeze Casting

Production steps of Saffil alumina fiber reinforced composites are as in the following:

1. Pure aluminum was melted and pure silicon was added into the molten aluminum.
2. The molten alloy was solidified
3. Saffil RF grade fibers were heated in steel molds up to 200 °C.
4. Pure magnesium, AlTi5B and AlSr10 master alloys were added into the pre-melted aluminum-silicon alloy.
5. Squeeze casting mold was heated to 190 °C.
6. Preforms in the steel molds were placed into the squeeze casting mold.
7. The molten alloy was poured into the mold at 800 °C and 750 °C.
8. Squeeze casting of the composite specimens was conducted.
9. Obtained aluminum covered steel preform molds were taken from the squeeze casting mold.

10. Steel preform molds covered by aluminum alloy was removed by the milling cutter machine.
11. Composite specimens (both bending test specimens and inserts) were taken from the steel mold by the 70 tons capacity vertical press.
12. The resultant bending specimens and inserts were grinded and polished.
13. Just before the insertion casting operation, inserts were grinded.
14. Insertion casting operation was done by locating the inserts into the die cavity of the squeeze casting mold.

During the experiments, the steel molds used in the infiltration of the Saffil fibers by the molten metal are given in Figure 3.2 and Figure 3.3.

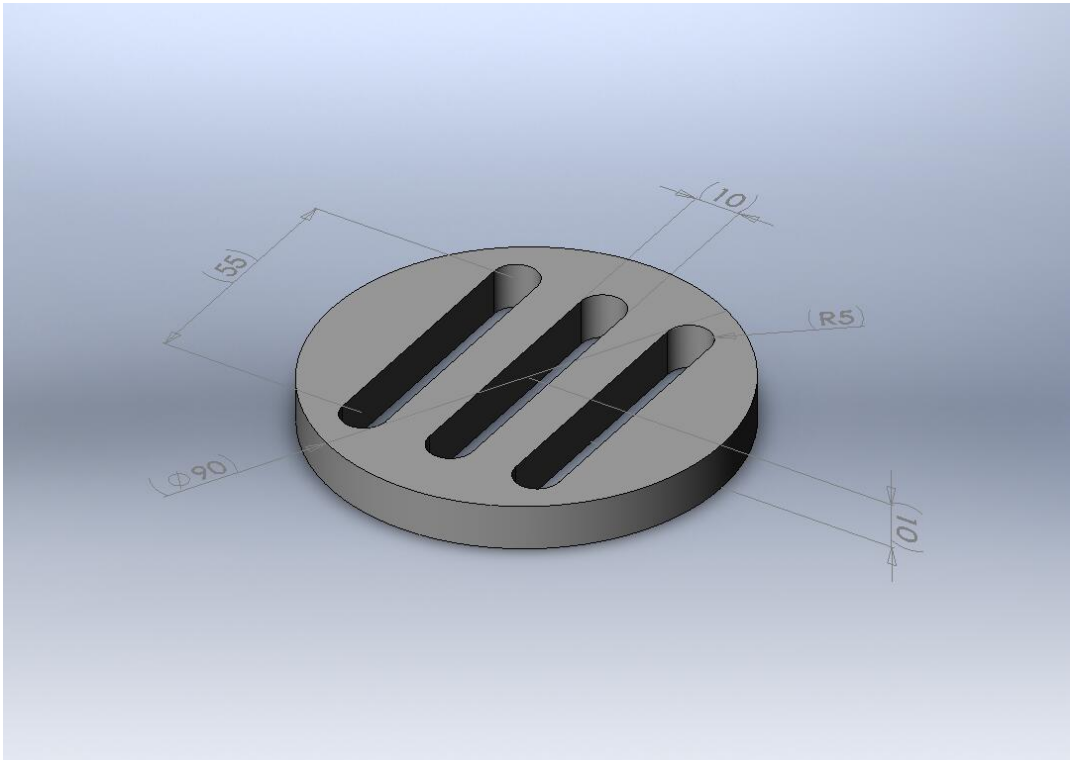

Figure 3.2 The steel mold used to produce three point bending test specimens

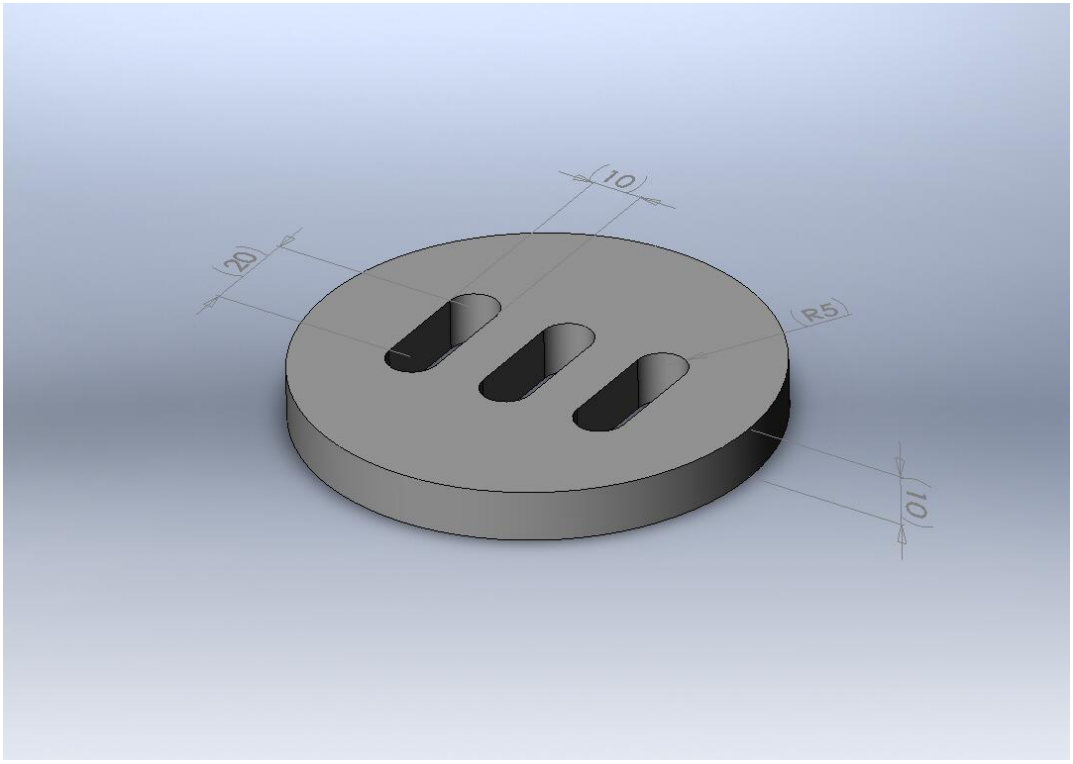

Figure 3.3 The steel mold used to infiltrate the inserts

Details of the squeeze casting operation are given in Appendix B.

In Figure 3.4 and Figure 3.5, details of the insertion casting molds can be seen.

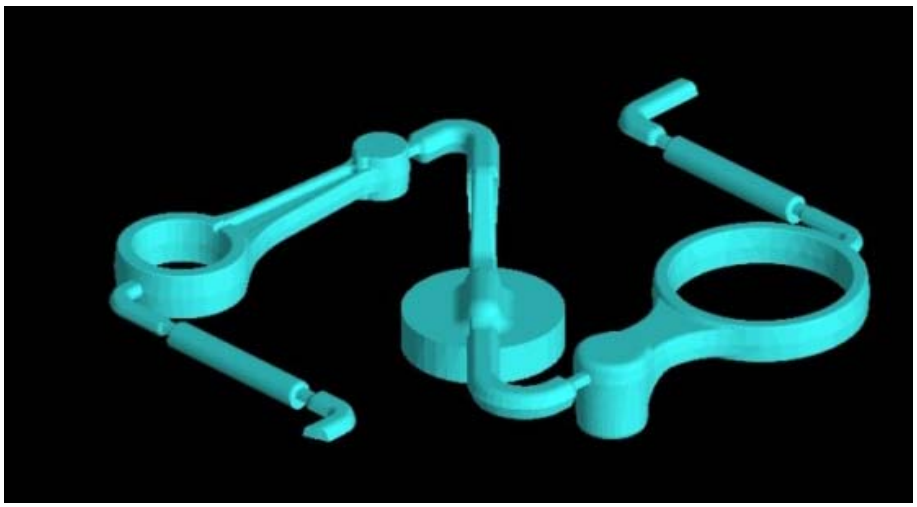

Figure 3.4 Details of the insertion casting mold 1

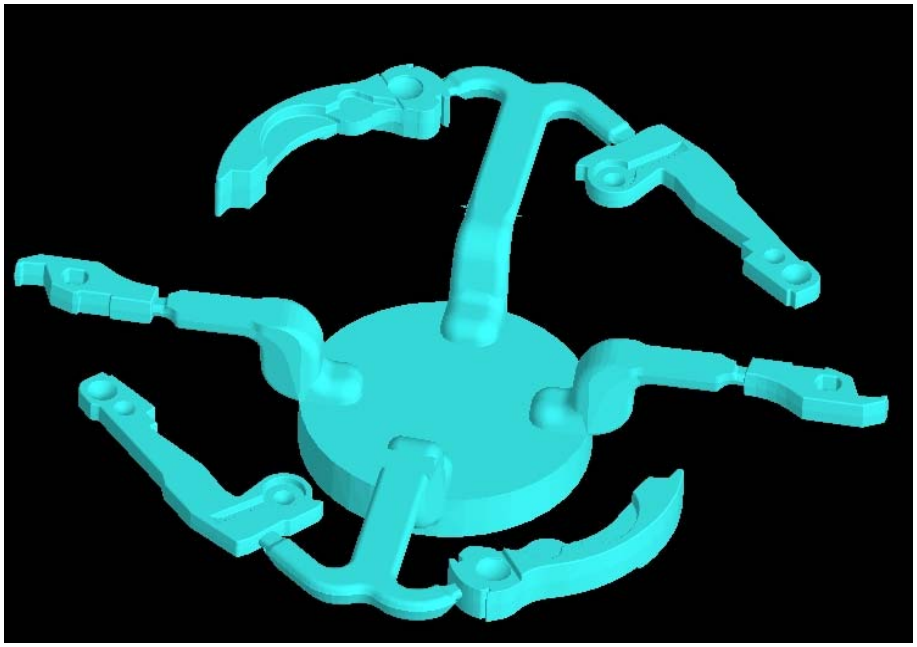

Figure 3.5 Details of the insertion casting mold 2

3.4 Mechanical Tests and Test Apparatus

Three point bending tests were performed by Shimadzu AGS-J (10 kN) test machine. Details of the specimen numbers were given in Table 3.7.

Table 3.7 Arrangement of specimens used in the experiments

Alloy	Volume Percents of Fibers						Infiltration Temperatures
	20 vol%	25 vol%	30 vol%	20 vol%	25 vol%	30 vol%	
AlSi7Mg0.8	3	3	3	3	3	3	750 °C
	3	3	3	3	3	3	800 °C
AlSi10Mg0.8	3	3	3	3	3	3	750 °C
	3	3	3	3	3	3	800 °C

Three point bending tests were carried out at a bending speed of 3 mm/min in Shimadzu AGS-J (10 kN) Test Machine.

Hardness tests were carried out Heckert Analog Hardness Test Machine where Brinell 62.5 kg hardness values acquired. Hardness measurement was performed both from the surfaces parallel to the fiber orientation and vertical to the fiber orientation.

The maximum fracture loads of the three-point bending test were obtained. Calculations of the three point bending tests were carried out by the following formula.

$$\sigma_{max} = \frac{3 \cdot F \cdot L}{2 \cdot b \cdot d^2} \tag{3.2}$$

Where F is the maximum load applied by the test machine, L is the span length of the specimen, b is the thickness and d is the width of the specimen. In the experiments, L, b and d values are approximately 48, 10 and 5 mm respectively.

3.5 Microscopy and Microstructural Analysis

In the experiments, composite specimens were examined by SEM and optical microscopy to determine their fracture surface, microstructure, fiber orientation characteristics. Details of these examinations are given in the following.

3.5.1 Sample Preparation

Samples for fracture surface examination were obtained from the fracture surfaces of three point bending test specimens. Fracture surfaces were cut from the bending test specimens by METKON METACUT M250 Cutting Machine and then purged from impurities by Retsch UR1 Ultrasonic Cleaner. Finally examination was performed by JEOL JSM-6400 Scanning Microscope.

Samples of image analysis and SEM study were prepared from the edges of the three point bending test specimens. Specimens were cut both from the surfaces parallel to the fiber orientation and vertical to the fiber orientation by METACUT M250 Cutting Machine. Obtained specimens were mounted in Bakelite resin by automatic Bakelite mounting machine of METKON HYDROPRESS 50. Mounted specimens were placed in a six-specimen sample holder of an automatic specimen mover of METKON FORCIMAT Specimen Mover. Grinding and polishing operations were performed by grinding and polishing machine of METKON FORCIPOL 2V. Grinding operation carried out from 180 grip SiC paper to 1000 grid SiC paper. Polishing operation performed using 1 μm and 0.3 μm Al_2O_3 suspension on a soft polishing coat. Finally specimens were purged from impurities by ultrasonic cleaning machine to remove any debris.

3.5.2 Scanning Electron Microscopy Analysis

Scanning electron microscopy analyses were carried out by JEOL JSM-6400 Scanning Microscope. Fracture surface examination and microstructural examination together with back scattered images were performed by this microscope. For SEM analysis, electrical conduction was established by applying Ag-paste to the specimens mounted in dielectric Bakelite resin.

3.5.3 Optical Microscopy Analysis

Optical microscopy analyses were carried out by SOIF XJF-6A optical microscopy to determine the microstructural characterization of the composites. Image analysis was performed by this optical microscope. Same specimens with SEM analysis were used in the image analysis of the composites.

3.6 Density Measurement

Density measurements of the composite specimens were done according to the Archimedes' Principle. Steps of the density measurement are as follows:

1. Weight of the specimen was measured in air with a sensitivity of 10^{-4} g under normal atmosphere.
2. Composite specimen was dipped into xylol (xylene) solution and weight of the specimen was measured in xylene.
3. The weights of the composited were measured with a sensitivity of 10^{-4} g.
4. The volume of the composite was calculated by the weight difference of the specimen hanging up in a cup of xylol and in air and dividing it to the density of xylol (0.861 g/cm^3).
5. The density of the composite was calculated by dividing the term weight of the specimen in air by the volume of the composite.

$$V_{specimen} = \frac{m_{specimen,air} - m_{specimen,xylene}}{\rho_{xylene}} \quad (3.3)$$

Where $m_{speciemen,air}$ is the weight of the specimen in air, $m_{specimen,xylene}$ is the weight of the specimen in xylene and ρ_{xylene} is the density of xylene (0.861 g/cm^3).

To have a comparison, theoretical densities were calculated by the rule of mixtures as shown below [1, 4]:

$$\rho_c = \rho_m \times (1 - V_f) + \rho_f \times V_f \quad (3.4)$$

Where ρ_c is the theoretical density of the composite, ρ_m is the density of the matrix metal, ρ_f is the density of the reinforcement phase (in this case fiber) and V_f is the fiber volume fraction of the composite.

CHAPTER 4

RESULTS AND DISCUSSION

In this study, the effects of alumina fiber addition and casting temperatures of the two different liquid alloys on the mechanical behavior of two different aluminum matrix composites were examined.

4.1 Microscopy and Microstructural Analysis

Microscopy and microstructural analysis contains the experimental results of scanning electron microscopy and optical microscopy. Results were grouped as:

1. Scanning Electron Microscopy results
    a. Saffil fibers' fiber orientation
    b. Fracture surface examination of composites
    c. Detailed microstructure analyses (back scattered images) of composites
2. Optical microscopy results (Image analyses of composites)

Details of the parameters state above are given in the following subtitles.

4.1.1 Scanning Electron Microscopy Results

Saffil fibers' orientation, fracture surfaces of the composites and detailed microstructure analyses of the composites were performed by the scanning electron

microscopy. Saffil fibers' SEM examination was performed to verify the technical data of the preforms to obtain the suitable fiber orientation for the composites. Fracture surface examination was performed to observe the fiber behavior after the fracture of the composite. Detailed microstructure analyses were performed to determine the phases exist in the composite product together with the distribution of the phases. To have the best contrast, back scattered images were also obtained.

In the figures Figure 4.1 through Figure 4.6, distribution of the Saffil fibers can be seen.

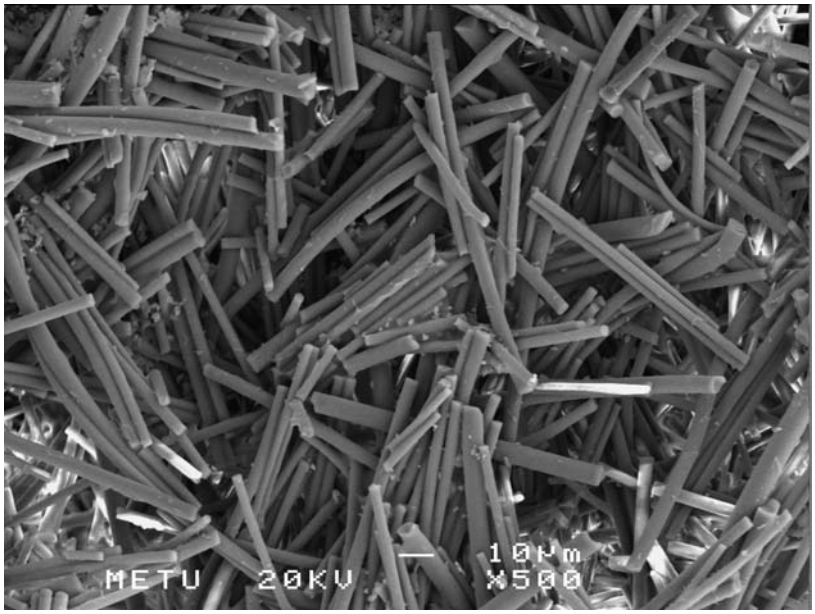

Figure 4.1 SEM image of 20 vol% Saffil fibers parallel to the fiber orientation

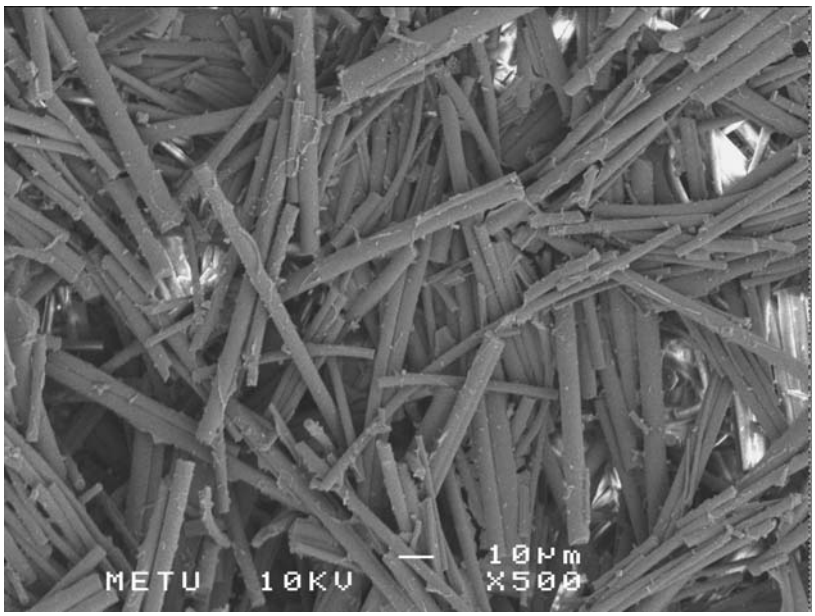

Figure 4.2 SEM image of 25 vol% Saffil fibers parallel to the fiber orientation

Figure 4.3 SEM image of 30 vol% Saffil fibers parallel to the fiber orientation

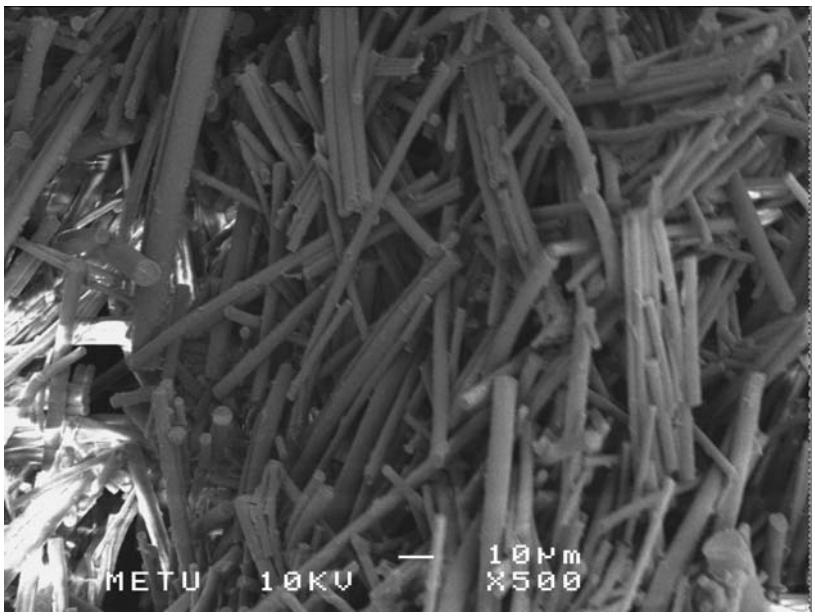

Figure 4.4 SEM image of 20 vol% Saffil fibers vertical to the fiber orientation

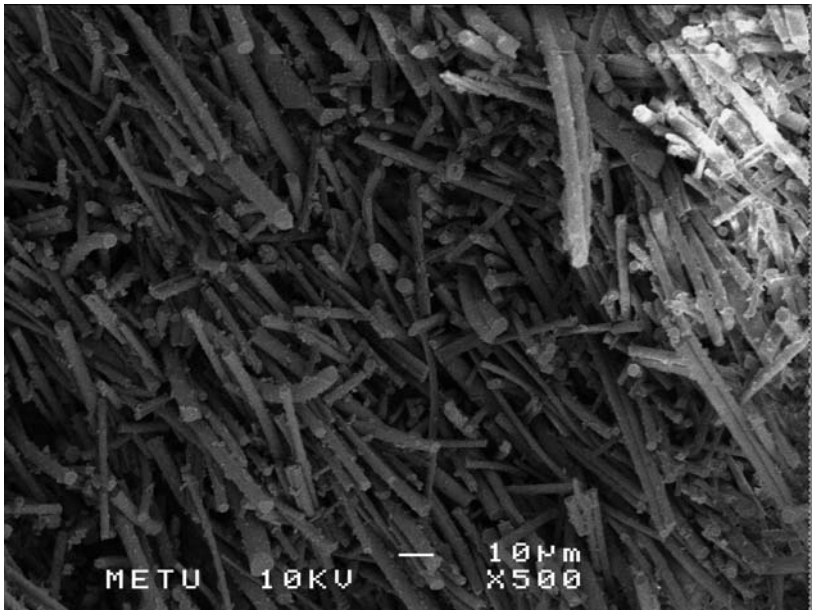

Figure 4.5 SEM image of 25 vol% Saffil fibers vertical to the fiber orientation

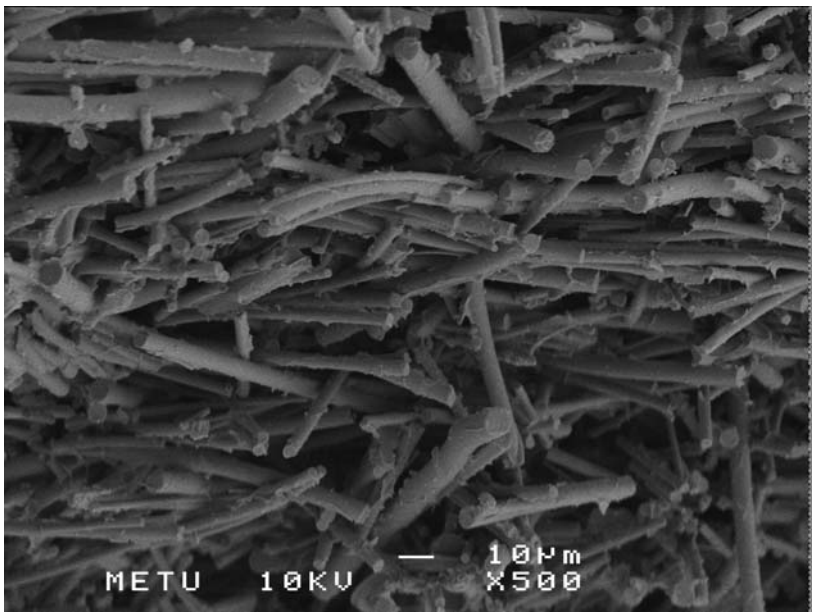

Figure 4.6 SEM image of 30 vol% Saffil fibers vertical to the fiber orientation

SEM analyses of the Saffil fibers showed that preforms have fibers distributed in a planar isotropic condition due to their production technique. Isotropic condition of the fibers was stated as at least 70% planar isotropy. SEM analyses of the preforms also showed that there exist fibers having diameters of >3μm and lengths of <150 μm.

In the case of fracture surface examination, for two different matrix alloys mainly AlSi7Mg0.8 and AlSi10Mg0.8 for two different infiltration temperatures of 750 °C and 800 °C at three different volume percentages of the reinforcement phases were examined. Figure 4.7 through Figure 4.22 show the fracture surface characteristics of the composites.

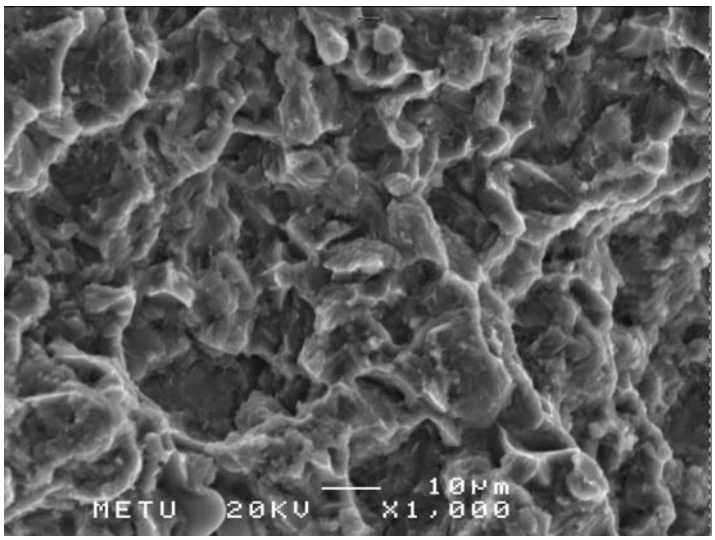

Figure 4.7 Fracture surface of AlSi7Mg0.8 alloy squeeze cast at 750 °C

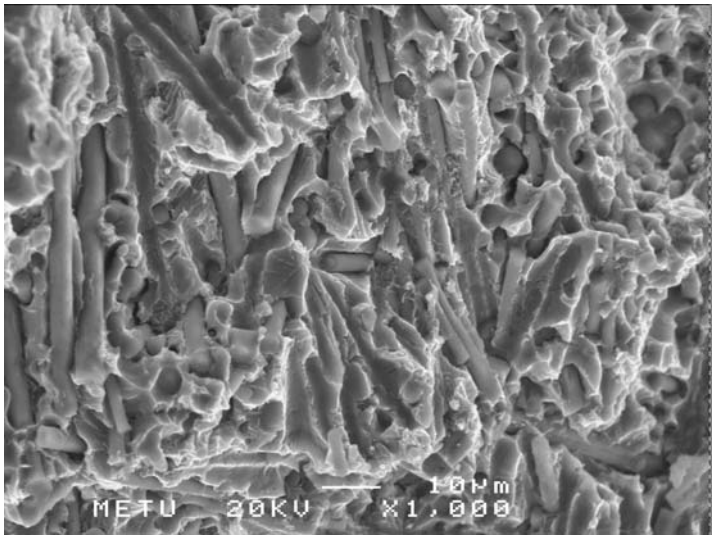

Figure 4.8 Fracture surface of AlSi7Mg0.8/20vol%Al_2O_3 reinforced composite squeeze cast at 750 °C

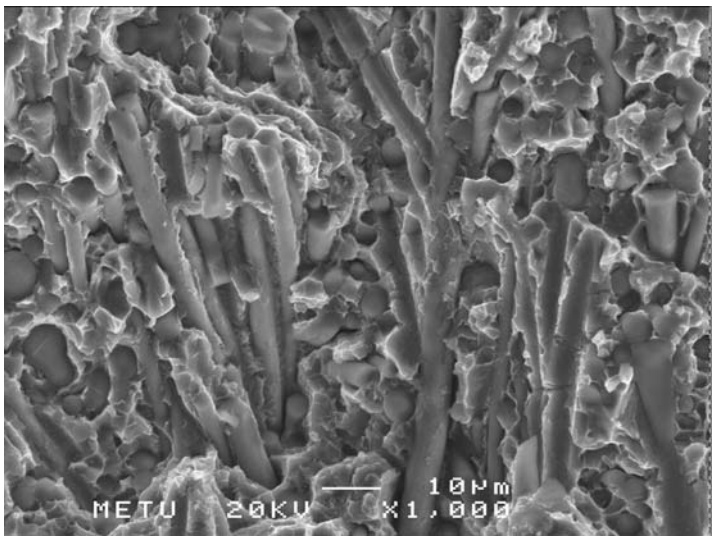

Figure 4.9 Fracture surface of AlSi7Mg0.8/25vol%Al_2O_3 reinforced composite squeeze cast at 750 °C

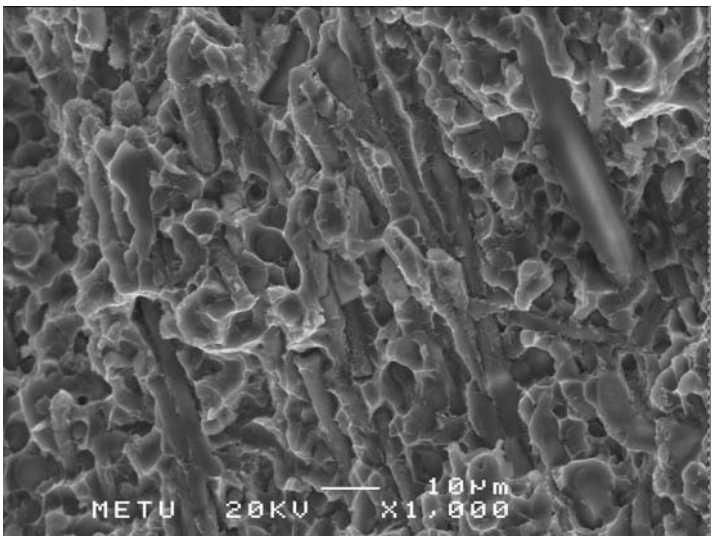

Figure 4.10 Fracture surface of AlSi7Mg0.8/30vol%Al_2O_3 reinforced composite squeeze cast at 750 °C

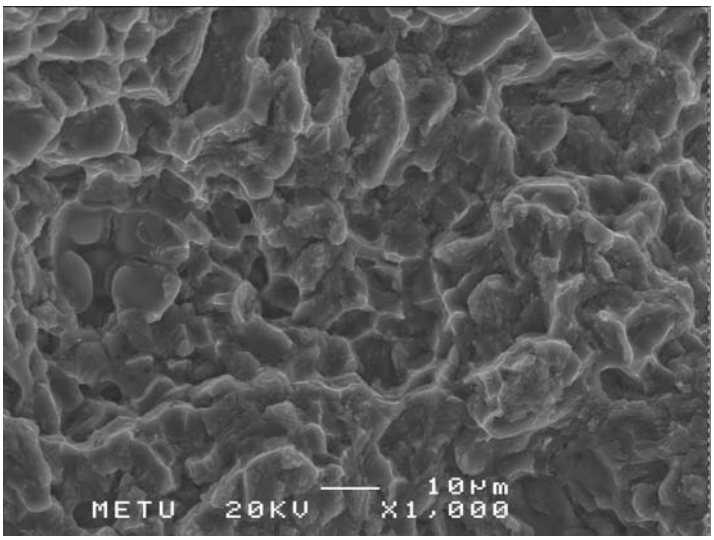

Figure 4.11 Fracture surface of AlSi7Mg0.8 alloy squeeze cast at 800 °C

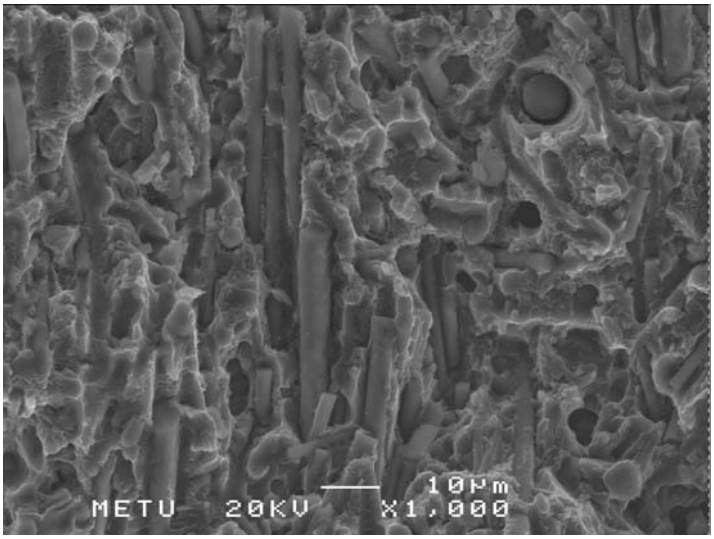

Figure 4.12 Fracture surface of AlSi7Mg0.8/20vol%Al_2O_3 reinforced composite squeeze cast at 800 °C

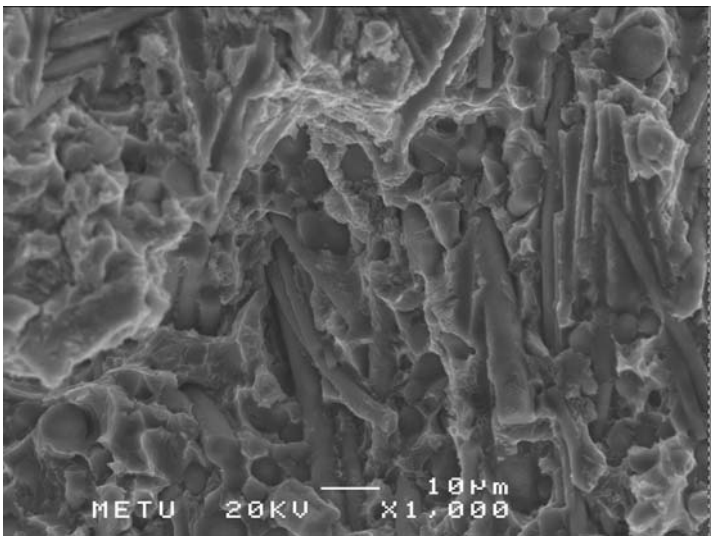

Figure 4.13 Fracture surface of AlSi7Mg0.8/25vol%Al_2O_3 reinforced composite squeeze cast at 800 °C

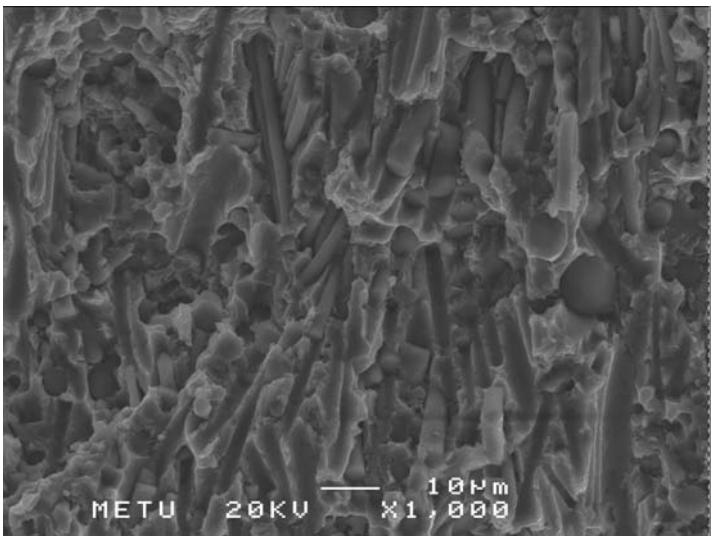

Figure 4.14 Fracture surface of AlSi7Mg0.8/30vol%Al_2O_3 reinforced composite squeeze cast at 800 °C

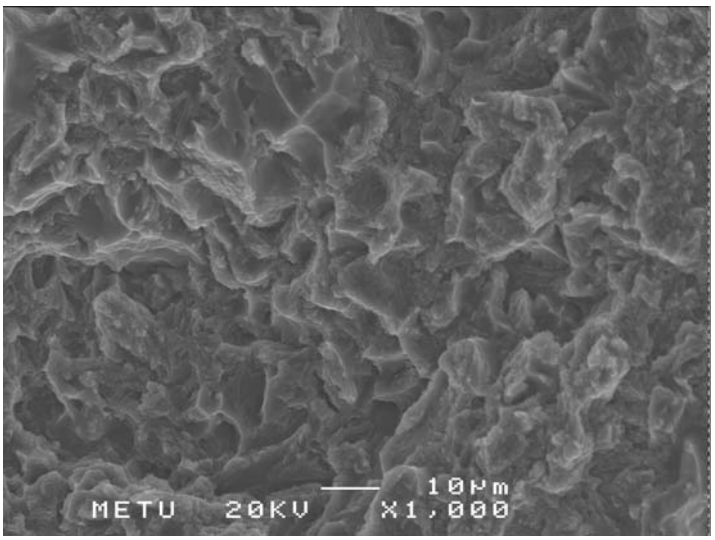

Figure 4.15 Fracture surface of AlSi10Mg0.8 alloy squeeze cast at 750 °C

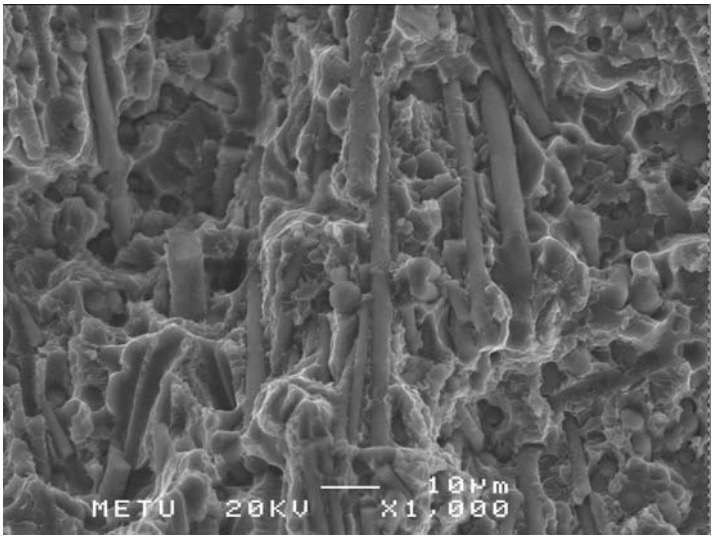

Figure 4.16 Fracture surface of AlSi10Mg0.8/20vol%Al_2O_3 reinforced composite squeeze cast at 750 °C

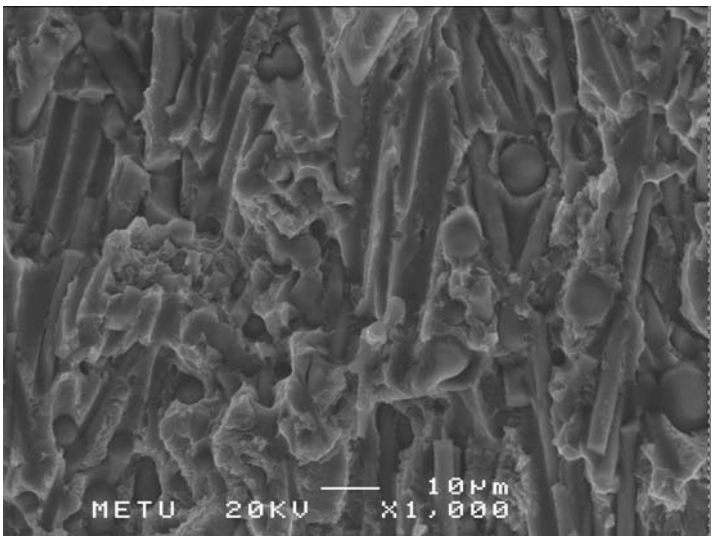

Figure 4.17 Fracture surface of AlSi10Mg0.8/25vol%Al_2O_3 reinforced composite squeeze cast at 750 °C

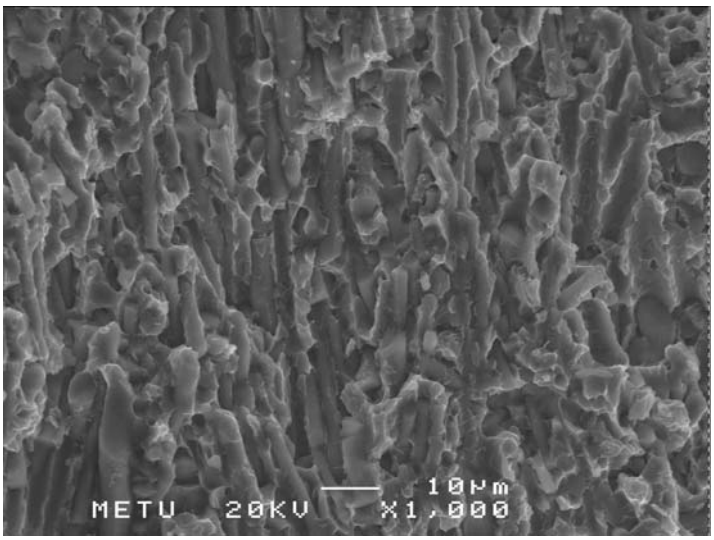

Figure 4.18 Fracture surface of AlSi10Mg0.8/30vol%Al_2O_3 reinforced composite squeeze cast at 750 °C

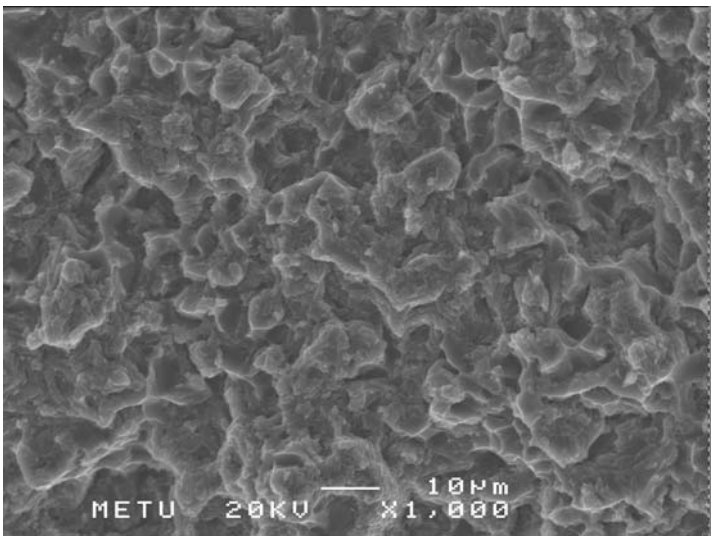

Figure 4.19 Fracture surface of AlSi10Mg0.8 alloy squeeze cast at 800 °C

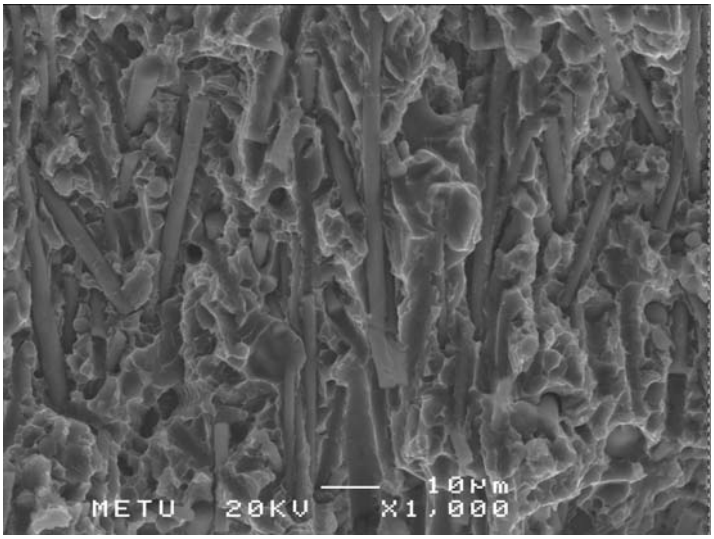

Figure 4.20 Fracture surface of AlSi10Mg0.8/20vol%Al_2O_3 reinforced composite squeeze cast at 800 °C

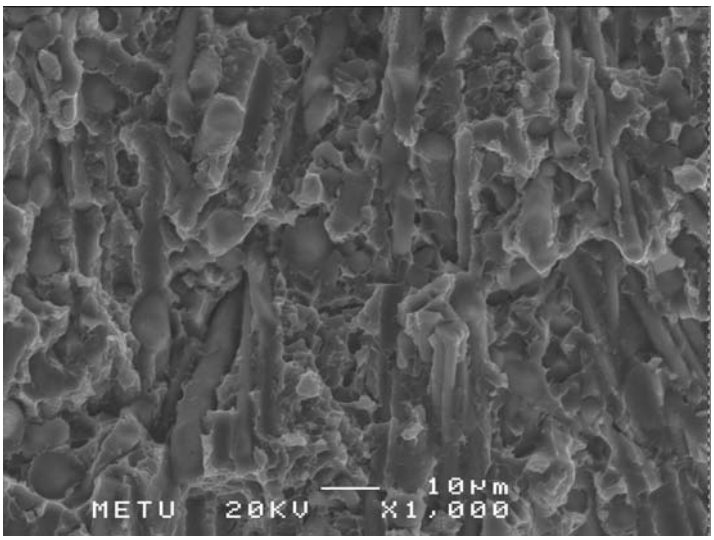

Figure 4.21 Fracture surface of AlSi10Mg0.8/25vol%Al_2O_3 reinforced composite squeeze cast at 800 °C

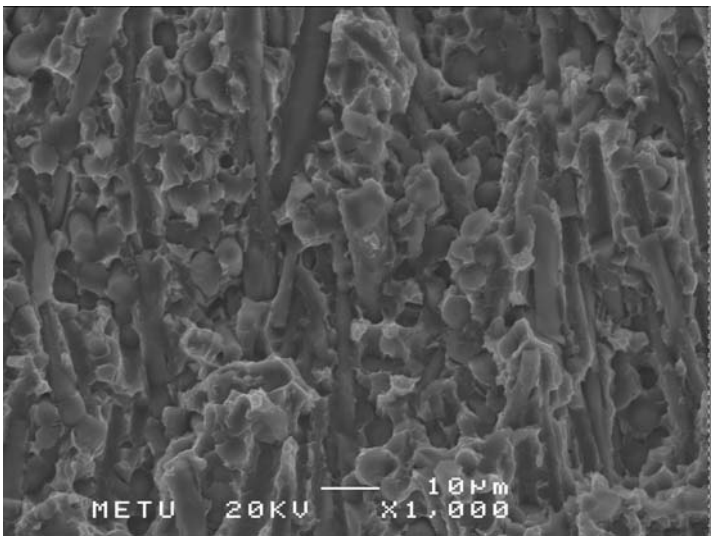

Figure 4.22 Fracture surface of AlSi10Mg0.8/25vol%Al_2O_3 reinforced composite squeeze cast at 800 °C

SEM study of fracture surfaces showed that both AlSi7Mg0.8/Al_2O_3 and AlSi10Mg0.8/Al_2O_3 composites revealed broken fibers, pulled-out fibers and de-bonded fibers in the fracture surfaces. Note that the highest energy absorbing mechanism is fiber pull-out mechanism [5].

In detailed fracture surface analyses by SEM, back scattered images of the composites showed the most appropriate fiber/matrix interface and orientation of the fibers in the composite. In figures from Figure 4.23 through Figure 4.76, except the 0 vol% composites i.e. matrix alloy, back scattered SEM images of the composites are given. Matrix alloy SEM images at X5000 magnification reveal the fibrous eutectic structure.

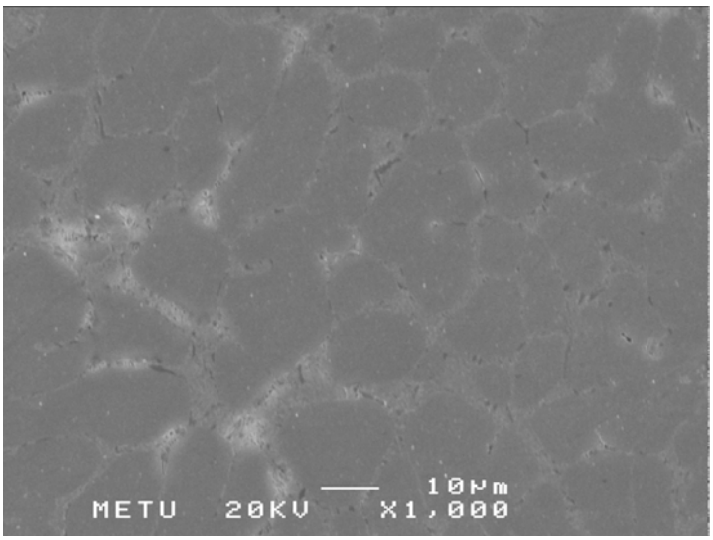

Figure 4.23 SEM image of AlSi7Mg0.8 alloy matrix squeeze cast at 750 °C at X1000 magnification

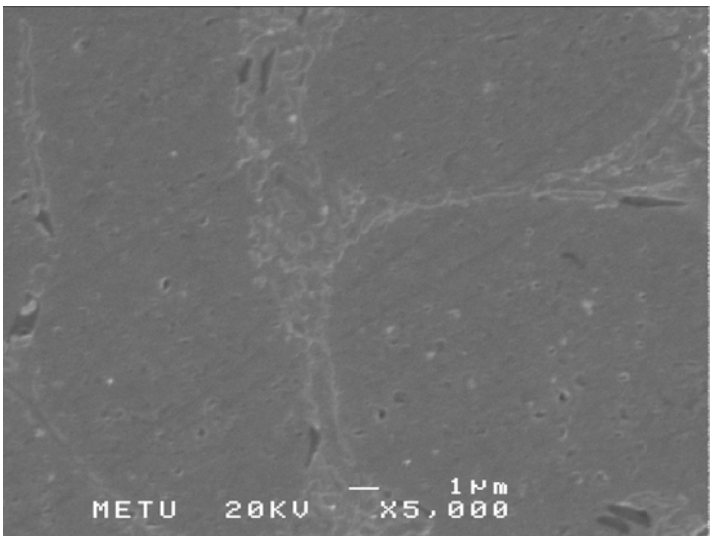

Figure 4.24 SEM image of AlSi7Mg0.8 alloy matrix squeeze cast at 750 °C at X5000 magnification, reveals fibrous eutectic

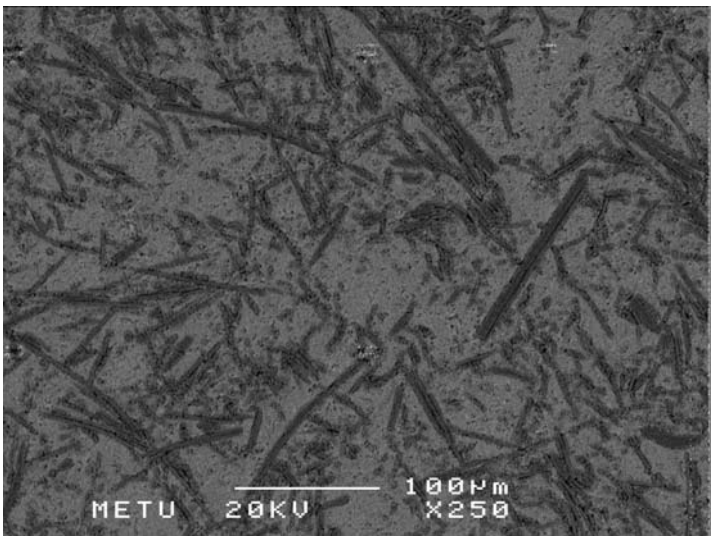

Figure 4.25 Back scattered SEM image of AlSi7Mg0.8/20vol%Al_2O_3 reinforced composite squeeze cast at 750 °C parallel to the fiber orientation at X250 magnification

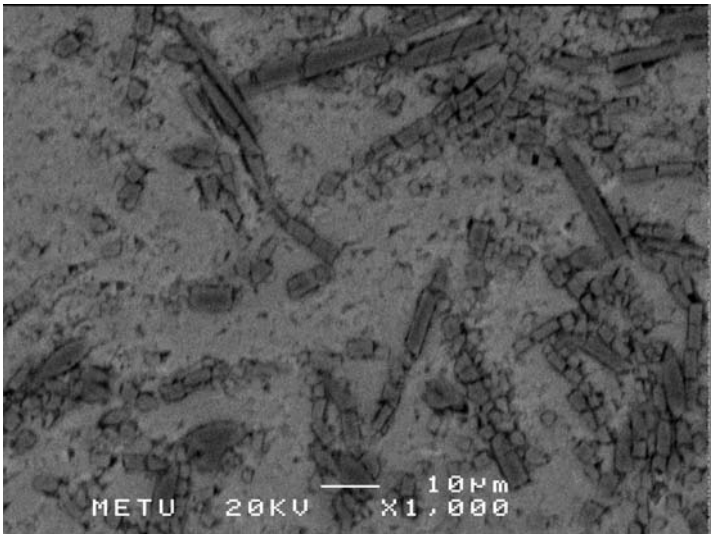

Figure 4.26 Back scattered SEM image of AlSi7Mg0.8/20vol%Al_2O_3 reinforced composite squeeze cast at 750 °C parallel to the fiber orientation at X1000 magnification

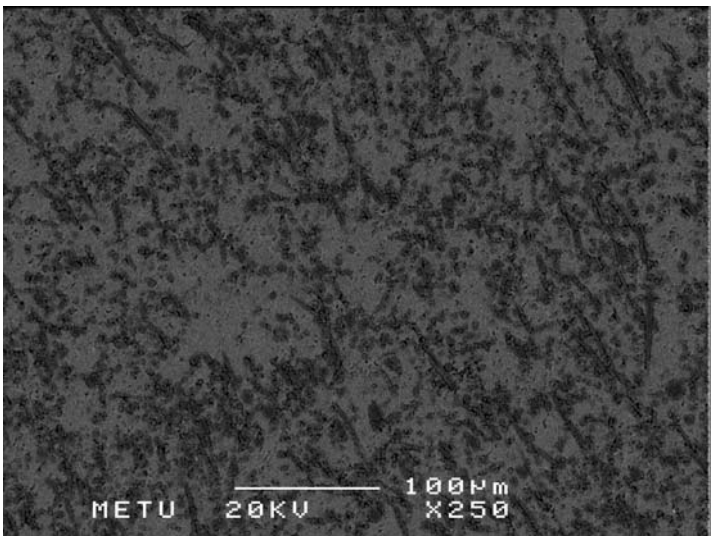

Figure 4.27 Back scattered SEM image of AlSi7Mg0.8/20vol%Al_2O_3 reinforced composite squeeze cast at 750 °C vertical to the fiber orientation at X250 magnification

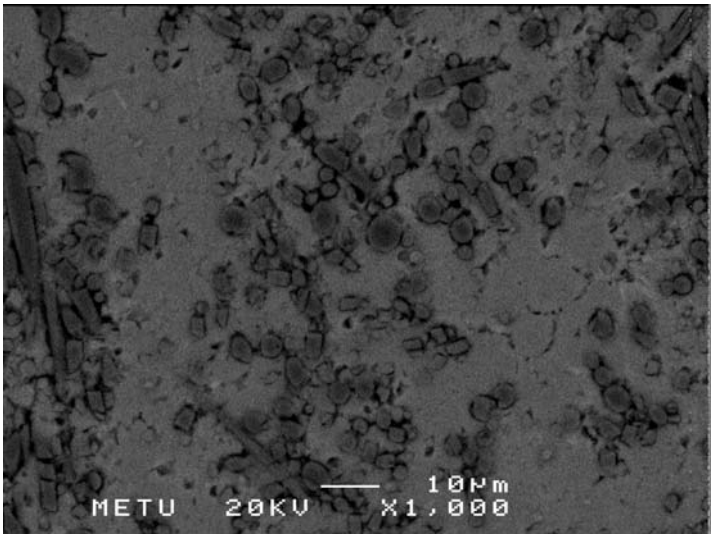

Figure 4.28 Back scattered SEM image of AlSi7Mg0.8/20vol%Al_2O_3 reinforced composite squeeze cast at 750 °C vertical to the fiber orientation at X1000 magnification

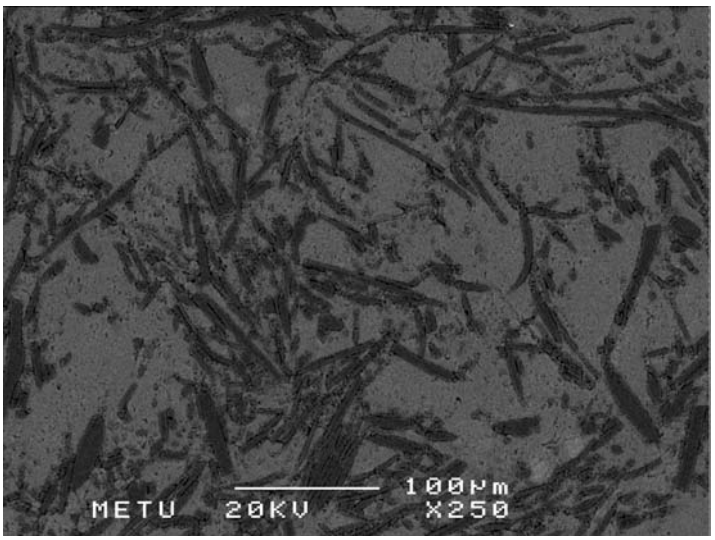

Figure 4.29 Back scattered SEM image of AlSi7Mg0.8/25vol%Al_2O_3 reinforced composite squeeze cast at 750 °C parallel to the fiber orientation at X250 magnification

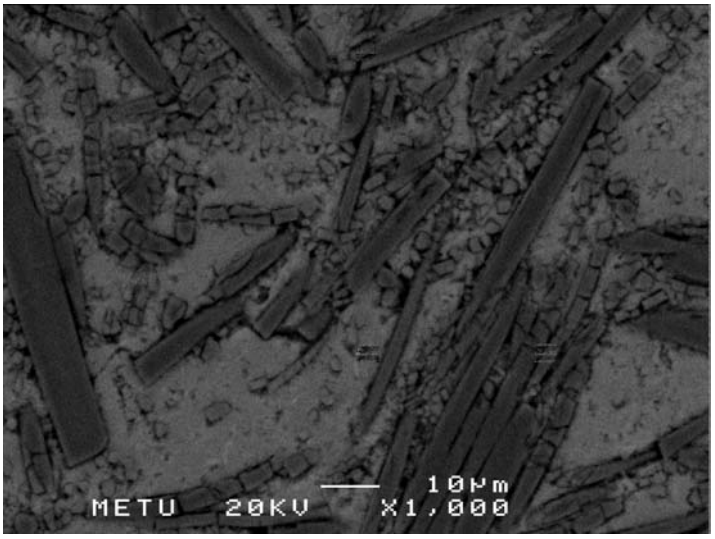

Figure 4.30 Back scattered SEM image of AlSi7Mg0.8/25vol%Al_2O_3 reinforced composite squeeze cast at 750 °C parallel to the fiber orientation at X1000 magnification

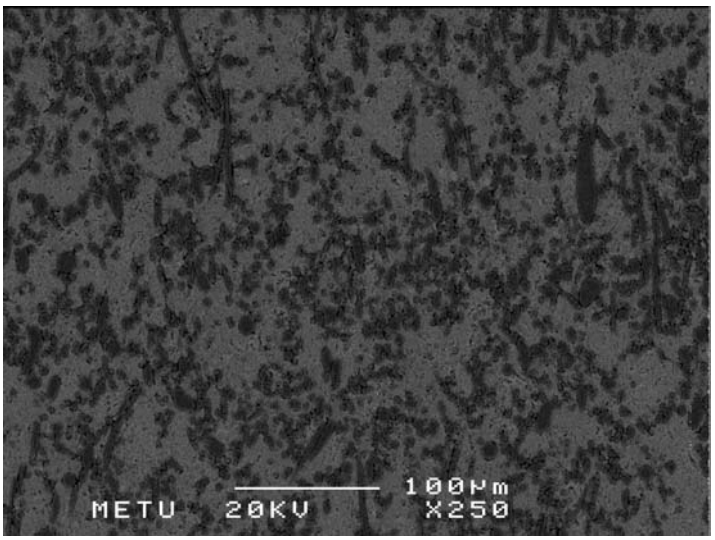

Figure 4.31 Back scattered SEM image of AlSi7Mg0.8/25vol%Al_2O_3 reinforced composite squeeze cast at 750 °C vertical to the fiber orientation at X250 magnification

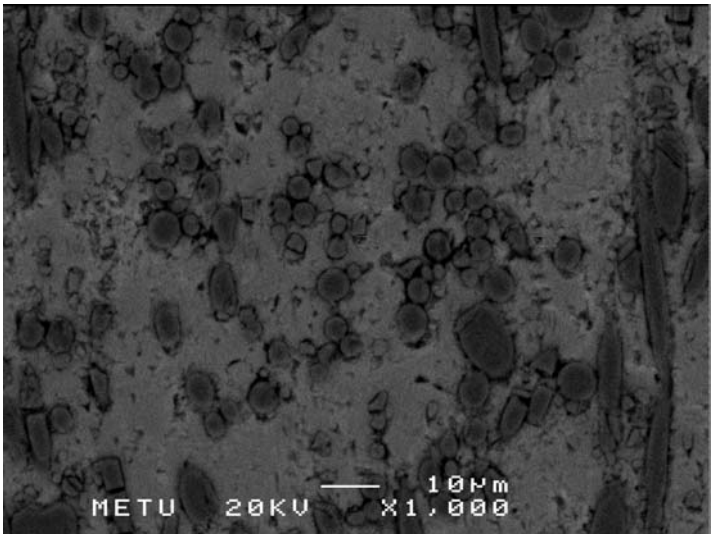

Figure 4.32 Back scattered SEM image of AlSi7Mg0.8/25vol%Al_2O_3 reinforced composite squeeze cast at 750 °C vertical to the fiber orientation at X1000 magnification

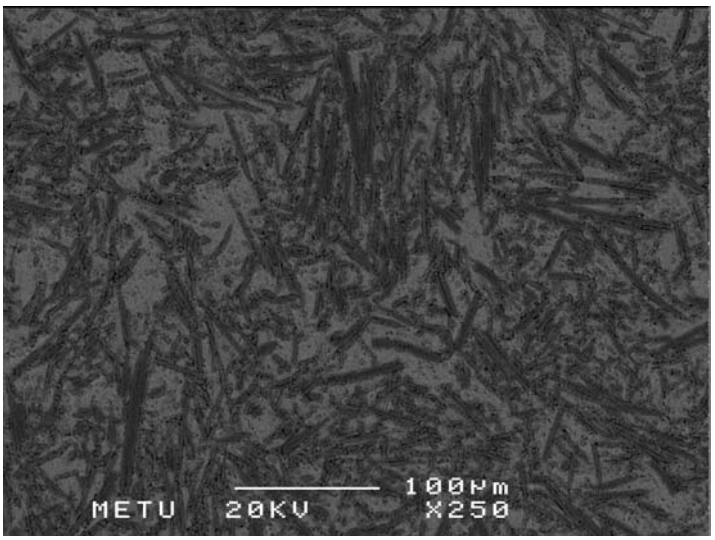

Figure 4.33 Back scattered SEM image of AlSi7Mg0.8/30vol%Al_2O_3 reinforced composite squeeze cast at 750 °C parallel to the fiber orientation at X250 magnification

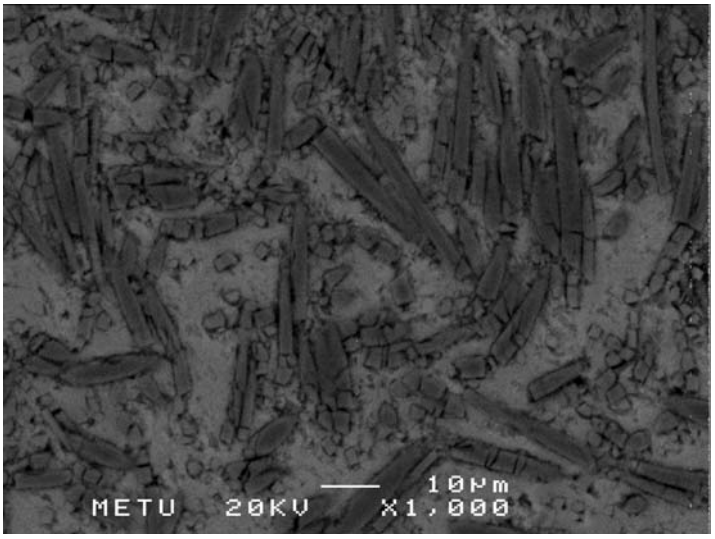

Figure 4.34 Back scattered SEM image of AlSi7Mg0.8/30vol%Al_2O_3 reinforced composite squeeze cast at 750 °C parallel to the fiber orientation at X1000 magnification

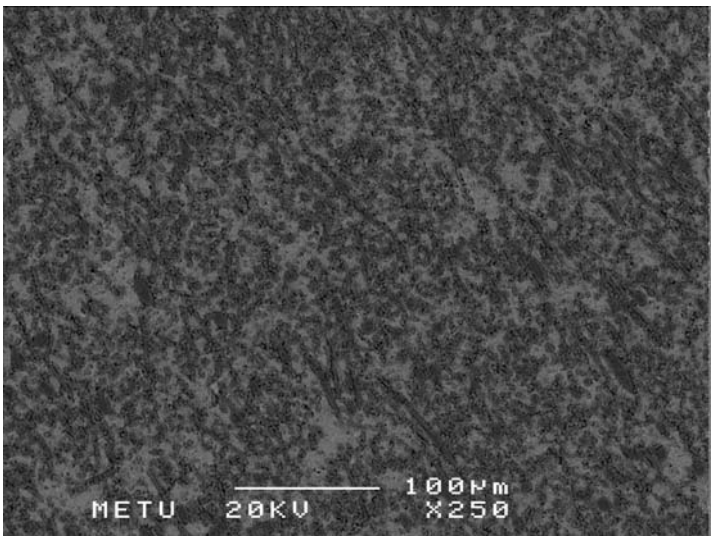

Figure 4.35 Back scattered SEM image of AlSi7Mg0.8/30vol%Al_2O_3 reinforced composite squeeze cast at 750 °C vertical to the fiber orientation at X250 magnification

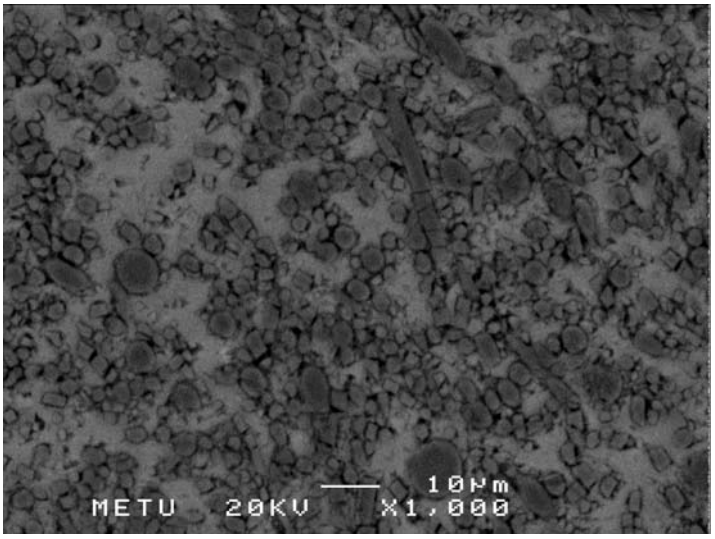

Figure 4.36 Back scattered SEM image of AlSi7Mg0.8/30vol%Al_2O_3 reinforced composite squeeze cast at 750 °C vertical to the fiber orientation at X1000 magnification

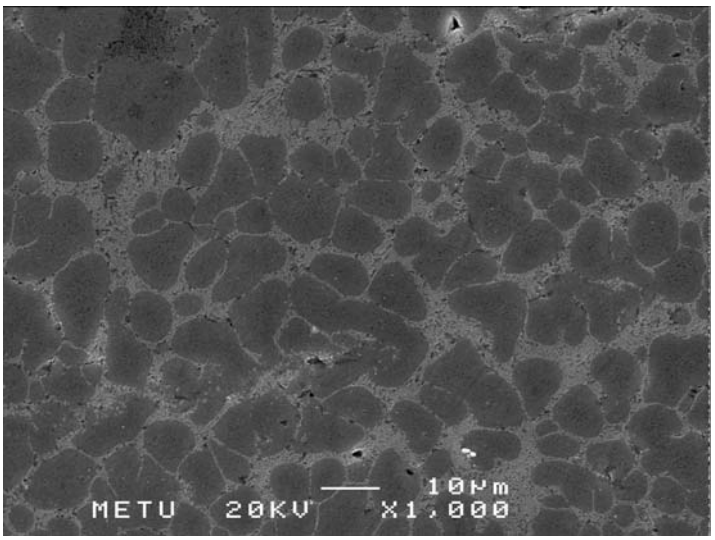

Figure 4.37 SEM image of AlSi7Mg0.8 alloy matrix squeeze cast at 800 °C at X1000 magnification

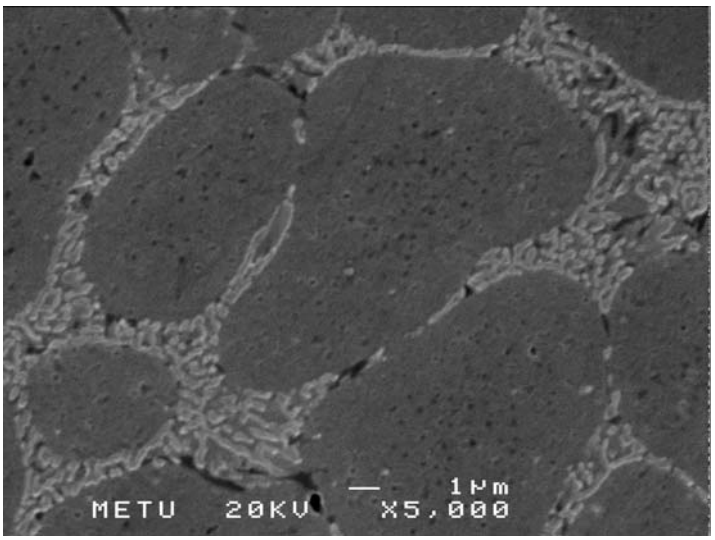

Figure 4.38 SEM image of AlSi7Mg0.8 alloy matrix squeeze cast at 800 °C at X5000 magnification, reveals fibrous eutectic

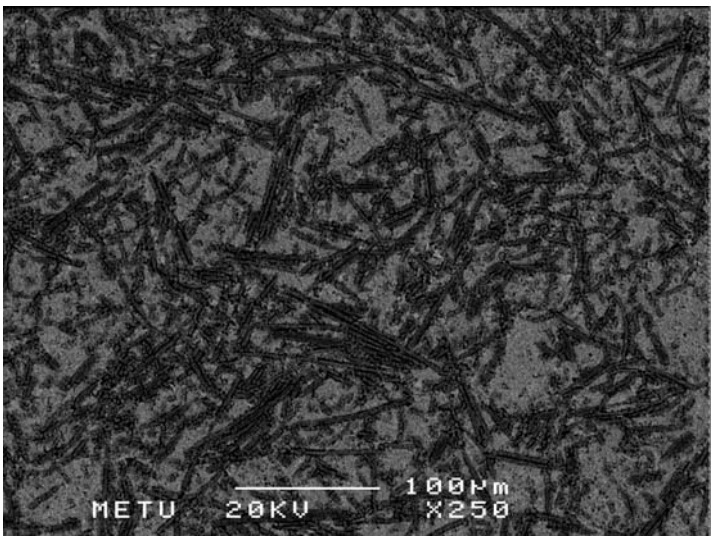

Figure 4.39 Back scattered SEM image of AlSi7Mg0.8/20vol%Al_2O_3 reinforced composite squeeze cast at 800 °C parallel to the fiber orientation at X250 magnification

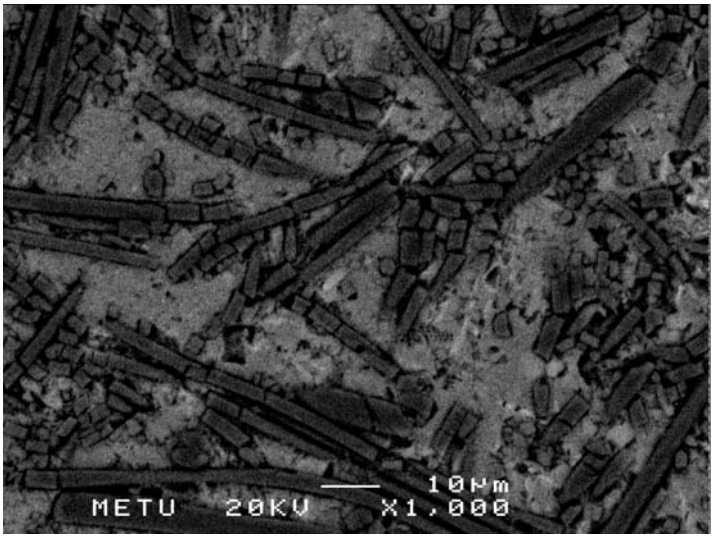

Figure 4.40 Back scattered SEM image of AlSi7Mg0.8/20vol%Al_2O_3 reinforced composite squeeze cast at 800 °C parallel to the fiber orientation at X1000 magnification

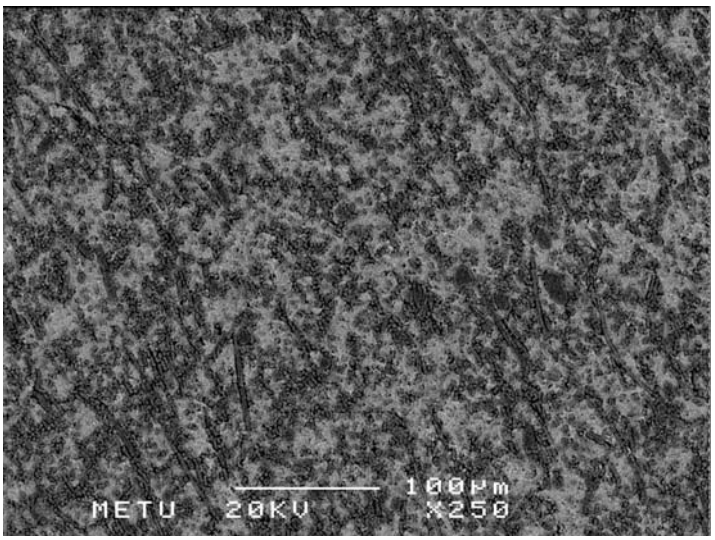

Figure 4.41 Back scattered SEM image of AlSi7Mg0.8/20vol%Al_2O_3 reinforced composite squeeze cast at 800 °C vertical to the fiber orientation at X250 magnification

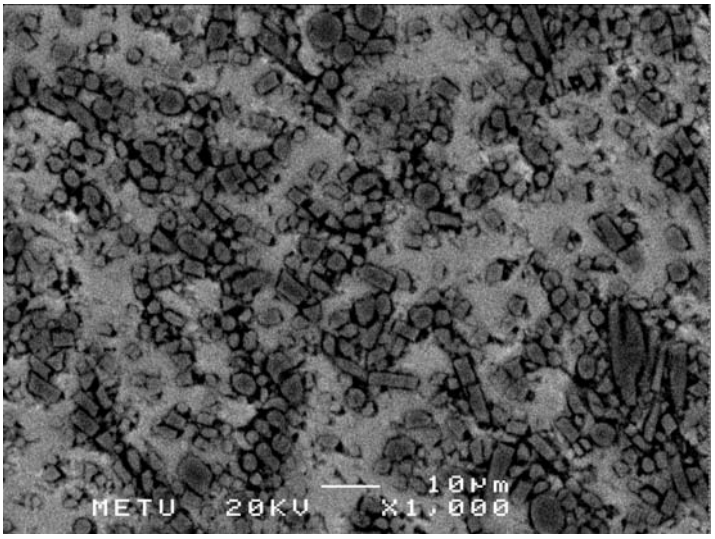

Figure 4.42 Back scattered SEM image of AlSi7Mg0.8/20vol%Al_2O_3 reinforced composite squeeze cast at 800 °C vertical to the fiber orientation at X1000 magnification

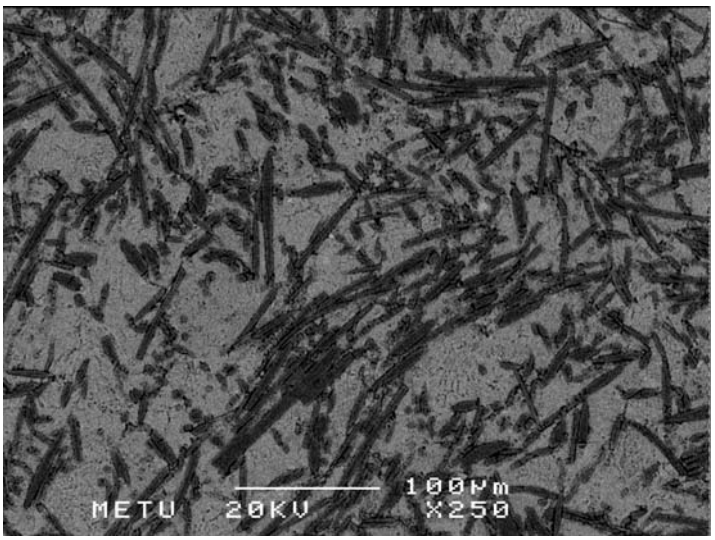

Figure 4.43 Back scattered SEM image of AlSi7Mg0.8/25vol%Al_2O_3 reinforced composite squeeze cast at 800 °C parallel to the fiber orientation at X250 magnification

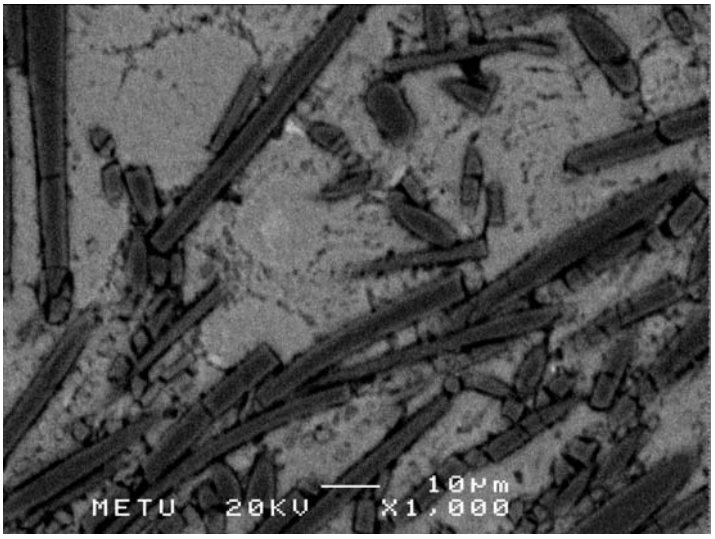

Figure 4.44 Back scattered SEM image of AlSi7Mg0.8/25vol%Al_2O_3 reinforced composite squeeze cast at 800 °C parallel to the fiber orientation at X1000 magnification

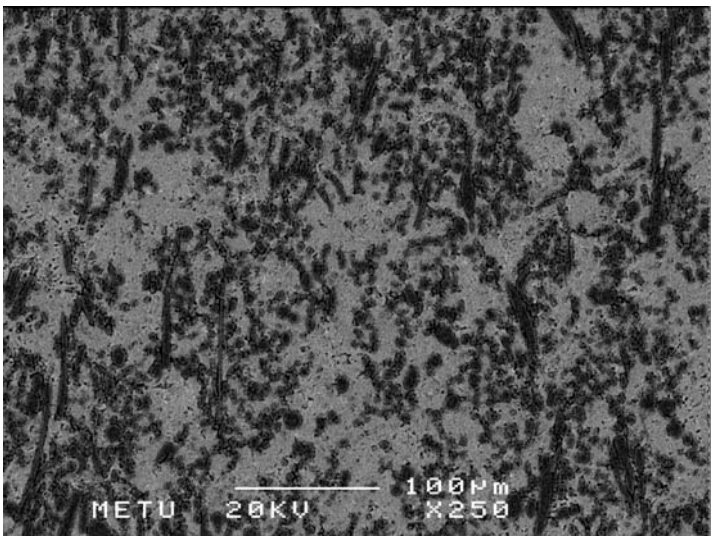

Figure 4.45 Back scattered SEM image of AlSi7Mg0.8/25vol%Al_2O_3 reinforced composite squeeze cast at 800 °C vertical to the fiber orientation at X250 magnification

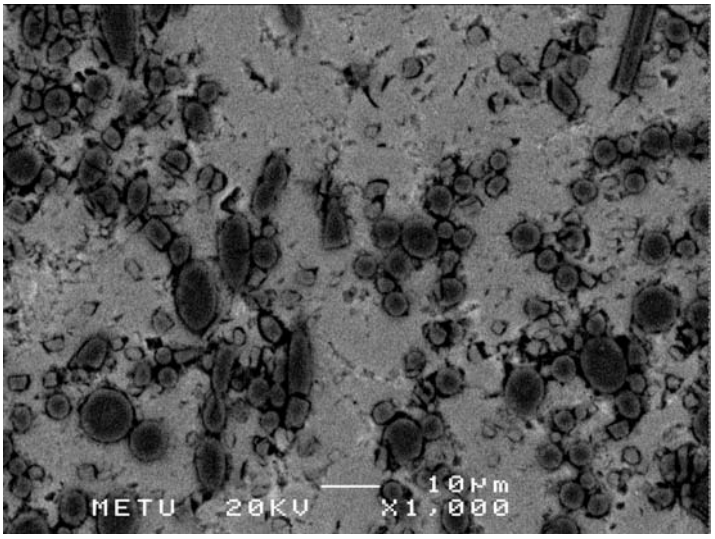

Figure 4.46 Back scattered SEM image of AlSi7Mg0.8/25vol%Al_2O_3 reinforced composite squeeze cast at 800 °C vertical to the fiber orientation at X1000 magnification

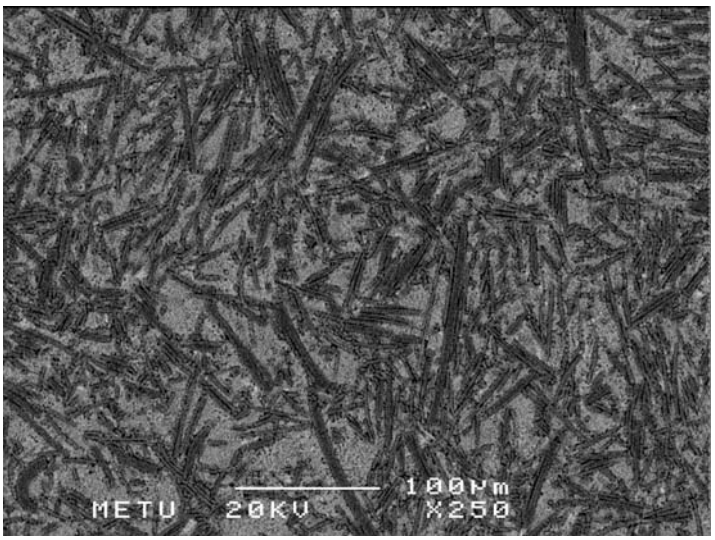

Figure 4.47 Back scattered SEM image of AlSi7Mg0.8/30vol%Al_2O_3 reinforced composite squeeze cast at 800 °C parallel to the fiber orientation at X250 magnification

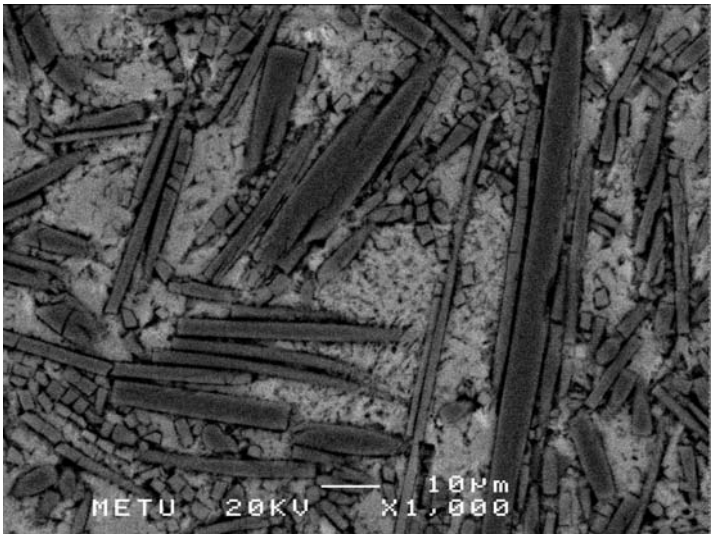

Figure 4.48 Back scattered SEM image of AlSi7Mg0.8/25vol%Al_2O_3 reinforced composite squeeze cast at 800 °C parallel to the fiber orientation at X1000 magnification

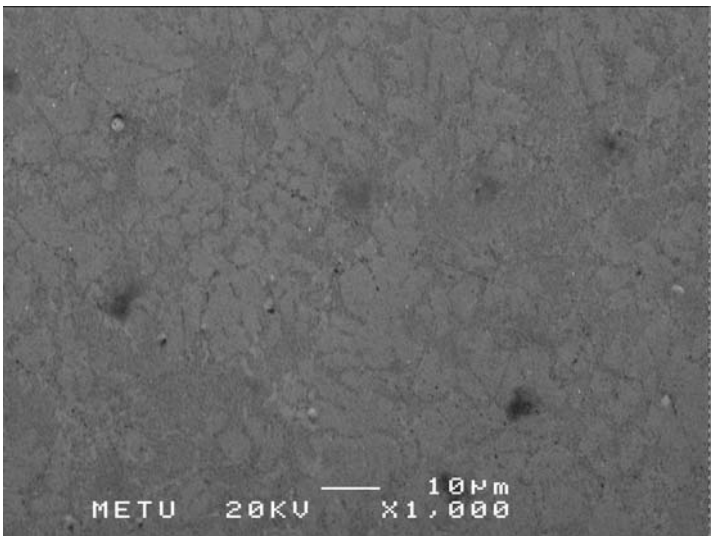

Figure 4.49 SEM image of AlSi10Mg0.8 alloy matrix squeeze cast at 750 °C at X1000 magnification

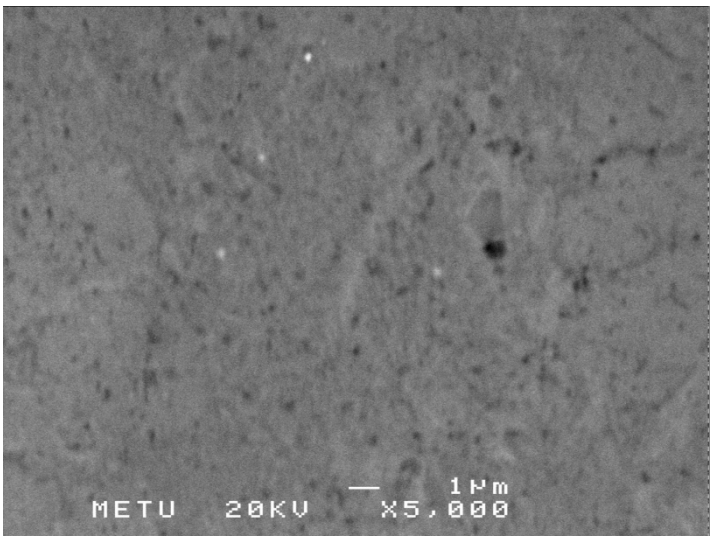

Figure 4.50 SEM image of AlSi10Mg0.8/ alloy matrix squeeze cast at 750 °C at X5000 magnification, reveals fibrous eutectic

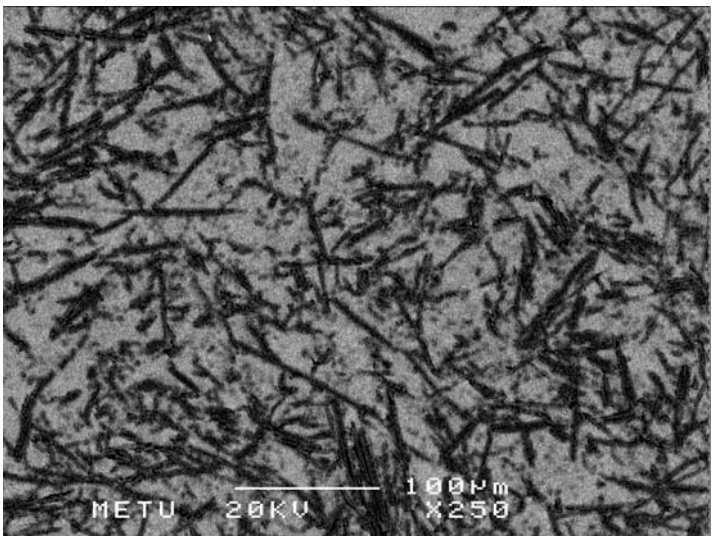

Figure 4.51 Back scattered SEM image of AlSi10Mg0.8/20vol%Al_2O_3 reinforced composite squeeze cast at 750 °C parallel to the fiber orientation at X250 magnification

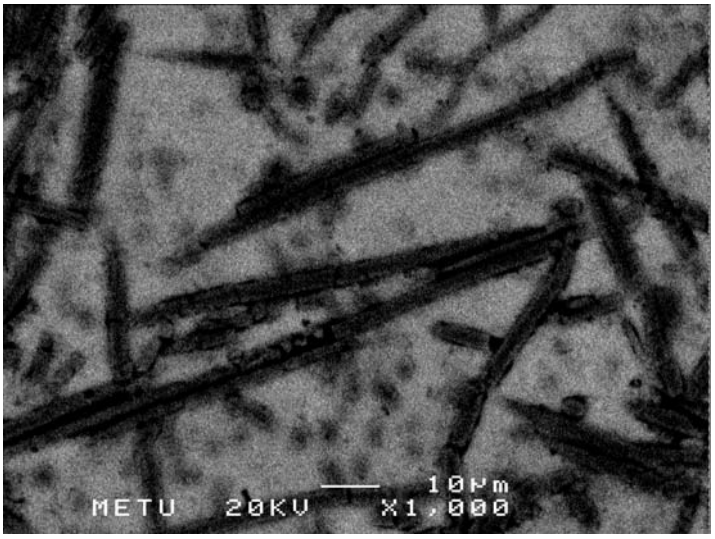

Figure 4.52 Back scattered SEM image of AlSi10Mg0.8/20vol%Al_2O_3 reinforced composite squeeze cast at 750 °C parallel to the fiber orientation at X1000 magnification

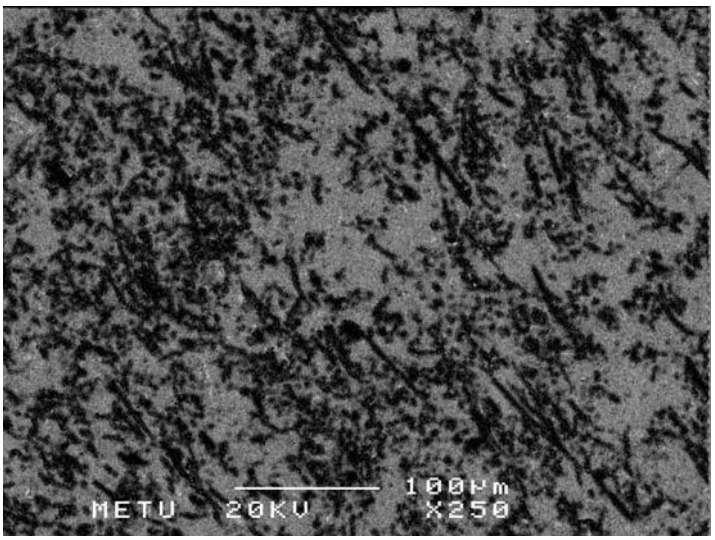

Figure 4.53 Back scattered SEM image of AlSi10Mg0.8/20vol%Al_2O_3 reinforced composite squeeze cast at 750 °C vertical to the fiber orientation at X250 magnification

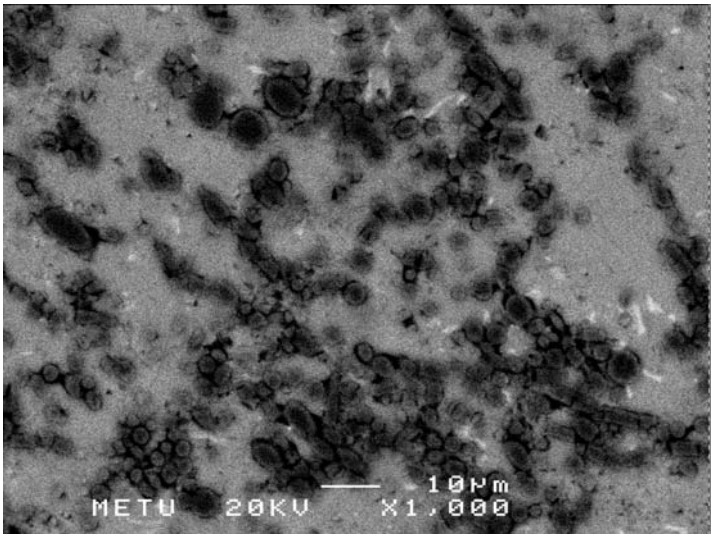

Figure 4.54 Back scattered SEM image of AlSi10Mg0.8/20vol%Al_2O_3 reinforced composite squeeze cast at 750 °C vertical to the fiber orientation at X1000 magnification

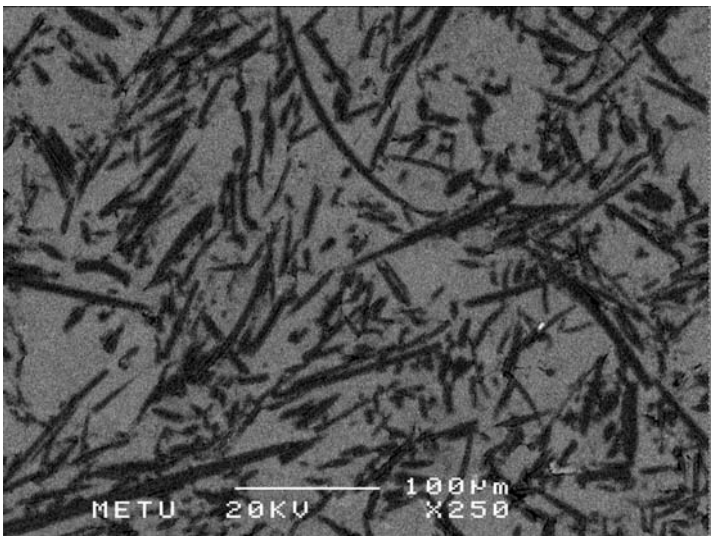

Figure 4.55 Back scattered SEM image of AlSi10Mg0.8/25vol%Al_2O_3 reinforced composite squeeze cast at 750 °C parallel to the fiber orientation at X250 magnification

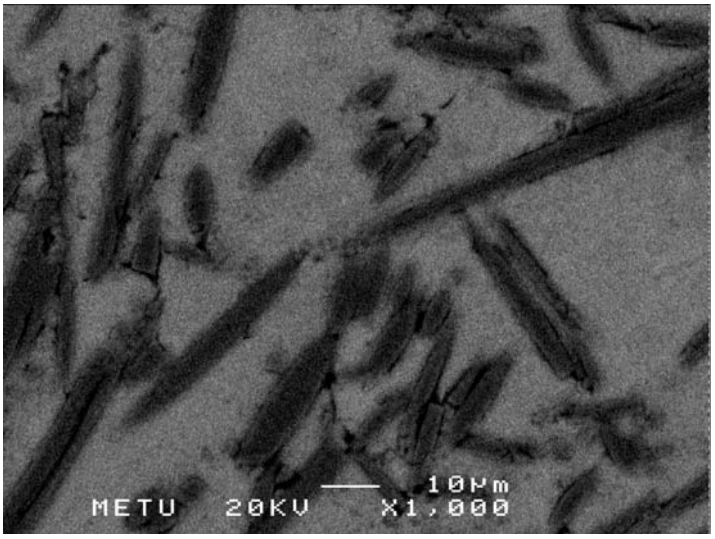

Figure 4.56 Back scattered SEM image of AlSi10Mg0.8/25vol%Al_2O_3 reinforced composite squeeze cast at 750 °C parallel to the fiber orientation at X1000 magnification

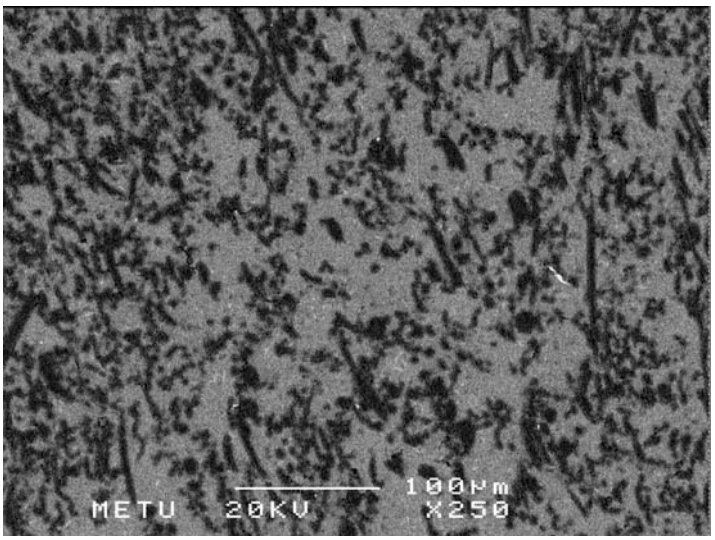

Figure 4.57 Back scattered SEM image of AlSi10Mg0.8/25vol%Al_2O_3 reinforced composite squeeze cast at 750 °C vertical to the fiber orientation at X250 magnification

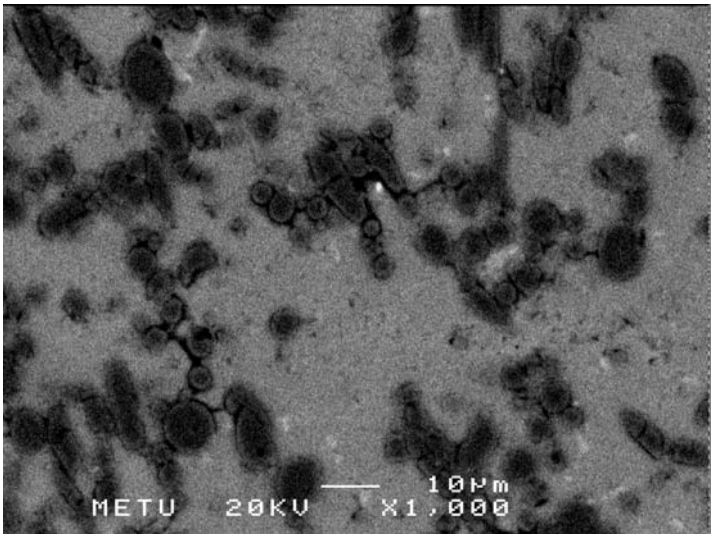

Figure 4.58 Back scattered SEM image of AlSi10Mg0.8/25vol%Al_2O_3 reinforced composite squeeze cast at 750 °C vertical to the fiber orientation at X1000 magnification

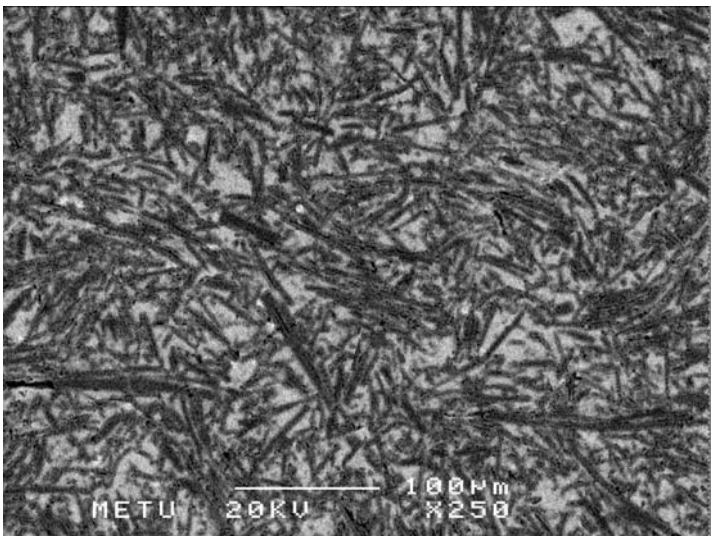

Figure 4.59 Back scattered SEM image of AlSi10Mg0.8/30vol%Al_2O_3 reinforced composite squeeze cast at 750 °C parallel to the fiber orientation at X250 magnification

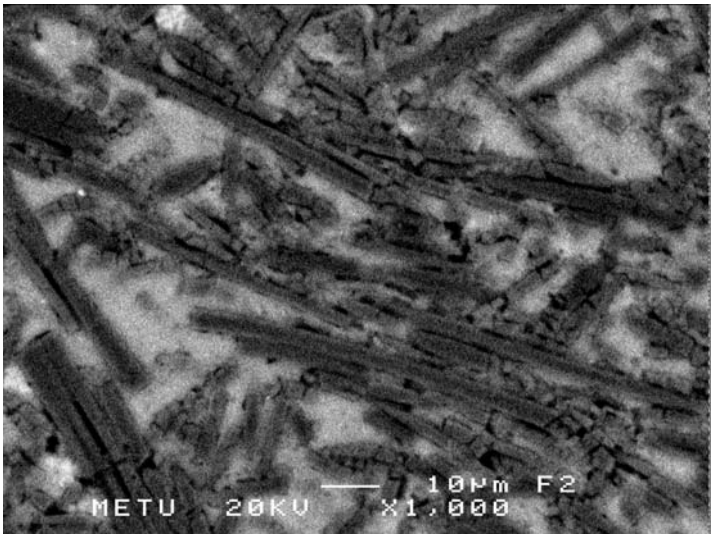

Figure 4.60 Back scattered SEM image of AlSi10Mg0.8/30vol%Al_2O_3 reinforced composite squeeze cast at 750 °C parallel to the fiber orientation at X1000 magnification

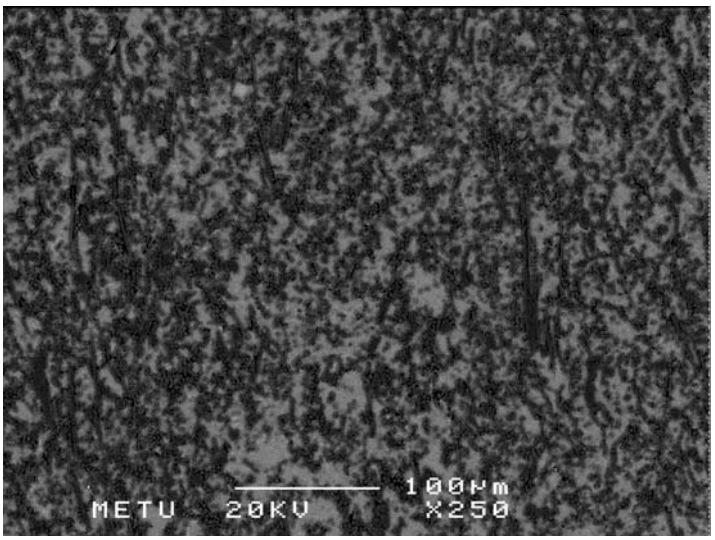

Figure 4.61 Back scattered SEM image of AlSi10Mg0.8/30vol%Al_2O_3 reinforced composite squeeze cast at 750 °C vertical to the fiber orientation at X250 magnification

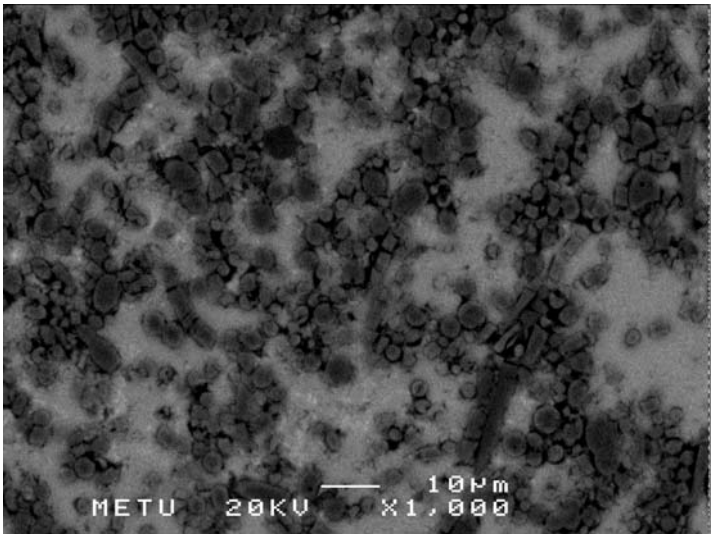

Figure 4.62 Back scattered SEM image of AlSi10Mg0.8/30vol%Al_2O_3 reinforced composite squeeze cast at 750 °C vertical to the fiber orientation at X1000 magnification

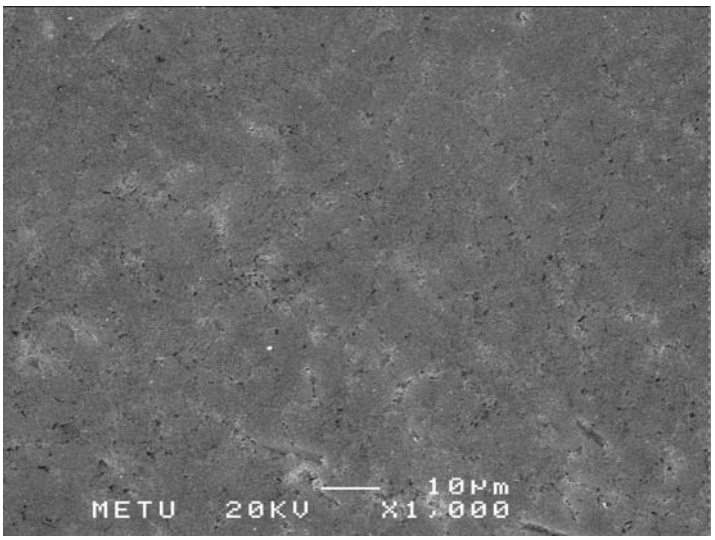

Figure 4.63 SEM image of AlSi10Mg0.8 alloy matrix squeeze cast at 800 °C at X1000 magnification

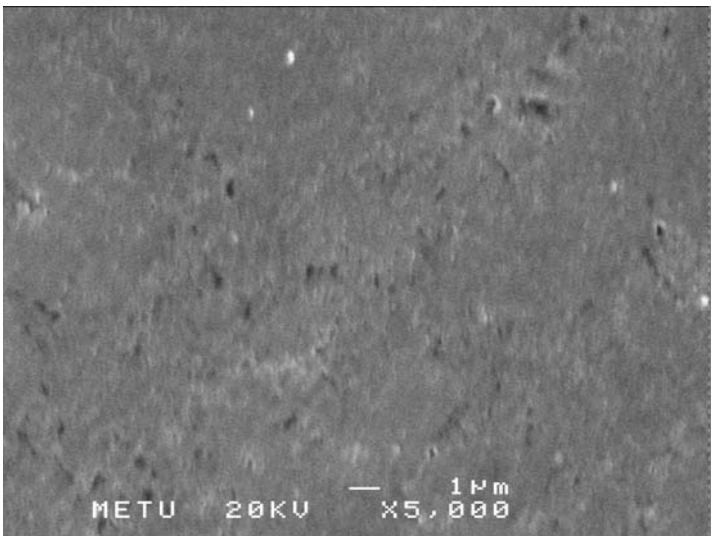

Figure 4.64 SEM image of AlSi10Mg0.8 alloy matrix squeeze cast at 800 °C at X5000 magnification, reveals fibrous eutectic

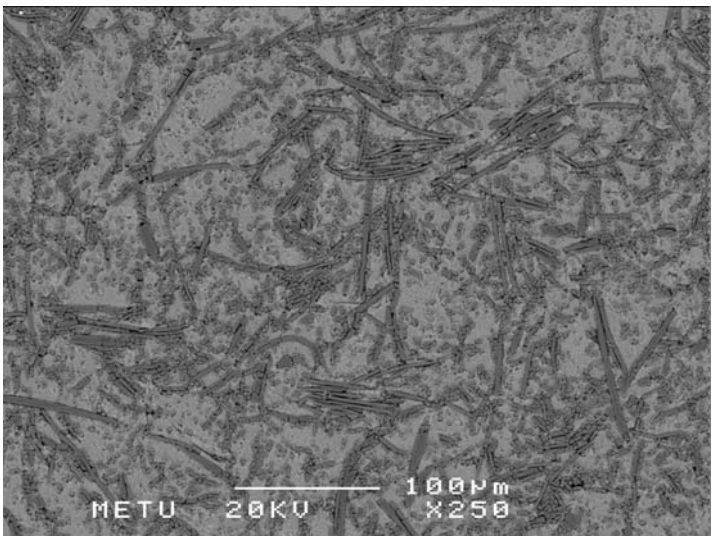

Figure 4.65 Back scattered SEM image of AlSi10Mg0.8/20vol%Al_2O_3 reinforced composite squeeze cast at 800 °C parallel to the fiber orientation at X250 magnification

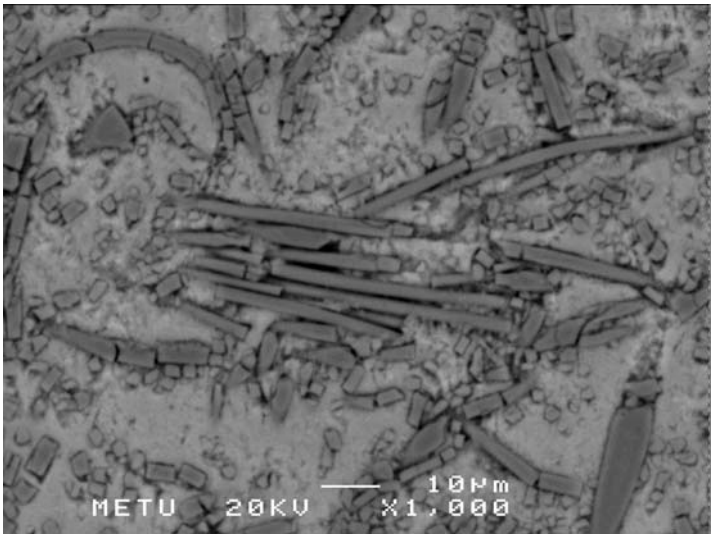

Figure 4.66 Back scattered SEM image of AlSi10Mg0.8/20vol%Al_2O_3 reinforced composite squeeze cast at 800 °C parallel to the fiber orientation at X1000 magnification

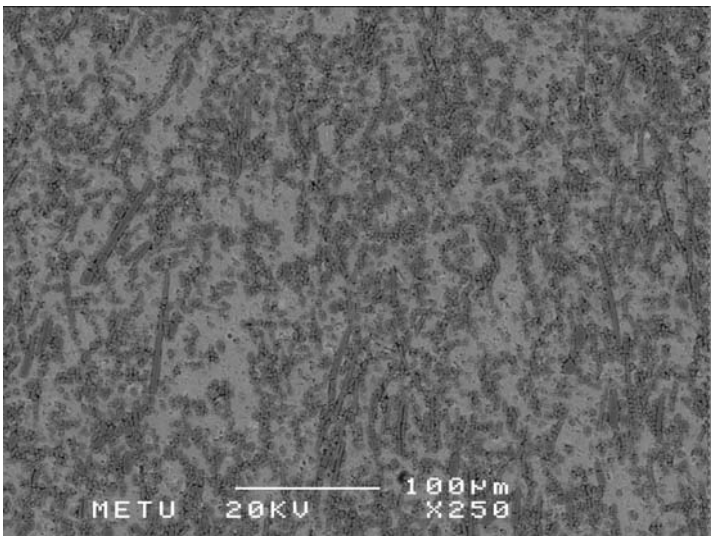

Figure 4.67 Back scattered SEM image of AlSi10Mg0.8/20vol%Al_2O_3 reinforced composite squeeze cast at 800 °C vertical to the fiber orientation at X250 magnification

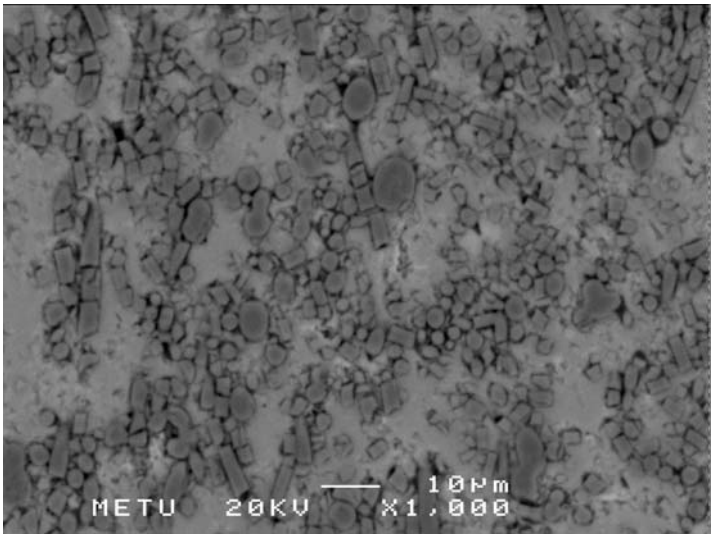

Figure 4.68 Back scattered SEM image of AlSi10Mg0.8/20vol%Al_2O_3 reinforced composite squeeze cast at 800 °C vertical to the fiber orientation at X1000 magnification

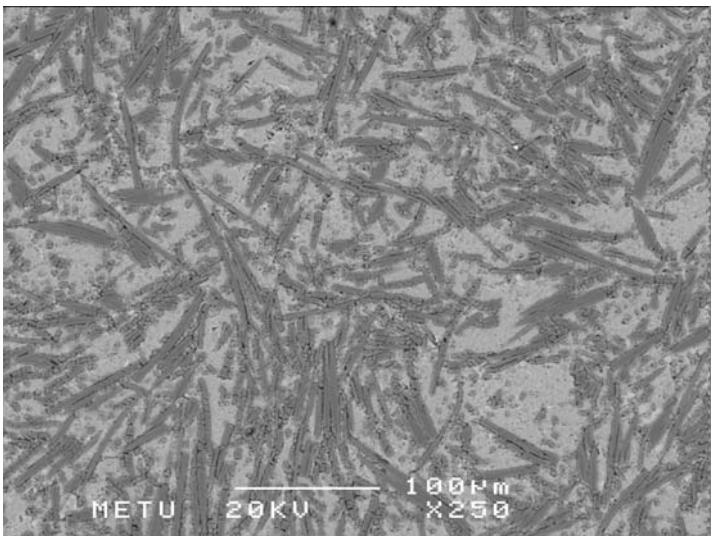

Figure 4.69 Back scattered SEM image of AlSi10Mg0.8/25vol%Al_2O_3 reinforced composite squeeze cast at 800 °C parallel to the fiber orientation at X250 magnification

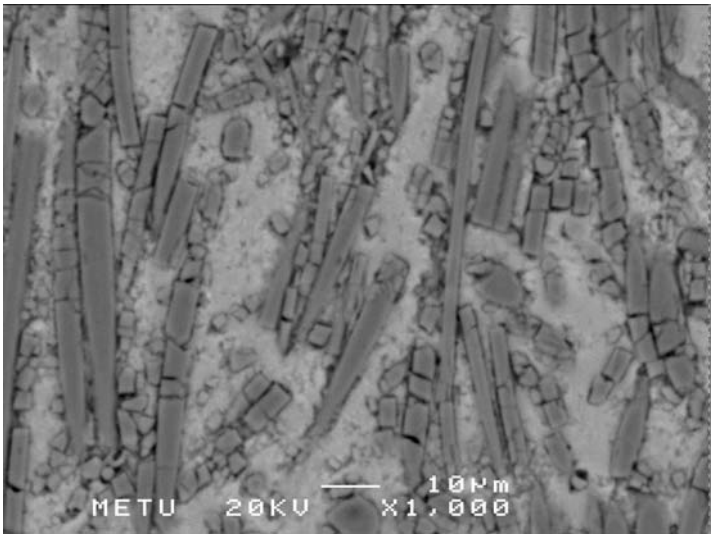

Figure 4.70 Back scattered SEM image of AlSi10Mg0.8/25vol%Al_2O_3 reinforced composite squeeze cast at 800 °C parallel to the fiber orientation at X1000 magnification

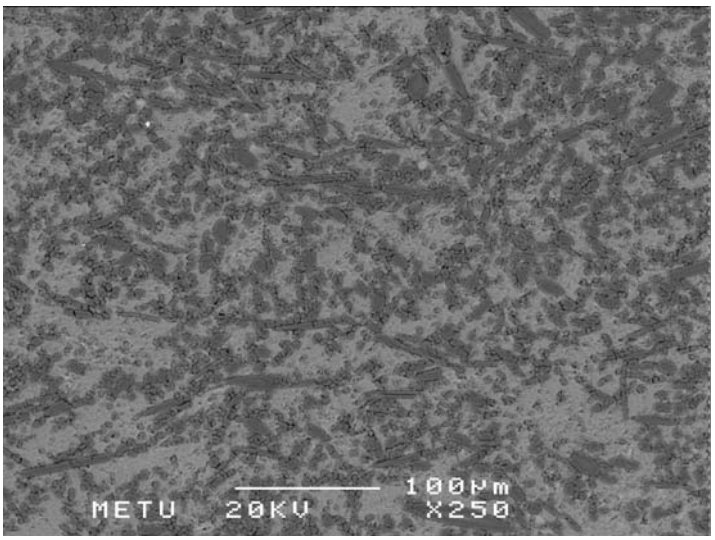

Figure 4.71 Back scattered SEM image of AlSi10Mg0.8/25vol%Al_2O_3 reinforced composite squeeze cast at 800 °C vertical to the fiber orientation at X250 magnification

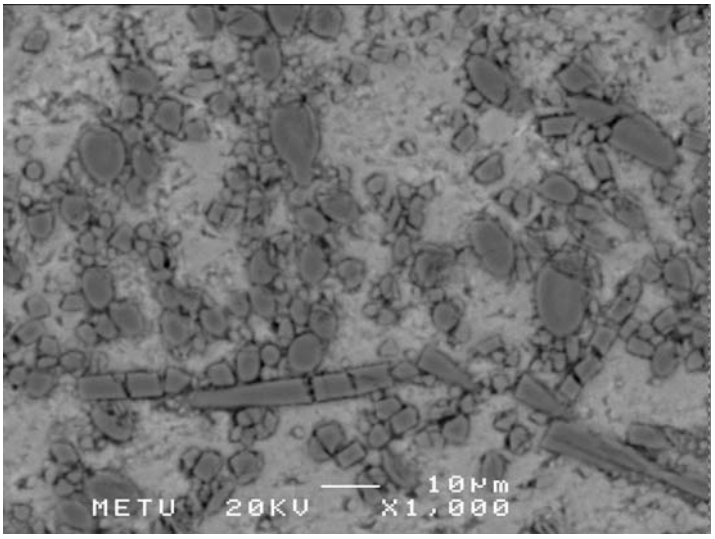

Figure 4.72 Back scattered SEM image of AlSi10Mg0.8/25vol%Al_2O_3 reinforced composite squeeze cast at 800 °C vertical to the fiber orientation at X1000 magnification

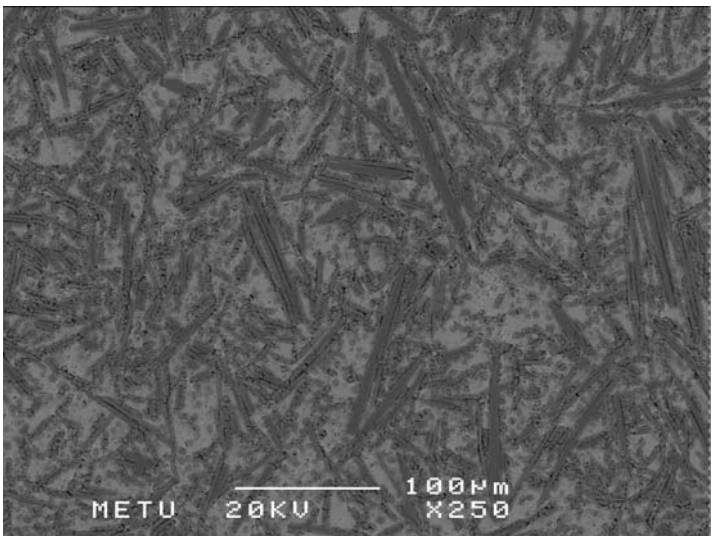

Figure 4.73 Back scattered SEM image of AlSi10Mg0.8/30vol%Al_2O_3 reinforced composite squeeze cast at 800 °C parallel to the fiber orientation at X250 magnification

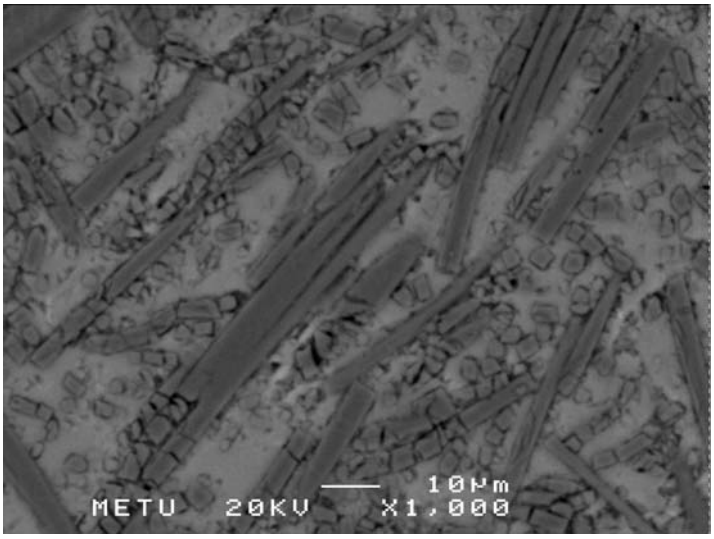

Figure 4.74 Back scattered SEM image of AlSi10Mg0.8/30vol%Al_2O_3 reinforced composite squeeze cast at 800 °C parallel to the fiber orientation at X1000 magnification

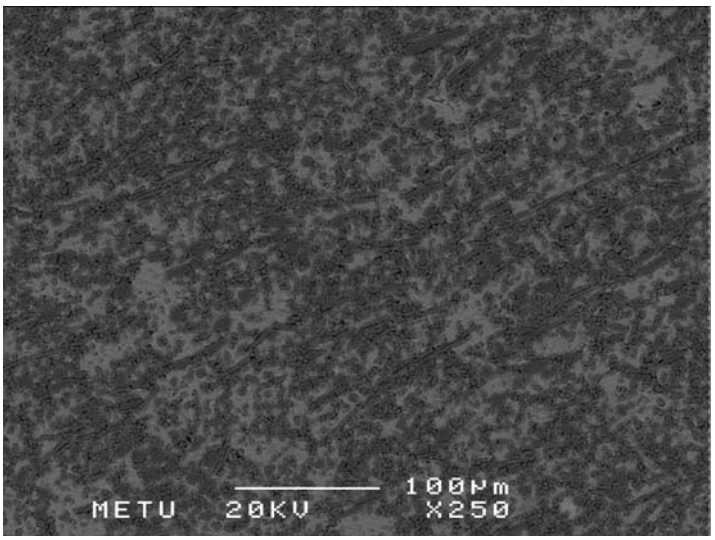

Figure 4.75 Back scattered SEM image of AlSi10Mg0.8/30vol%Al_2O_3 reinforced composite squeeze cast at 800 °C vertical to the fiber orientation at X250 magnification

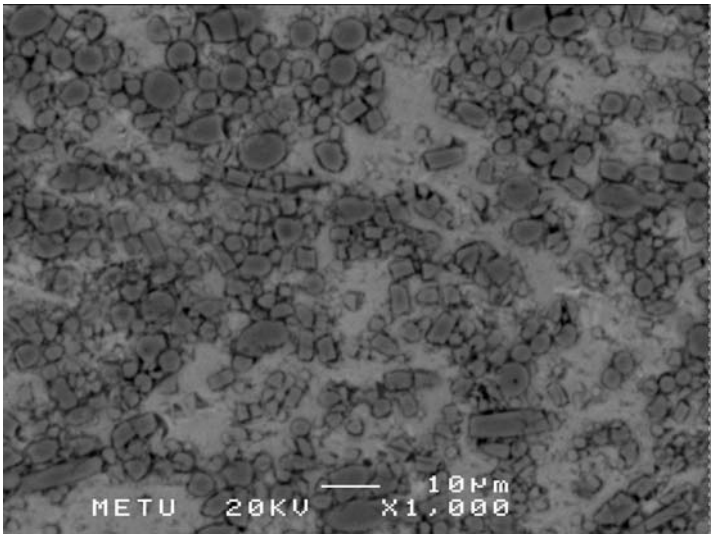

Figure 4.76 Back scattered SEM image of AlSi10Mg0.8/30vol%Al_2O_3 reinforced composite squeeze cast at 800 °C vertical to the fiber orientation at X1000 magnification

Back scattered SEM images of the composites parallel to the fiber orientation showed that planar isotropic condition of the fibers of the preforms had not been deteriorated by the applied pressure during the squeeze casting operation. Moreover SEM images also showed that an appropriate fiber/matrix adhesion was achieved by the squeeze casting conditions. However, in SEM images it was also seen micro-porosities which were inevitable due to the very high driving forces that had arisen during infiltration.

In addition to the back scattered SEM images, normal SEM images were also taken. However, due to ability of having large contrast between reinforcement and matrix phases in back scattered images, normal SEM images are not given in SEM study of composites. One of the normal SEM images is shown in the Figure 4.77.

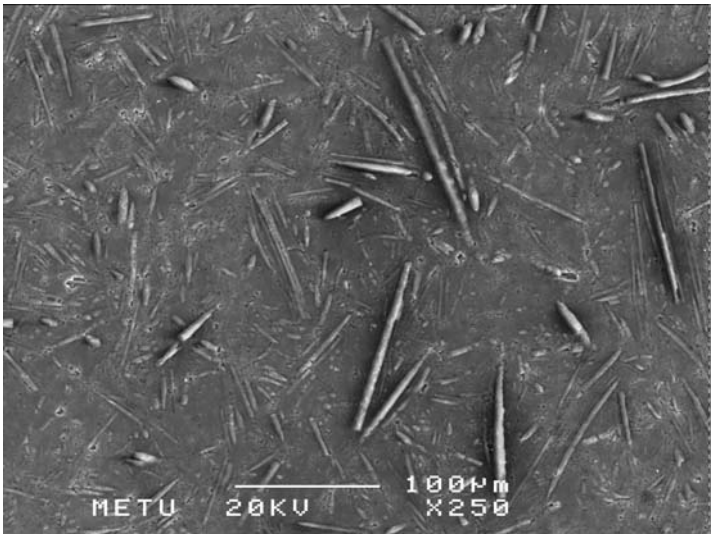

Figure 4.77 SEM image of AlSi10Mg0.8/30vol%Al_2O_3 reinforced composite squeeze cast at 800 °C parallel to the fiber orientation at X250 magnification

4.1.2 Optical Microscopy Results

Optical microscopy study was carried out to investigate the vol% of Saffil fibers in the composite, i.e. image analysis. Image analyses were conducted by Dewinter Materials Plus 4.1 Image Analyzing Program and Soif XJP-6A optical microscope. The program makes a contrast between two phases and finds an area ratio of the two phases. The image analyses were performed at 100X magnifications. The area ration changed into the volume ratio of the composite by multiplying the area percent by a unit height yielding the volume percent of the composite. Finally the results were compared with the theoretical results, which were 20, 25 and 30 vol%. An example of the image analyses results is given in Figure 4.78.

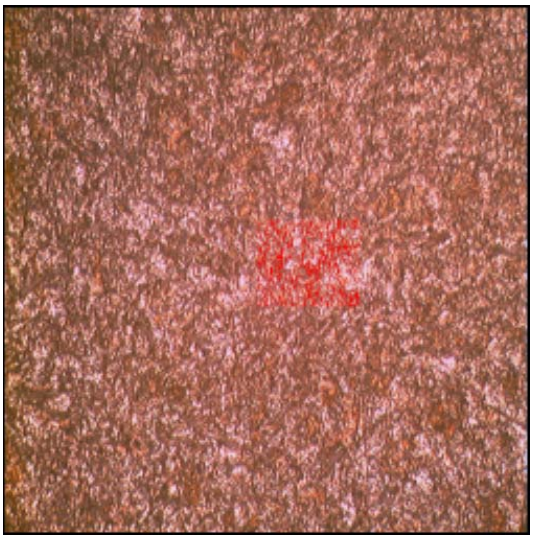

Figure 4.78 The sample image after image analyzing at 100X magnification

One of the microstructure test reports is given in Table 4.1.

Table 4.1 Image analysis result of AlSi7Mg0.8/30vol%Saffil composite infiltrated at 750 °C from vertical to the fiber orientation

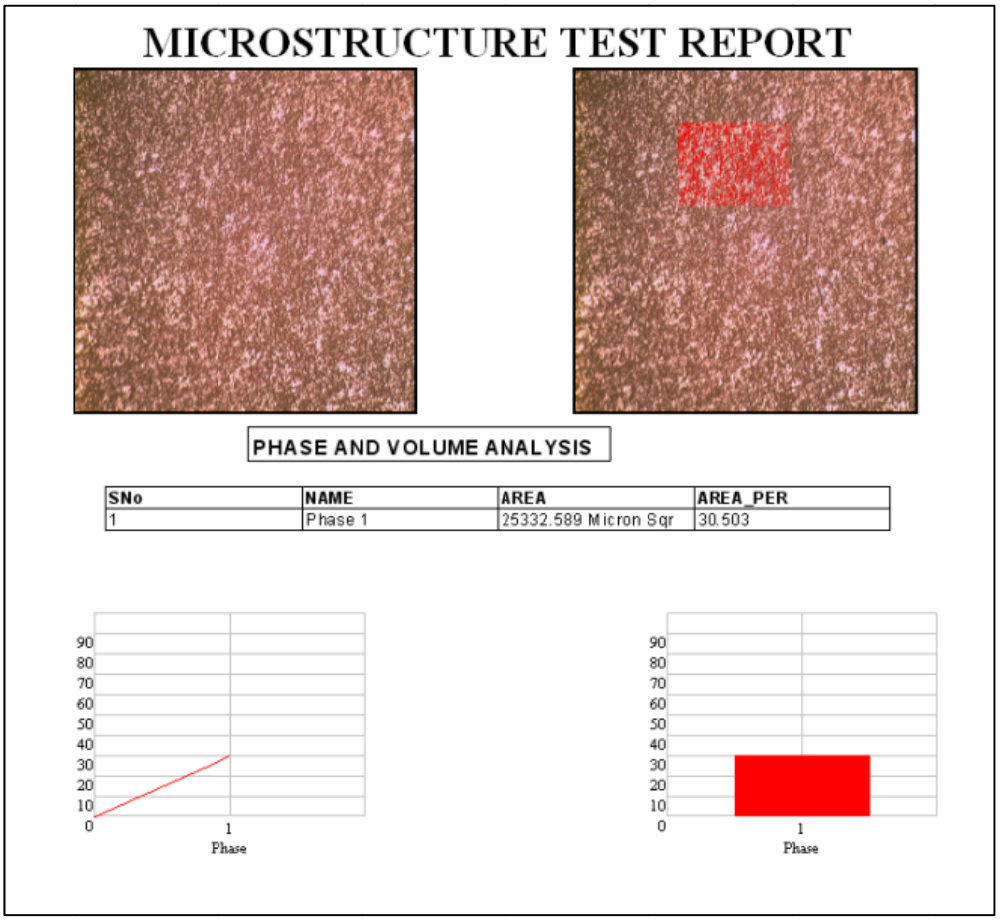

Details of the image analyzing reports are given in Appendix C.

In Table 4.2 and Table 4.3, image analyzing results of the specimens are given.

Table 4.2 Image analyses results of the composite specimens

Alloy	Infiltration Temperature (°C)	vol% of the Reinforcement	Orientation of the Fibers	
			Parallel	Vertical
AlSi7Mg0.8	750	20 vol%	20.017	20.771
		25 vol%	25.214	25.590
		30 vol%	30.155	30.513
	800	20 vol%	21.822	21.083
		25 vol%	26.996	26.109
		30 vol%	30.469	30.452
AlSi10Mg0.8	750	20 vol%	20.110	20.115
		25 vol%	25.528	25.470
		30 vol%	31.250	30.267
	800	20 vol%	20.836	20.350
		25 vol%	25.512	26.095
		30 vol%	32.121	31.230

Table 4.3 Deviations of the image analyzing results compared to the theoretical values

Alloy	Infiltration Temperature (°C)	vol% of the Reinforcement	Deviation of the Results from Theoretical Values According to the Fiber Orientation (%)	
			Parallel	Vertical
AlSi7Mg0.8	750	20 vol%	0.08	3.71
		25 vol%	0.85	2.31
		30 vol%	0.51	1.68
	800	20 vol%	8.35	5.14
		25 vol%	7.39	4.25
		30 vol%	1.54	1.48
AlSi10Mg0.8	750	20 vol%	0.55	0.57
		25 vol%	2.07	1.85
		30 vol%	4.00	0.88
	800	20 vol%	4.01	1.72
		25 vol%	2.01	4.20
		30 vol%	6.60	3.94

From the image analyses results, it was seen that calculated results had positive deviation from the theoretical values. This difference was mainly because of local fiber breakages together with high contrast required for the microscope. It was also observed that there had been no definite trend in the deviation values compared to the volume percentages of the reinforcement phase.

Optical microscopy results also include insert/backing alloy interface analyses. In Figure 4.79 and Figure 4.80, insert/backing alloy interface can be seen.

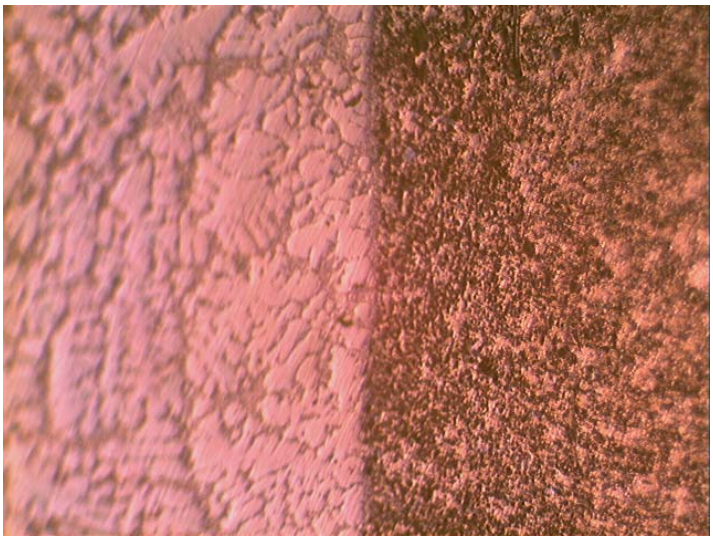

Figure 4.79 Optical microscopy image of insert/backing alloy interface at X100 magnification

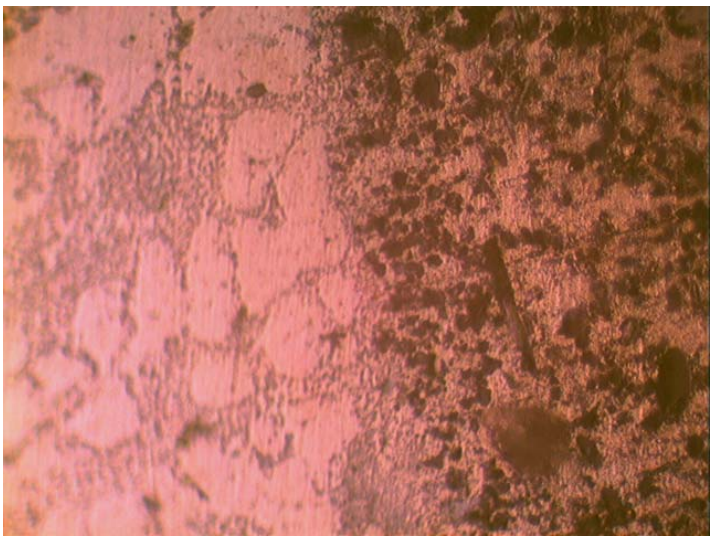

Figure 4.80 Optical microscopy image of insert/backing alloy interface at X400 magnification

Details of the image analyses of insert/backing alloy can be seen in Appendix C.

Insertion casting operation was done in 100 tons capacity vertical press. Component alloy (metal surrounding the insert) was AlSi10Mg0.8 due to its higher filling ability compared to AlSi7Mg0.8 alloy. Two different connecting rods were casted. Inserts were grinded before the insertion casting operation to remove the alumina layer exists around the insert.

Although insert/component alloy interface was successfully created, it was noted that extremely thin sections (≈ 1 or 2 mm) should be avoided near the insert. These thin sections can inhibit the insertion casting by favoring the molten metal velocity in the mold cavity of the component. It was seen that this condition had not affected the insert/component alloy interface, but affected the overall geometry of the component. In Figure 4.81, the connecting rod produced after the insertion casting operation.

Figure 4.81 Connecting rod obtained from the insertion casting operation

During the insertion casting operation, it was seen that an appropriate insert/backing alloy interface could be achieved by these process parameters.

4.2 XRD Analyses Results

XRD analyses of the Saffil fibers and composites were done. The reinforcement phase, i.e. Saffil fibers, mainly consists of δ-Al_2O_3 and small amount of SiO_2 as stated in the technical datasheet of the manufacturer. Composite specimens were also analyzed to check whether any degradable chemical reaction occurred between fiber and matrix phases or not. XRD results of the composite specimens showed

that both matrix alloy and Saffil fibers existed in the structure. Delta alumina structure of the Saffil fibers did not changed after the processing.

4.2.1 XRD Analyses of the Preforms

XRD analyses of the preforms showed that the reinforcement phase consisted of δ-Al_2O_3. In the following figure, XRD pattern can be seen. It was seen that δ-Al_2O_3 gives 2θ peaks at 36°, 39°, 45°, 46°, 60° and 67°. In Figure 4.82, (h k l) values of the peaks of δ-Al_2O_3 are given.

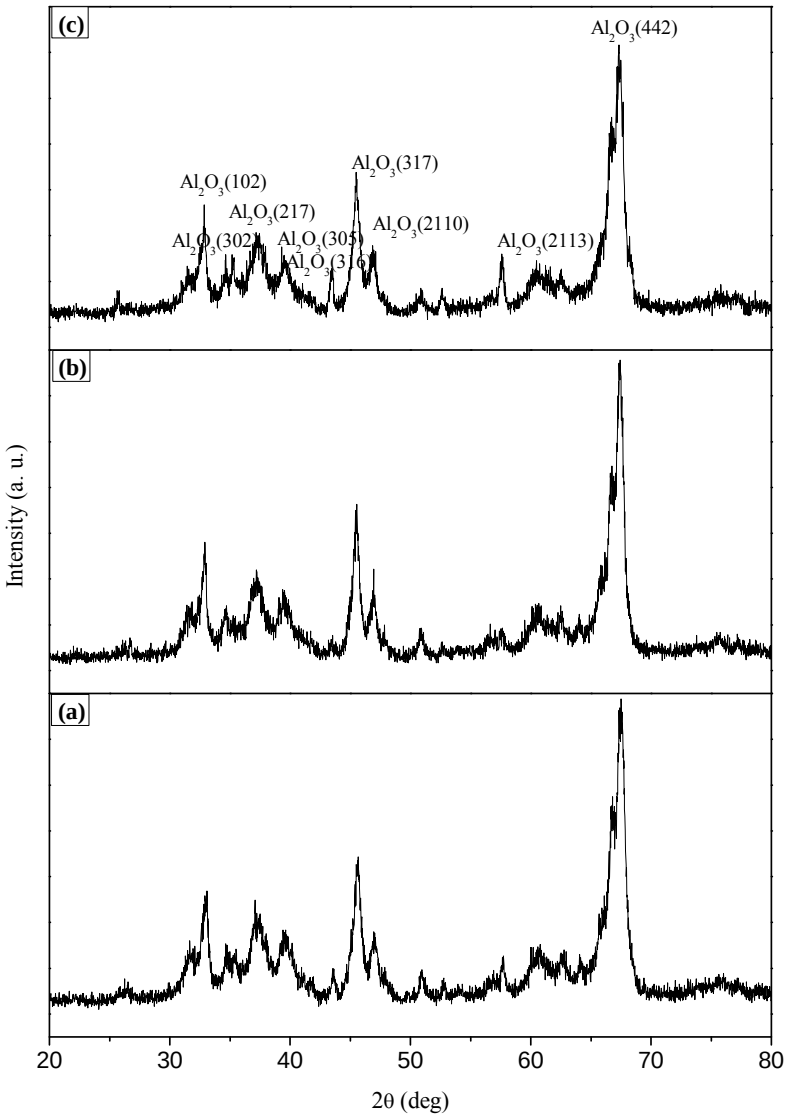

Figure 4.82 XRD analyses of the preforms (a) 20vol%, (b) 25 vol% and (c) 30 vol% Saffil fibers

4.2.2 XRD Analyses of the Composite Specimens

XRD analyses of the composite specimens showed that there had been no chemical reaction between the fiber and the matrix phases since there had been no other

phase observed in the XRD patterns. This showed that any chemical reaction between the fiber and the reinforcement was not kinetically possible.

It was seen that Al gives 2θ peaks at 38°, 44°, 65°, 78° and 82°; Si gives 2θ peaks at 28°, 47°, 56°, 76° and 86°; and δ-Al_2O_3 gives 2θ peaks at 36°, 39°, 45°, 46° and 67°. Detailed XRD patterns of the searched phases are given in Appendix D.

In the XRD patterns given in figures from Figure 4.83 through 4.87, note that 2θ peaks of Al and Al_2O_3 are very close to each other in the 2θ regions of 36-39° and 44-46°. There exists a δ-Al_2O_3 peak from (3 0 5) plane next to Al peak from (1 1 1) plane. Similarly, next to Al peak from (2 0 0) plane, there exists a δ-Al_2O_3 peak from (3 1 7) plane.

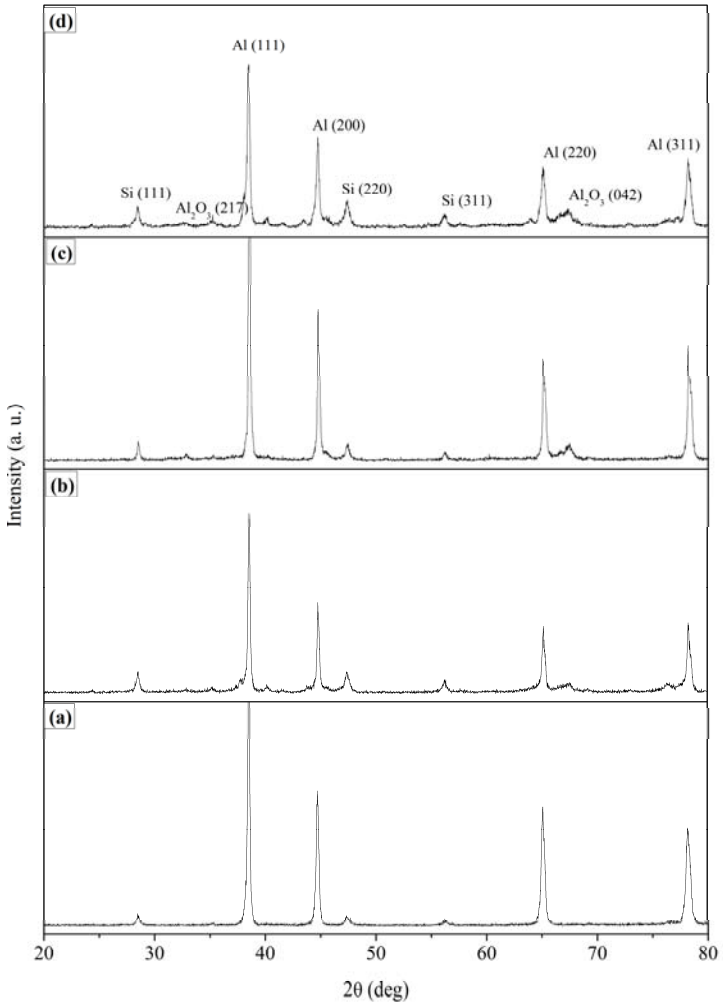

Figure 4.83 XRD analysis of AlSi7Mg0.8 matrix composite infiltrated at 750 °C (a) 0 vol% fiber reinforced, (b) 20 vol% fiber reinforced, (c) 25 vol% fiber reinforced and (d) 30 vol% fiber reinforced

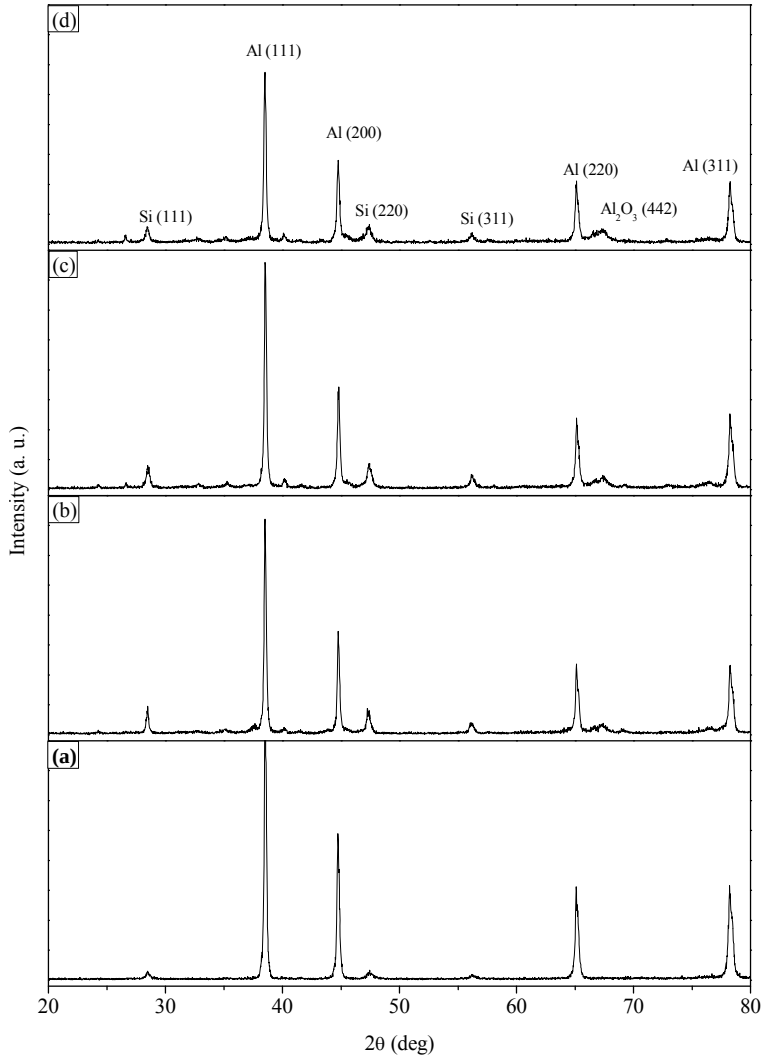

Figure 4.84 XRD analysis of AlSi7Mg0.8 matrix composite infiltrated at 800 °C (a) 0 vol% fiber reinforced, (b) 20 vol% fiber reinforced, (c) 25 vol% fiber reinforced and (d) 30 vol% fiber reinforced

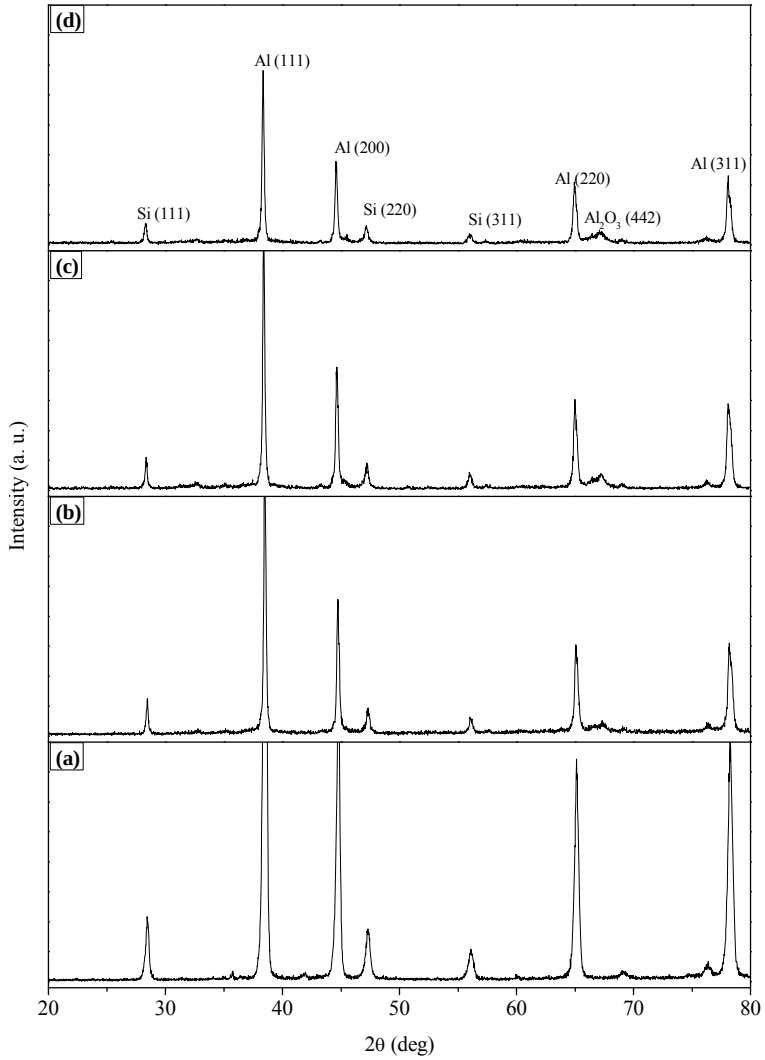

Figure 4.85 XRD analysis of AlSi10Mg0.8 matrix composite infiltrated at 750 °C (a) 0 vol% fiber reinforced, (b) 20 vol% fiber reinforced, (c) 25 vol% fiber reinforced and (d) 30 vol% fiber reinforced

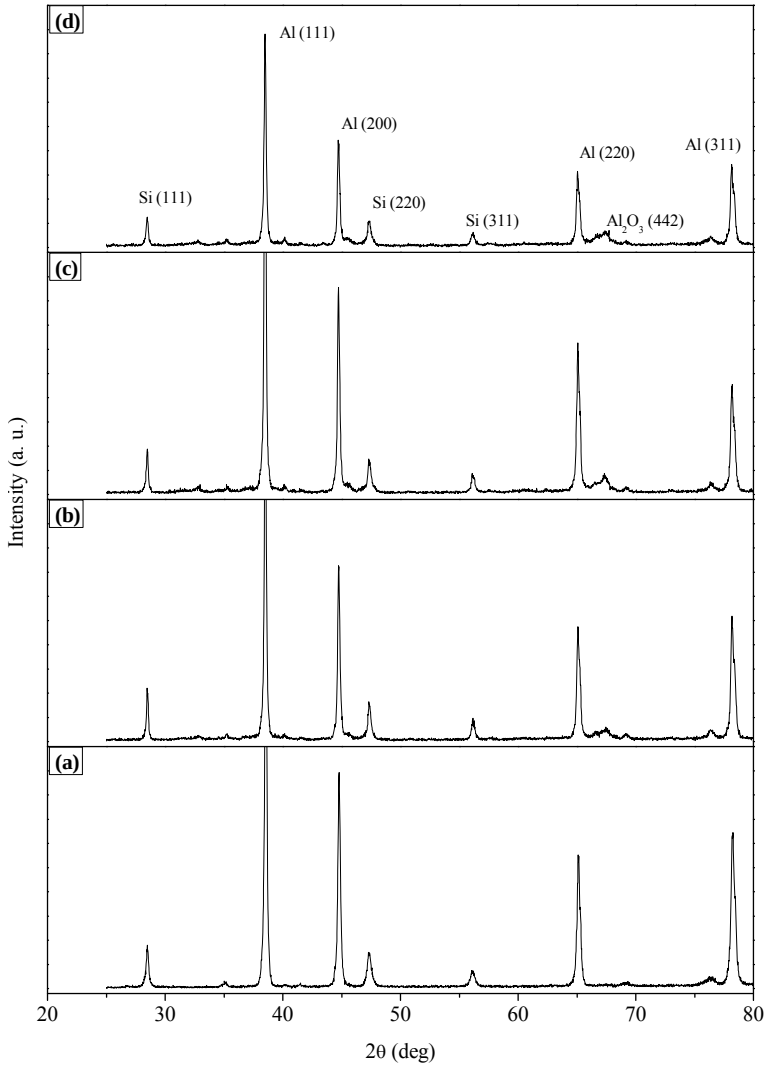

Figure 4.86 XRD analysis of AlSi10Mg0.8 matrix composite infiltrated at 800 °C (a) 0 vol% fiber reinforced, (b) 20 vol% fiber reinforced, (c) 25 vol% fiber reinforced and (d) 30 vol% fiber reinforced

4.3 Mechanical Test Results

Mechanical tests were divided into two parts, which are three point bending test and hardness test. Details of the tests are given in the following subtitles.

4.3.1 Three Point Bending Test Results

Three point bending tests were performed to observe the flexural strength of the composite specimens. In Table 4.4, average flexural strength values of the composites with respect to their infiltration temperature, fiber volume percent and matrix alloy types are given.

Table 4.4 Average flexural strength values of the composite specimens

Matrix Alloy	Infiltration Temperature (°C)	Vol% of the Fiber	Average Flexural Strength of the Composite (MPa)	Standard Deviation
AlSi7Mg0.8	750	0 vol%	571	145
		20 vol%	595	59
		25 vol%	706	5
		30 vol%	740	138
	800	0 vol%	455	97
		20 vol%	566	128
		25 vol%	674	93
		30 vol%	711	100
AlSi10Mg0.8	750	0 vol%	739	73
		20 vol%	780	160
		25 vol%	866	160
		30 vol%	908	320
	800	0 vol%	649	139
		20 vol%	760	171
		25 vol%	859	127
		30 vol%	881	155

All composite specimens showed brittle fracture. Due to the brittle characteristic of the fibers, which dominated the composite fracture behavior rather than the matrix, composites showed a brittle fracture behavior. In the case of AlSi7Mg0.8 matrix composites, increasing the vol% of fibers caused an increase in strength values directly. Also in the case of AlSi10Mg0.8 matrix composites, increasing the vol% of fibers caused an increase in strength values directly.

Infiltration temperature had another effect on the flexural strength of the composite specimens. For AlSi10Mg0.8 matrix composites, lower infiltration temperature i.e. 750 °C favored higher flexural strength values due to smaller grain size of the matrix phase. However for AlSi7Mg0.8 matrix composites, the situation is somewhat different. For 20 vol% reinforcement phase, lower infiltration temperature favored higher flexural strength; but for 25 and 30 vol% reinforcement phase, higher infiltration temperature favored higher flexural strength possibly due to the higher infiltration ability at higher temperatures. From the phase diagram of Al-Si system, it is seen that temperature of first solid phase appears in the alloy is higher as the silicon content of the alloy decreases (before the eutectic point). Therefore it is possible to say that flexural strength decrease of AlSi7Mg0.8 alloy can be correlated with the lower infiltration ability of the alloy at lower temperature compared to AlSi10Mg0.8 alloy. In the following figure, average flexural strength values of the composite specimens are given. Detailed results are given in Appendix E.

Effect of the silicon content of the alloys showed that higher silicon containing alloy showed higher flexural strength values compared to the lower silicon containing alloy. In Table 4.5, this effect can be seen in numerical values.

Table 4.5 Effect of Si on the flexural strength of the matrix

Name of the alloy	Flexural Strength (MPa)	Standard Deviation (MPa)
AlSi7Mg0.8 (@ 750 °C)	571	145
AlSi7Mg0.8 (@ 800 °C)	455	97
AlSi10Mg0.8 (@ 750 °C)	739	73
AlSi10Mg0.8 (@ 800 °C)	649	139

Squeeze casting temperature also affects the flexural strength of the matrix. Lower squeeze casting temperature favors the higher flexural strength values of the matrix. Higher flexural strength values could be explained by the use of

temperature range of the solidification. As the temperature range allowed for the alloy increases, the grain size of the alloy increases yielding lowered the strength of the alloy.

From the data obtained from three point bending test, fiber efficiency of the composites were calculated by the use of equation (2.10) and the surface area of the fibers were calculated by the use of equation (2.5) as shown in Table 4.6.

Table 4.6 Fiber efficiencies and the specific surface areas of 10^6 fibers

Name of the composite	Fiber Efficiency	Specific surface area (m^2/m^3)
AlSi7Mg0.8/20vol%Saffil (@ 750 °C)	0.63	3.3
AlSi7Mg0.8/25vol%Saffil (@ 750 °C)	0.65	4.4
AlSi7Mg0.8/30vol%Saffil (@ 750 °C)	0.59	5.7
AlSi7Mg0.8/20vol%Saffil (@ 800 °C)	0.59	3.3
AlSi7Mg0.8/25vol%Saffil (@ 800 °C)	0.61	4.4
AlSi7Mg0.8/30vol%Saffil (@ 800 °C)	0.56	5.7
AlSi10Mg0.8/20vol%Saffil (@ 750 °C)	0.96	3.3
AlSi10Mg0.8/25vol%Saffil (@ 750 °C)	0.88	4.4
AlSi10Mg0.8/30vol%Saffil (@ 750 °C)	0.79	5.7
AlSi10Mg0.8/20vol%Saffil (@ 800 °C)	0.93	3.3
AlSi10Mg0.8/25vol%Saffil (@ 800 °C)	0.88	4.4
AlSi10Mg0.8/30vol%Saffil (@ 800 °C)	0.76	5.7

Fiber efficiency values showed that most efficiently reinforced composites were AlSi10Mg0.8/20vol%Saffil reinforced ones. This result also necessitates that more improvements on 25 and 30 vol% fibers can be done as the future work.

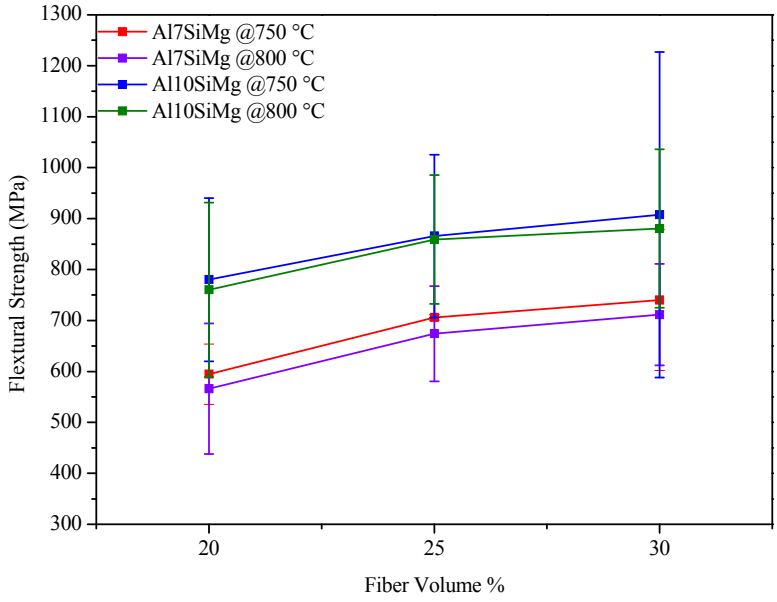

Figure 4.87 Three point bending test results of the composite specimens

From Figure 4.88, it is seen that lowest flexural strength belongs to AlSi7Mg0.8/20 vol% Saffil reinforced composite infiltrated at 800 °C; highest flexural strength belongs to AlSi10Mg0.8/30 vol% Saffil reinforced composite infiltrated at 750 °C.

4.3.2 Hardness Test Results

Hardness tests of the composite specimens were performed both from the vertical and parallel to the fiber orientation of the composites. Since hardness values of the materials are important parameters in selecting the materials resistant to the plastic flow, these tests were performed for the composite specimens. In Figure 4.89 and

Figure 4.90, hardness test results of the composites can be seen. Detailed results of hardness tests are also given in Appendix F.

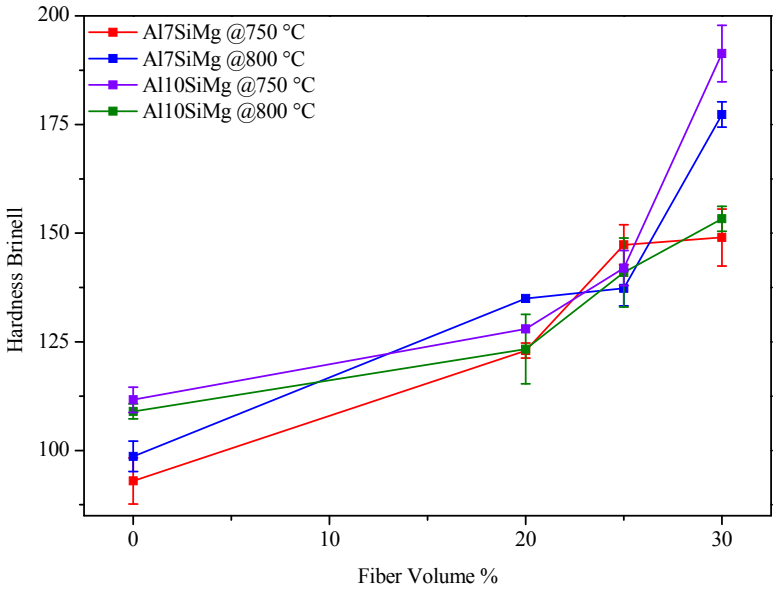

Figure 4.88 Hardness results of the composite specimens taken from the parallel to the fiber orientation

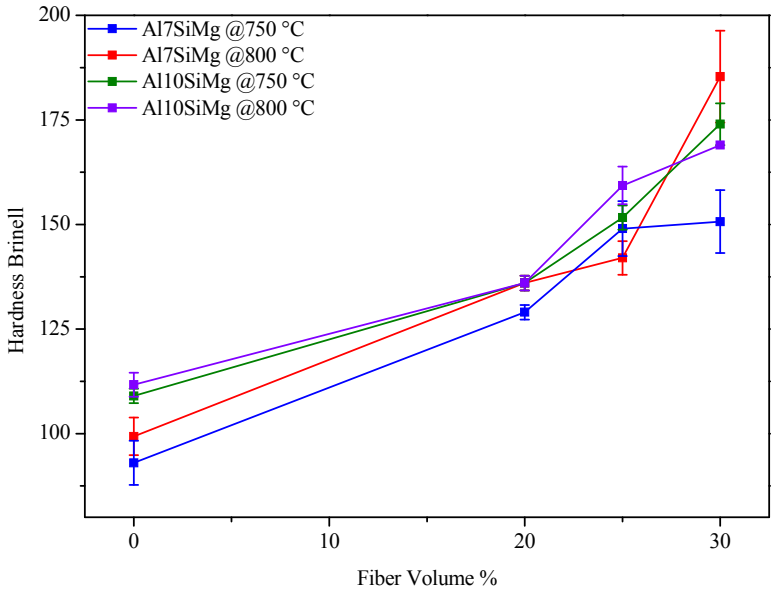

Figure 4.89 Hardness results of the composite specimens taken from the vertical to the fiber orientation

From the figures, it is seen that, increasing the fiber content of the composites yields higher hardness values. Increasing the fiber content of the composites decreases the grain size of the alloy resulting in higher hardness values. Moreover, increasing the fiber content of the reinforcement phase increases the hardness value by hindering the dislocation motion [19]. The highest hardness values for parallel and vertical orientation of the fibers were obtained for 30 vol% Saffil fiber reinforced AlSi7Mg0.8 alloy as 177 and 185 respectively.

4.4 Density Measurement

Density measurement was performed to find out the difference between the theoretical density values with the experimental density values due to the micro-porosities, which were inevitable in infiltration process, of the composite specimens. In the following figures from Figure 4.91 through Figure 4.94,

experimental and theoretical density values are given. Detailed results are given in Appendix G.

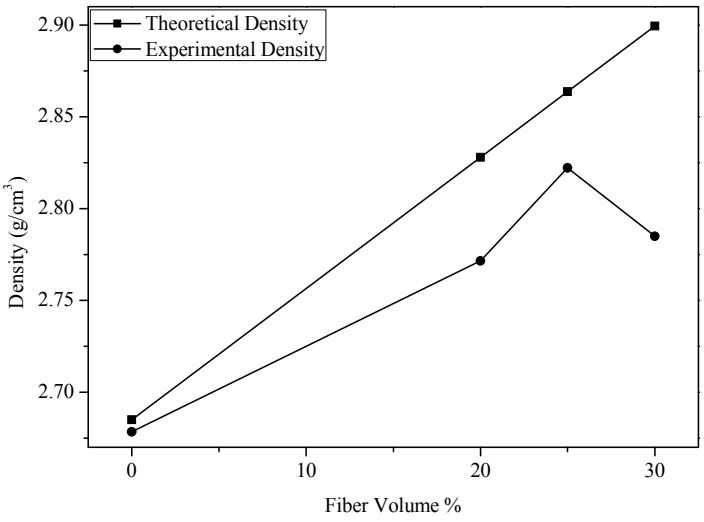

Figure 4.90 Theoretical and experimental densities of AlSi7Mg0.8 matrix composite cast at 750 °C and reinforced by Saffil fibers

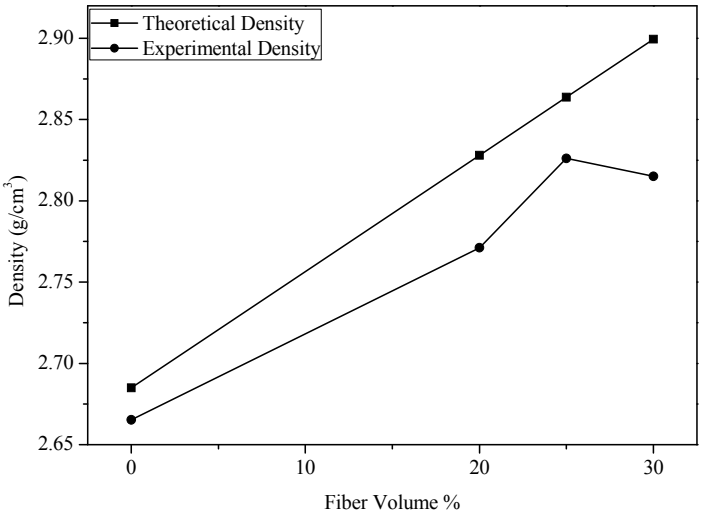

Figure 4.91 Theoretical and experimental densities of AlSi7Mg0.8 matrix composite cast at 800 °C and reinforced by Saffil fibers

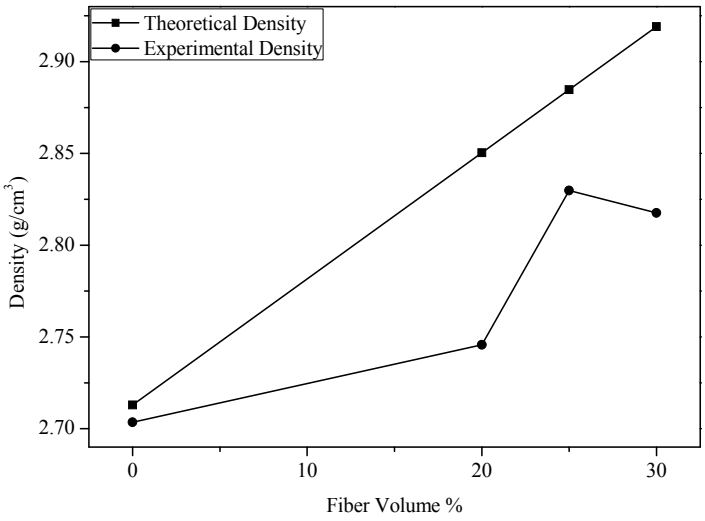

Figure 4.92 Theoretical and experimental densities of AlSi10Mg0.8 matrix composite cast at 750 °C and reinforced by Saffil fibers

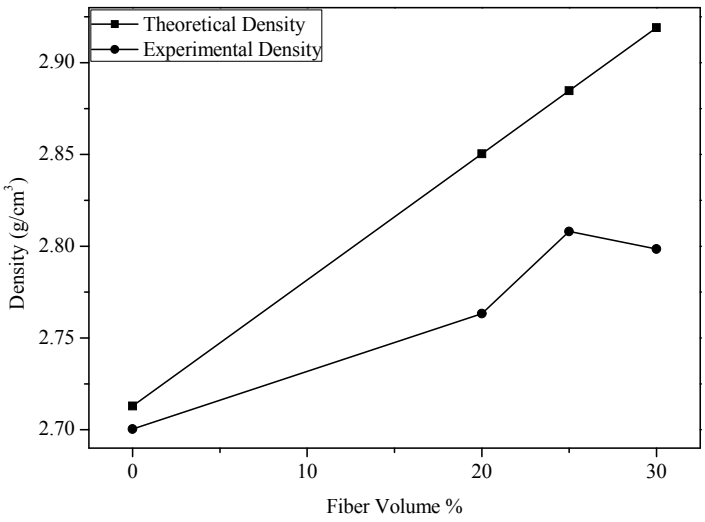

Figure 4.93 Theoretical and experimental densities of AlSi10Mg0.8 matrix composite cast at 800 °C and reinforced by Saffil fibers

From the figures it is seen that theoretical density values are always greater than the experimental density values. This difference is the evidence of micro-porosities exists in the composite structure. This is mainly related to high pressures needed to infiltrate the porous preforms [30].

The difference between the theoretical and the experimental density values is the highest in 30 vol% fiber reinforced composites. This is mainly due to the increasing fiber cross-links and interaction in the preforms. As fiber cross-links and interaction increases, porosity level of the composite increases. In addition to cross-link effect, movement of fibers also enhances the micro-porosities in the specimens. Application of the force results movement of the fibers.

4.5 Insertion Casting

Insertion casting was conducted to have final components for automotive and defense applications. In the following figures, sample parts for automotive and defense applications can be seen.

Figure 4.94 Components obtained from insertion casting for automotive applications

Figure 4.95 Components obtained from insertion casting for defense applications

Insertion casting operation was performed by the use of 100 tons capacity vertical press. Setting the die temperature to 200 °C and molten temperature to 800 °C resulted reasonable interface between insert/backing alloy.

Many difficulties observed in the insertion casting operation. Insertion casting was not successful for all the components for every time. First of all, insert dimensions became the major struggling parameter in the casting. In the die cavity, gap between the mold cavity and the insert determined the backing alloy's covering ability of the insert. This situation was observed especially for the small components, i.e. defense applications. In the case of large gaps between the insert and the die cavity, i.e. automotive applications, this impediment effects were not observed. However, during the insertion casting operation of the automotive parts, another difficulty was observed for the squeeze casting operation. Although there were enough gaps between the insert and the mold cavity for the backing alloy to

caver the insert, thin sections of the die cavity close to the inserts caused the backing alloy eruption from the die. In spite of the difficulties faced during insertion casting, appropriate insert/backing alloy interfaces were obtained. By introducing smaller inserts to the small parts and avoiding thin sections of the die cavity, insertion casting of these parts could be achieved excellent degree of casting. In the following figure a more suitable sketch of the insert for the small parts can be seen.

Figure 4.96 Sample drawing of the more suitable inserts for the defense application parts

CHAPTER 5

CONCLUSION

In the present study, the following conclusions can be drawn after investigating the effects of silicon content of the matrix alloy, vol% of the fiber and infiltration temperature on mechanical behavior and physical properties of Saffil alumina short fiber reinforced aluminum matrix metal matrix composites together with the effects on insert/component interface.

1. Detailed microstructure analyses conducted by SEM showed that micro-porosity could be observed in the cross-links of the fiber network as expected. SEM micrographs also showed that an appropriate fiber/matrix interface due to existence of pulled fibers in the fracture surface was achieved under the squeeze casting parameters of the experiments. Moreover to the existence of the pulled-out fibers, non-existence of broken fibers in the fracture surface also stood for the appropriate fiber/matrix interface.

2. Image analyses showed that an appropriate insert/backing alloy interface had been achieved. Moreover, there no fiber damage or displacement was observed by the phase analyses of the microstructures of the composites. Results were also close to the theoretical values of the composites both from the vertical and parallel to the fiber orientation. Deviation of the experimental values from the theoretical values was in the range of 0.57% to 5.14%.

3. Three point bending test results indicated that increasing the fiber content caused to increase flexural strength values of the composites. AlSi10Mg0.8 alloy matrix composites reinforced with 30 vol% Saffil fibers had the highest strength values. Compared to non-reinforced alloy 169 MPa increase in flexural strength value was obtained for AlSi10Mg0.8 matrix composites infiltrated at 750 °C and reinforced with 30 vol% Saffil fibers. 23% increase was gained compared to non-reinforced alloy.

4. The effect of the infiltration temperature showed different conclusion for AlSi10Mg0.8 and AlSi7Mg0.8 alloy matrix composites. For AlSi10Mg0.8 matrix composites lower infiltration temperature favored higher strength values due to smaller grain sizes of the matrix alloy. However for AlSi7Mg0.8 alloy matrix composites, except 20 vol% reinforced ones, lower infiltration temperature caused lower strength values due to higher solidus temperature characteristic due to its alloy content that had decreased infiltration ability of the alloy.

5. The effect of the amount of silicon in the matrix alloy was determined that AlSi10Mg0.8 alloy showed higher flexural strength values than AlSi7Mg0.8 alloy. The difference was 168 MPa and 194 MPa for 750 °C and 800 °C squeeze casting temperatures respectively.

6. Hardness results increased by increasing the fiber volume fraction of the composites.

7. XRD analyses of preforms showed that preforms were mainly composed of delta alumina. XRD analyses also showed that there had been no phase other than alumina fiber and aluminum matrix alloy.

8. Density measurements revealed that difference between theoretical and experimental values of composites' density results was increase as the fiber

content increase. The maximum difference was obtained for 30 vol% fiber reinforced composites. Contrary to the theoretical values, 30 vol% fiber reinforced composites showed lower density results than the 25 vol% fiber reinforced ones. This was mainly due to the increasing the fiber cross-links which caused the micro-porosity level to increase and air build up in front of the liquid front.

9. Fiber efficiency of the composites was calculated. The results showed that highest fiber efficiency was obtained from AlSi10Mg0.8/20vol%Saffil reinforced and squeeze cast at 750 °C composite as 0.96 and the lowest efficiency was obtained from AlSi7Mg0.8/30vol%Saffil reinforced and squeeze cast at 800 °C composite as 0.59. The reason why higher fiber efficiency was almost 1.00 for AlSi10Mg0.8/20vol%Saffil reinforced and squeeze cast at 750 °C composite was the Mg content of the matrix. Mg content of the matrix alloy were the most efficient parameter for the composite reinforced 20 vol% Saffil fibers at the corresponding experimental parameters.

10. Image analyses results of the insertion casting operation showed that a complete insert/backing alloy interface was achieved. It was observed that most important parameters of the insertion casting operation were the gap between the die cavity and the insert, and thin cross cross-section of the die cavity near the insert. Avoiding thin sections of the die together with large gaps between insert and the die cavity could yield even better insert/component interface.

REFERENCES

1. K.K. Chawla, *Composite Materials Science and Engineering*. 2nd Edition ed. 1998, New-York: Springer-Verlag.

2. D.D.L. Chung, *Composite Materials: Functional Materials for Modern Technologies*. 2003, London: Springer-Verlag.

3. K.U. Kainer, ed. *Metal Matrix Composites Custom-made Materials for Automotive and Aerospace Engineering*. 2006, WILEY-VCH Verlag GmbH & Co. KGaA: Weinheim.

4. N. Chawla and K.K. Chawla, *Metal Matrix Composites*. 2006, New York: Springer Science+Business Media, Inc.

5. S. Suresh, A. Mortensen, and A. Needleman, eds. *Fundamentals of Metal Matrix Composites*. 1993, Butterworth-Heinemann: Boston.

6. P.K. Rohatgi, *Metal-matrix Composites.* Defence Science Journal, 1993. **43**: p. 329-349.

7. D.B. Miracle and S.L. Donaldson, eds. *Composites*. ASM Handbook. Vol. 21. 2001, ASM International.

8. V.V. Vasilev and E. Morozov, *Advanced Mechanics of Composite Materials*. 2007, Elsevier Science B.V.

9. S.T. Mileiko, *Metal and Ceramic Based Composites*. Composite Materials Series. Vol. 12. 1997, Amsterdam: Elsevier Science B.V.

10. A. Sundarrajan, A. Mortensen, T.Z. Kattamis, and M.C. Flemings, *Kinetic undercooling in solidification of a hypereutectic Al–Si alloy: Effect of*

solidifying within a ceramic preform composite. Acta Materialia, 1998. **46**: p. 91-99.

11. M. Rodríguez-Reyes, M.I. Pech-Canul, J.C. Rendón-Angeles, and J. López-Cuevas, *Limiting the development of Al_4C_3 to prevent degradation of Al/SiC_p composites processed by pressureless infiltration.* Composites Science and Technology, 2006. **66**: p. 1056–1062.

12. F. Gul and M. Acilar, *Effect of the reinforcement volume fraction on the dry sliding wear behavior of Al–10Si/SiCp composites produced by vacuum infiltration technique.* Composites Science and Technology, 2004. **64**: p. 1959-1970.

13. E. Carreño-Morelli, T. Cutard, R. Schaller, and C. Bonjour, *Processing and characterization of aluminium-based MMCs produced by gas pressure infiltration.* Materials Science and Engineering A, 1998. **251**: p. 48-57.

14. A. Demir and N. Altinkok, *Effect of gas pressure infiltration on microstructure and bending strength of porous Al_2O_3/SiC-reinforced aluminum matrix composites.* Composites Science and Technology, 2004. **64**: p. 2067-2074.

15. O. Beffort, S. Long, C. Cayron, J. Kuebler, and P.A. Buffat, *Alloying effects on microstructure and mechanical properties of high volume fraction of SiC-particule reinforced Al-MMCs made by squeeze casting infiltration.* Composites Science and Technology, 2007. **67**: p. 737-745.

16. Q. Zhang, G. Wu, G. Chen, L. Jiang, and B. Luan, *The thermal expansion and mechanical properties of high reinforcement content SiCp/Al composites fabricated by squeeze casting technology.* Composites: Part A, 2003. **34**: p. 1023-1027.

17. T. Matsunaga, K. Matsuda, T. Hatayama, K. Shinozaki, and M. Yoshida, *Fabrication of continuous carbon fiber-reinforced aluminum–magnesium alloy composite wires using ultrasonic infiltration method.* Composites: Part A, 2007. **38**: p. 1902-1911.

18. T. Matsunaga, K. Ogata, T. Hatayama, K. Shinozaki, and M. Yoshida, *Effect of acoustic cavitation on ease of infiltration of molten aluminum alloys into carbon fiber bundles using ultrasonic infiltration method.* Composites: Part A, 2007. **38**: p. 771-778.

19. P. Rohatgi, ed. *Solidification of Metal Matrix Composites*. 1990, The Minerals, Metals & Materials Society: Warrendale.

20. J.R. Davis, ed. *Aluminum and Aluminum Alloys*. ASM Handbook. 1993, ASM International: Ohio.

21. S.C. Kurnaz, *Production of saffil fiber reinforced Zn-Al (ZA 12) base metal matrix composites using infiltration technique and study of their properties.* Materials Science and Engineering A, 2003. **346**: p. 108-115.

22. S. Nagarajan, B. Dutta, and M.K. Surappa, *The effect of SiC particles on the size and morphology of eutectic silicon in cast A356/SiCp composites.* Composites Science and Technology, 1999. **59**: p. 897-902.

23. J.L. Murray and A.J. McAlister, *The Al-Si (Aluminum-Silicon) System.* Journal of Phase Equilibria, 1984. **5**: p. 74-84.

24. S. Amini, S. Javadpour, M.S. Jamshidi, and S. Amini, *Manufacturing and Property Evaluation of A356/SAFFIL and Hybrid A356/(SiCP+SAFFIL) Composites via Squeeze Casting Process*, in *Proceeding of the Conference of Metallurgists*. 2003: Vancuver , Canada.

25. K.K. Chawla, *Ceramic Matrix Composites*. 1993, London: Chapman & Hall.

26. N.P. Cheremisinoff, ed. *Sythesis and Properties*. Handbook of Ceramics and Composites. Vol. 1. 1990, Marcel Dekker, Inc.: New York.

27. H. Fredriksson and U. Åkerlind, *Materials Processing during Casting*. 2006, West Sussex: John Wiley & Sons Ltd.

28. D.M. Stefanescu, *Science and Engineering of Casting Solidification*. 2002, New York: Kluwer Academic / Plenum Publishers.

29. P. Rohatgi, *Foundry Processing of Metal Matrix Composites.* Modern Casting, 1988. **78**: p. 47-50.

30. A. Mortensen, L.J. Masur, J.A. Cornie, and M.C. Flemings, *Infiltration of Fibrous Preforms by a Pure Metal: Part I. Theory.* Metallurgical Transactions A, 1989. **20**: p. 2535-2547.

31. Ö. Keleş, *Production and Characterization of Saffil Alumina Fiber Reinforced Squeeze Cast Aluminum Matrix Composites*, in *Metallurgical and Materials Engineering*. 2008, Middle East Technical University: Ankara.

32. T. Choh and T. Oki, *Wettability of silicon carbide by aluminum and aluminum alloy.* Materials Science and Technology, 1987. **3**: p. 378-385.

33. R. Warren and C.-H. Andersson, *Silicon carbide fibres and their potential for use in composite materials. II.* Composites, 1984. **15**: p. 101-111.

34. M. Fishkis, *Interface and fracture surface in Saffil/Al-Cu-Mg metal matrix composites.* Journal of Materials Sicience, 1991: p. 2651-2661.

35. A. Mortensen and I. Jin, *Solidification processing of metal matrix composites.* International Materials Reviews, 1992. **37**: p. 101-128.

36. D.L. McDanels, *Tungsten fiber reinforced copper matrix composites.* Metallurgical Transactions A, 1965. **223**: p. 636-642.

37. C.M. Friend, *The effect of matrix properties on reinforcement in short alumina fiber – aluminum metal matrix composites.* Journal of Materials Sicience, 1987. **22**: p. 3005-3010.

38. H. Lianxi, Y. Yiwen, L. Shoujing, and X. Xinying, *Investigation on the kinetics of infiltration of liquid aluminum into an alumina fibrous preform.* Journal of Materials Processing Technology, 1999. **94**: p. 227-230.

Appendix A: Spectral Analyses of the Matrix Alloys

Table A.1 Spectrometer analyses of AlSi7Mg0.8 matrix composites infiltrated at 800 °C

Element	Point 1	Point 2	Point 3	Average
Al	91.8	91.9	91.7	91.8
Si	7.0	6.9	7.0	7.0
Fe	0.191	0.173	0.182	0.182
Cu	0.0031	0.0033	0.0034	0.0033
Mn	0.0010	0.0010	0.0010	0.0010
Mg	0.827	0.830	0.852	0.836
Zn	0.0050	0.0050	0.0050	0.0050
Cr	0.0044	0.0050	0.0026	0.0040
Ni	0.0050	0.0050	0.0050	0.0050
Ti	0.0867	0.0885	0.0878	0.0877
Be	0.0001	0.0001	0.0001	0.0001
Ca	0.0005	0.0005	0.0005	0.0005
Li	0.0001	0.0001	0.0001	0.0001
Pb	0.0020	0.0020	0.0020	0.0020
Sn	0.0100	0.0100	0.0100	0.0100
Sr	0.0084	0.0085	0.0091	0.0087
V	0.0136	0.0139	0.0126	0.0134
Na	0.0005	0.0005	0.0005	0.0005
Bi	0.0050	0.0050	0.0050	0.0050
Zr	0.0020	0.0020	0.0020	0.0020
B	0.0015	0.0014	0.0015	0.0015
Ga	0.0154	0.0168	0.0169	0.0164
Cd	0.0010	0.0010	0.0010	0.0010
Co	0.0030	0.0030	0.0030	0.0030
Ag	0.0010	0.0010	0.0010	0.0010
Hg	0.0030	0.0030	0.0030	0.0030
In	0.0020	0.0020	0.0020	0.0020

Table A.2 Spectrometer analyses of AlSi7Mg0.8 matrix composites infiltrated at 750 °C

Element	Point 1	Point 2	Point 3	Average
Al	91.4	91.3	91.1	91.3
Si	7.3	7.3	7.6	7.4
Fe	0.230	0.217	0.218	0.222
Cu	0.0068	0.0051	0.0040	0.0053
Mn	0.0010	0.0010	0.0010	0.0010
Mg	0.776	0.934	0.809	0.840
Zn	0.0050	0.0050	0.0050	0.0050
Cr	0.0125	0.0083	0.0077	0.0095
Ni	0.0050	0.0050	0.0050	0.0050
Ti	0.1730	0.1660	0.1510	0.1633
Be	0.0001	0.0001	0.0001	0.0001
Ca	0.0005	0.0005	0.0005	0.0005
Li	0.0001	0.0001	0.0001	0.0001
Pb	0.0020	0.0020	0.0020	0.0020
Sn	0.0100	0.0100	0.0100	0.0100
Sr	0.0209	0.0230	0.0187	0.0209
V	0.0184	0.0173	0.0181	0.0179
Na	0.0005	0.0005	0.0005	0.0005
Bi	0.0050	0.0050	0.0050	0.0050
Zr	0.0020	0.0020	0.0020	0.0020
B	0.0083	0.0080	0.0053	0.0072
Ga	0.0221	0.0235	0.0214	0.0223
Cd	0.0010	0.0010	0.0010	0.0010
Co	0.0030	0.0030	0.0030	0.0030
Ag	0.0010	0.0010	0.0010	0.0010
Hg	0.0030	0.0030	0.0030	0.0030
In	0.0020	0.0020	0.0020	0.0020

Table A.3 Spectrometer analyses of AlSi10Mg0.8 matrix composites infiltrated at 750 °C

Element	Point 1	Point 2	Point 3	Average
Al	88.4	88.4	88.4	88.4
Si	10.5	10.4	10.4	10.4
Fe	0.177	0.174	0.170	0.174
Cu	0.0032	0.0031	0.0035	0.0033
Mn	0.0010	0.0010	0.0010	0.0010
Mg	0.774	0.765	0.778	0.772
Zn	0.0050	0.0050	0.0050	0.0050
Cr	0.0041	0.0036	0.0034	0.0037
Ni	0.0050	0.0050	0.0050	0.0050
Ti	0.0822	0.0824	0.0845	0.0830
Be	0.0001	0.0001	0.0001	0.0001
Ca	0.0007	0.0005	0.0005	0.0006
Li	0.0001	0.0001	0.0001	0.0001
Pb	0.0025	0.0020	0.0020	0.0022
Sn	0.0100	0.0100	0.0100	0.0100
Sr	0.0076	0.0071	0.0076	0.0074
V	0.0130	0.0141	0.0128	0.0133
Na	0.0005	0.0005	0.0005	0.0005
Bi	0.0050	0.0050	0.0050	0.0050
Zr	0.0020	0.0020	0.0020	0.0020
B	0.0011	0.0014	0.0017	0.0014
Ga	0.0160	0.0150	0.0149	0.0153
Cd	0.0010	0.0010	0.0010	0.0010
Co	0.0030	0.0030	0.0030	0.0030
Ag	0.0010	0.0010	0.0010	0.0010
Hg	0.0030	0.0030	0.0030	0.0030
In	0.0020	0.0020	0.0020	0.0020

Table A.4 Spectrometer analyses of AlSi10Mg0.8 matrix composites infiltrated at 750 °C

Element	Point 1	Point 2	Point 3	Average
Al	88.4	88.3	88.2	88.3
Si	10.4	10.5	10.6	10.5
Fe	0.178	0.178	0.176	0.177
Cu	0.0034	0.0030	0.0029	0.0031
Mn	0.0010	0.0010	0.0010	0.0010
Mg	0.757	0.727	0.751	0.745
Zn	0.0050	0.0050	0.0050	0.0050
Cr	0.0040	0.0058	0.0044	0.0047
Ni	0.0050	0.0050	0.0050	0.0050
Ti	0.0971	0.0953	0.0938	0.0954
Be	0.0001	0.0001	0.0001	0.0001
Ca	0.0005	0.0005	0.0005	0.0005
Li	0.0001	0.0001	0.0001	0.0001
Pb	0.0020	0.0020	0.0020	0.0020
Sn	0.0100	0.0100	0.0100	0.0100
Sr	0.0040	0.0036	0.0037	0.0038
V	0.0119	0.0128	0.0131	0.0126
Na	0.0005	0.0005	0.0005	0.0005
Bi	0.0050	0.0050	0.0050	0.0050
Zr	0.0020	0.0020	0.0020	0.0020
B	0.0025	0.0023	0.0025	0.0024
Ga	0.0173	0.0141	0.0153	0.0156
Cd	0.0010	0.0010	0.0010	0.0010
Co	0.0030	0.0030	0.0030	0.0030
Ag	0.0010	0.0010	0.0010	0.0010
Hg	0.0030	0.0030	0.0030	0.0030
In	0.0020	0.0020	0.0020	0.0020

Appendix B: Details of the Squeeze Casting Operation

Table B.1 Squeeze casting parameters of AlSi7Mg0.8 alloy matrix inserts

Temp. of Infiltration (°C)	Temp. of Lower Mold (°C)	Temp. of Upper Mold (°C)	Temp. of Preform (°C)	Temp. of Molten Metal (°C)	Vol% of the Reinforcement
750	200	196	-	751	0 vol%
	226	205	195	755	20 vol%
	195	184	220	749	25 vol%
	192	190	215	752	30 vol%
800	190	188	-	802	0 vol%
	172	165	180	800	20 vol%
	185	180	218	805	25 vol%
	188	179	200	801	30 vol%

Table B.2 Squeeze casting parameters of AlSi7Mg0.8 alloy matrix three point bending test specimens

Temp. of Infiltration (°C)	Temp. of Lower Mold (°C)	Temp. of Upper Mold (°C)	Temp. of Preform (°C)	Temp. of Molten Metal (°C)	Vol% of the Reinforcement
750	200	196	-	751	0 vol%
	226	205	195	755	20 vol%
	195	184	220	749	25 vol%
	192	190	215	752	30 vol%
800	175	175	-	803	0 vol%
	172	170	200	813	20 vol%
	173	170	204	810	25 vol%
	174	175	210	803	30 vol%

Table B.3 Squeeze casting parameters of AlSi10Mg0.8 alloy matrix three point bending test specimens

Temp. of Infiltration (°C)	Temp. of Lower Mold (°C)	Temp. of Upper Mold (°C)	Temp. of Preform (°C)	Temp. of Molten Metal (°C)	Vol% of the Reinforcement
750	203	201	-	751	0 vol%
	179	180	222	756	20 vol%
	188	184	210	749	25 vol%
	198	189	211	753	30 vol%
800	201	200	-	810	0 vol%
	186	183	224	805	20 vol%
	183	175	211	796	25 vol%
	182	186	200	804	30 vol%

Table B.4 Squeeze casting parameters of AlSi10Mg0.8 alloy matrix inserts

Temp. of Infiltration (°C)	Temp. of Lower Mold (°C)	Temp. of Upper Mold (°C)	Temp. of Preform (°C)	Temp. of Molten Metal (°C)	Vol% of the Reinforcement
750	199	200	-	750	0 vol%
	198	194	225	760	20 vol%
	184	180	220	757	25 vol%
	193	197	206	747	30 vol%
800	185	190	-	800	0 vol%
	185	188	227	805	20 vol%
	174	170	220	808	25 vol%
	182	176	220	805	30 vol%

Appendix C: Reports of the Image Analyses

Table C.1 Image analysis result of AlSi7Mg0.8/20 vol% Saffil composite infiltrated at 750 °C from parallel to the fiber orientation

MICROSTRUCTURE TEST REPORT

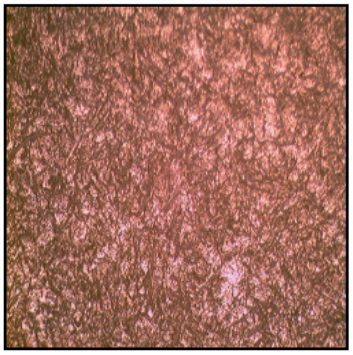

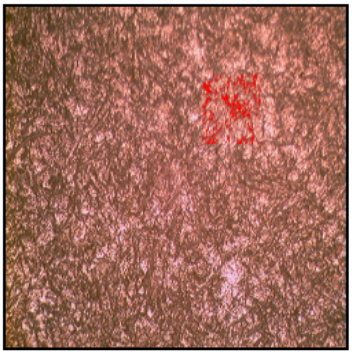

PHASE AND VOLUME ANALYSIS

SNo	NAME	AREA	AREA_PER
1	Phase 1	7376.116 Micron Sqr	20.071

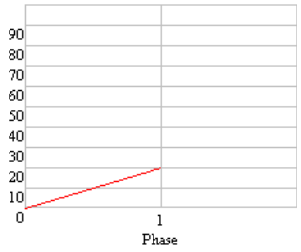

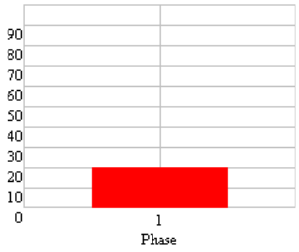

Table C.2 Image analysis result of AlSi7Mg0.8/20vol%Saffil composite infiltrated at 750 °C from vertical to the fiber orientation

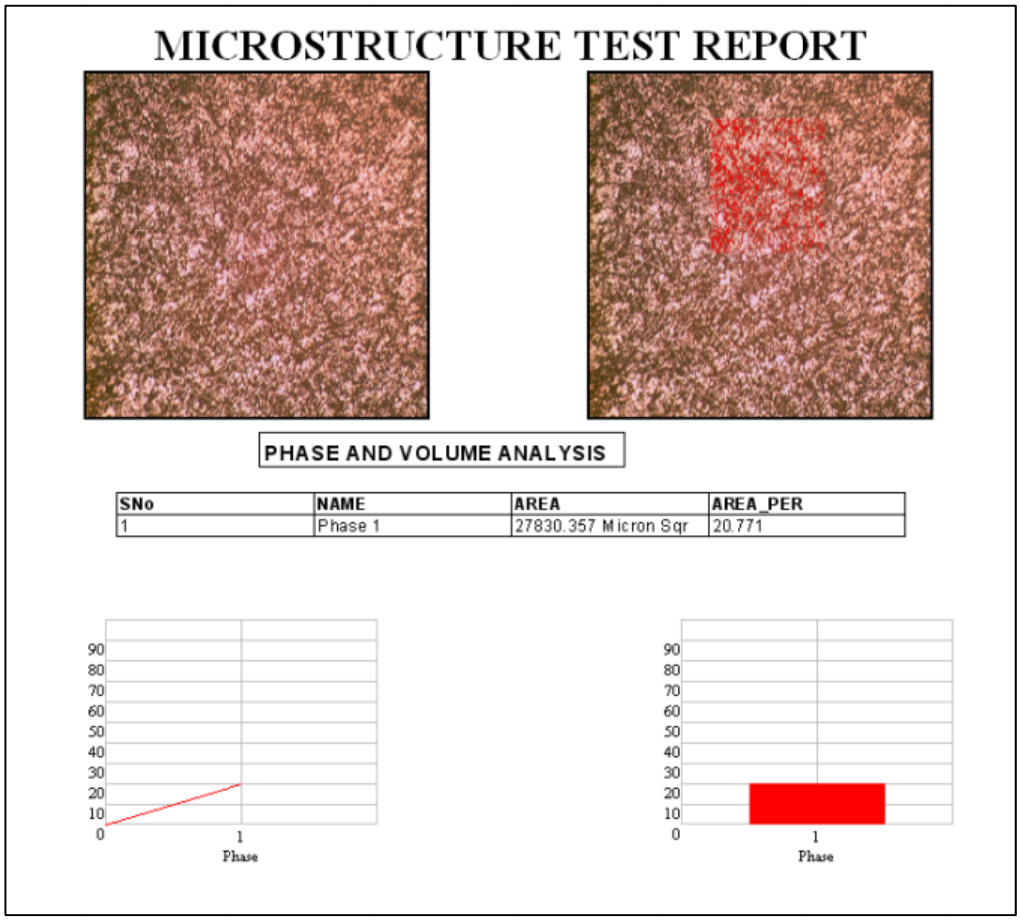

Table C.3 Image analysis result of AlSi7Mg0.8/25vol%Saffil composite infiltrated at 750 °C from parallel to the fiber orientation

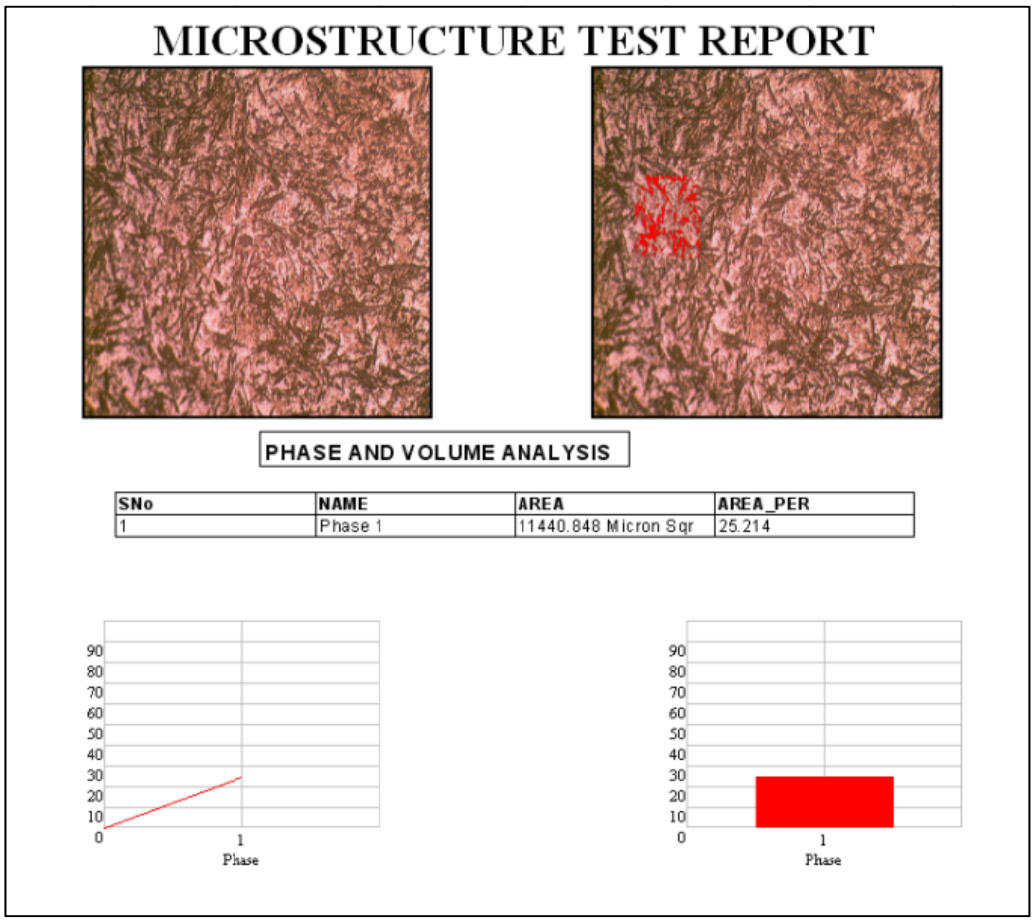

Table C.4 Image analysis result of AlSi7Mg0.8/25vol%Saffil composite infiltrated at 750 °C from vertical to the fiber orientation

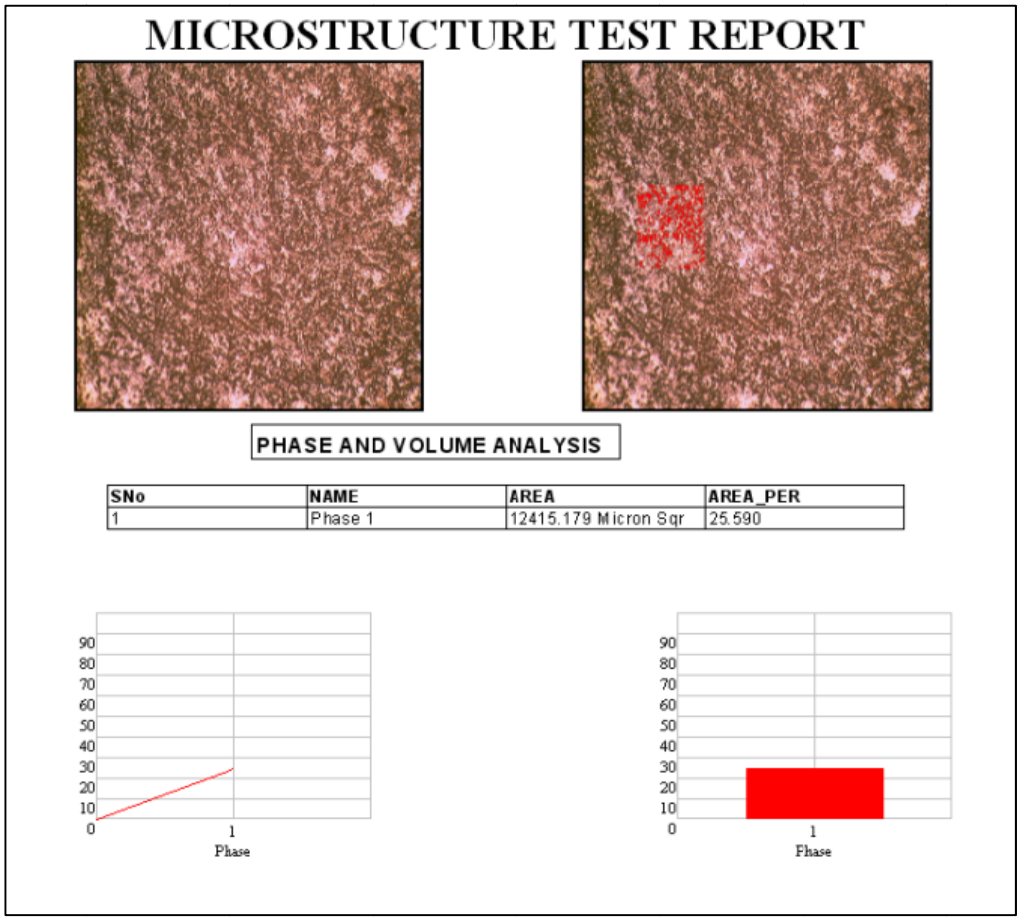

Table C.5 Image analysis result of AlSi7Mg0.8/30 vol% Saffil composite infiltrated at 750 °C from parallel to the fiber orientation

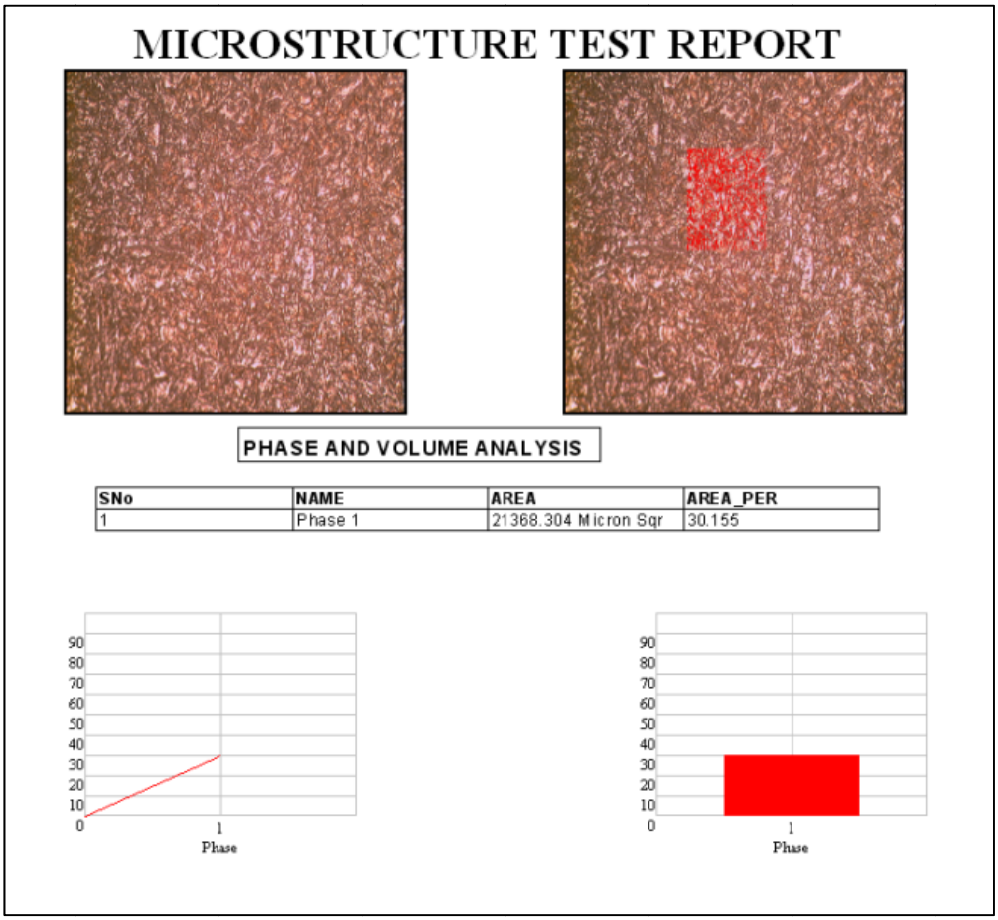

Table C.6 Image analysis result of AlSi7Mg0.8/30vol%Saffil composite infiltrated at 750 °C from vertical to the fiber orientation

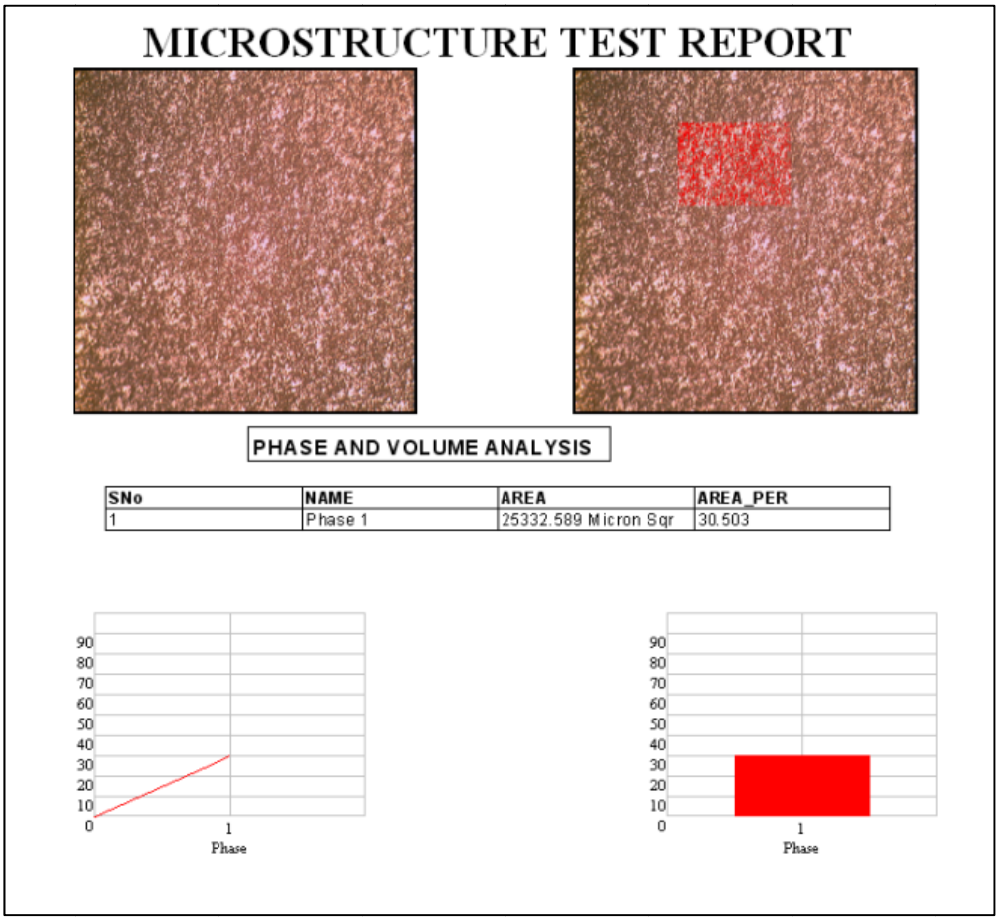

Table C.7 Image analysis result of AlSi7Mg0.8/20 vol% Saffil composite infiltrated at 800 °C from parallel to the fiber orientation

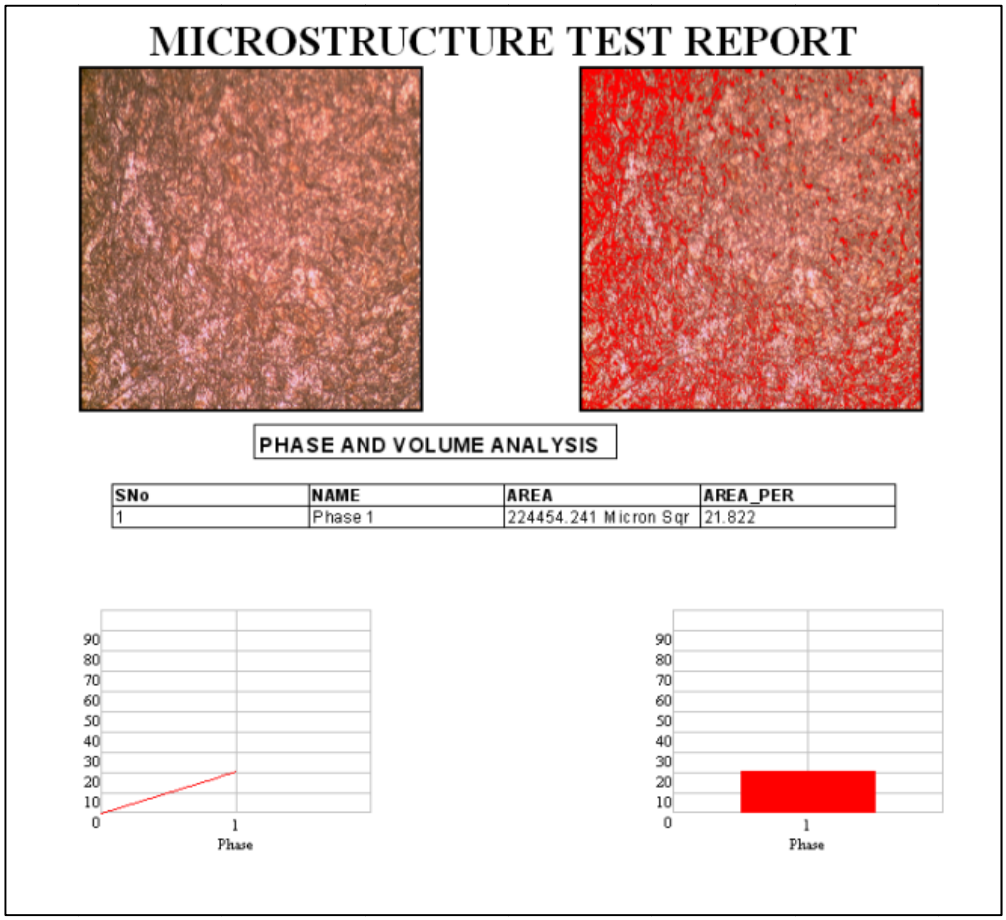

Table C.8 Image analysis result of AlSi7Mg0.8/20 vol% Saffil composite infiltrated at 800 °C from vertical to the fiber orientation

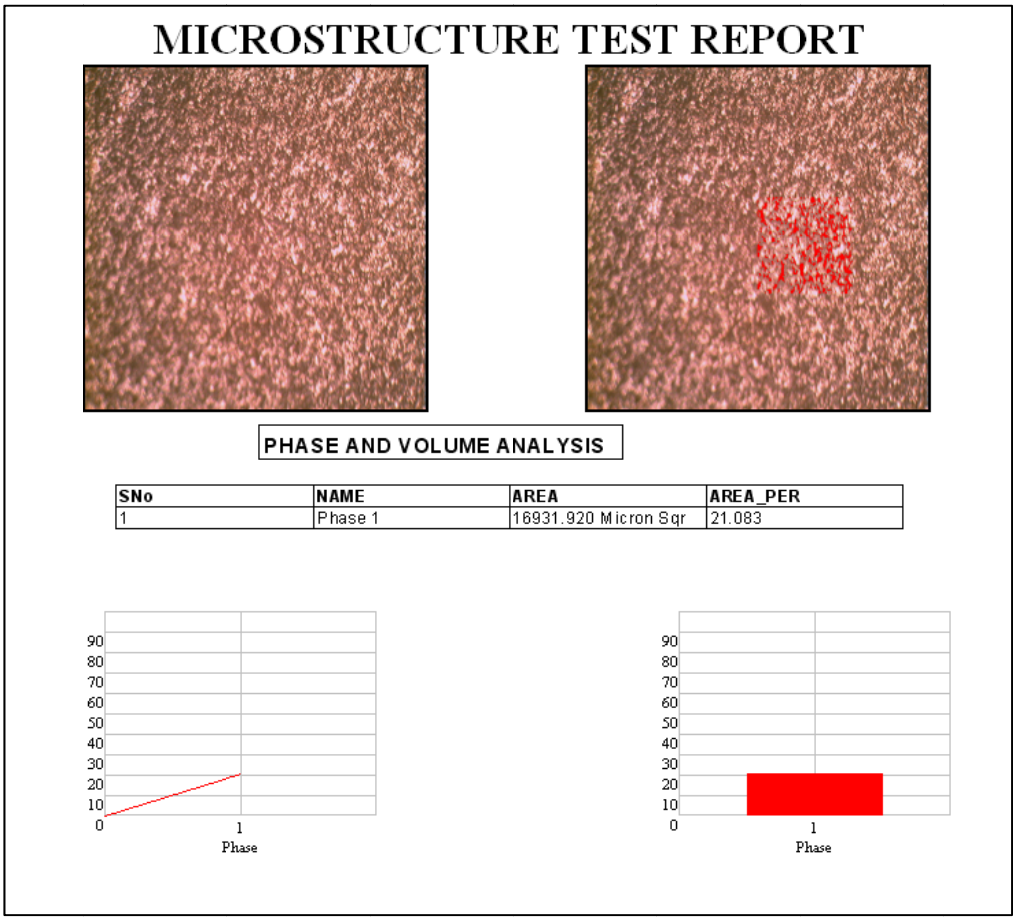

Table C.9 Image analysis result of AlSi7Mg0.8/25vol%Saffil composite infiltrated at 800 °C from parallel to the fiber orientation

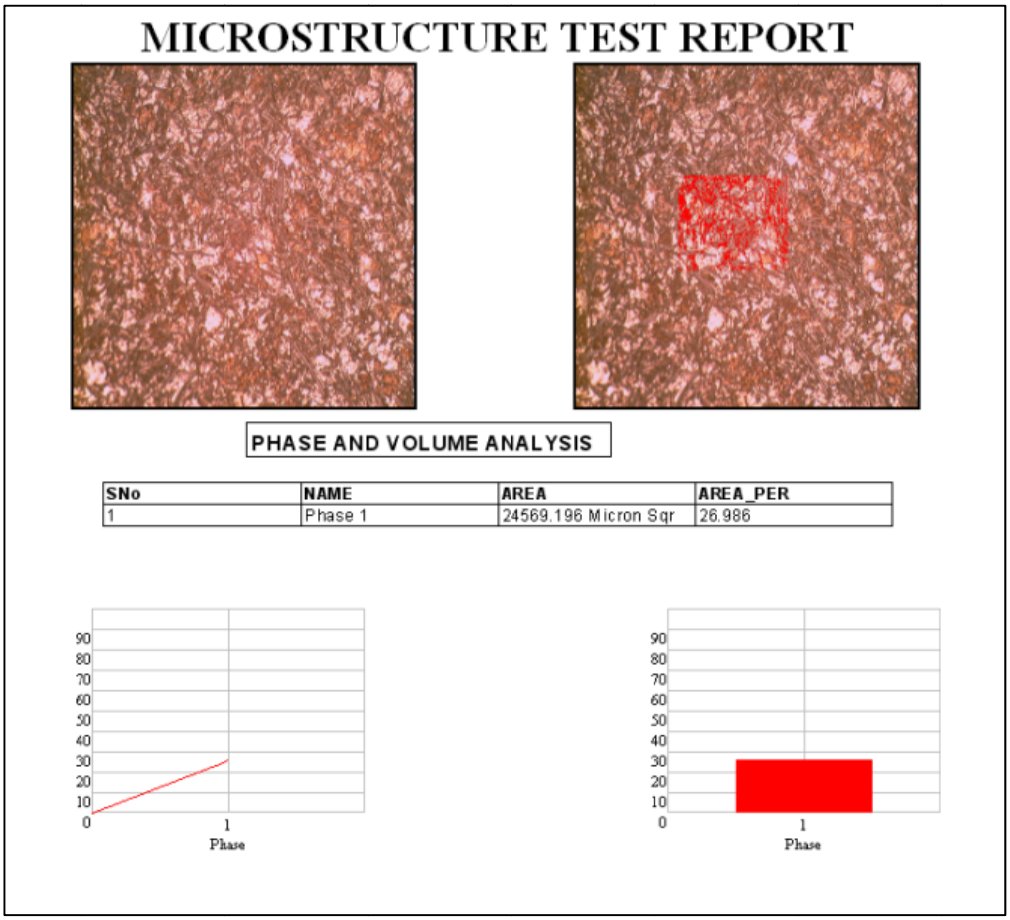

Table C.10 Image analysis result of AlSi7Mg0.8/25vol%Saffil composite infiltrated at 800 °C from vertical to the fiber orientation

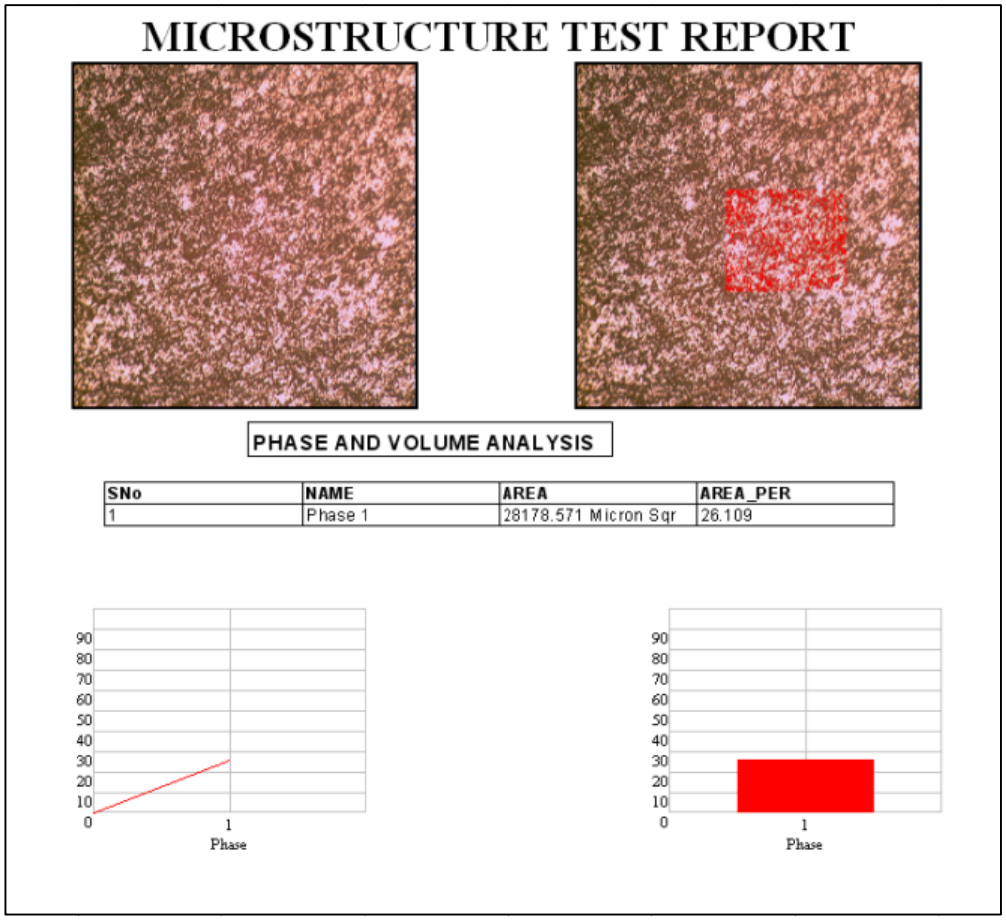

Table C.11 Image analysis result of AlSi7Mg0.8/30vol%Saffil composite infiltrated at 800 °C from parallel to the fiber orientation

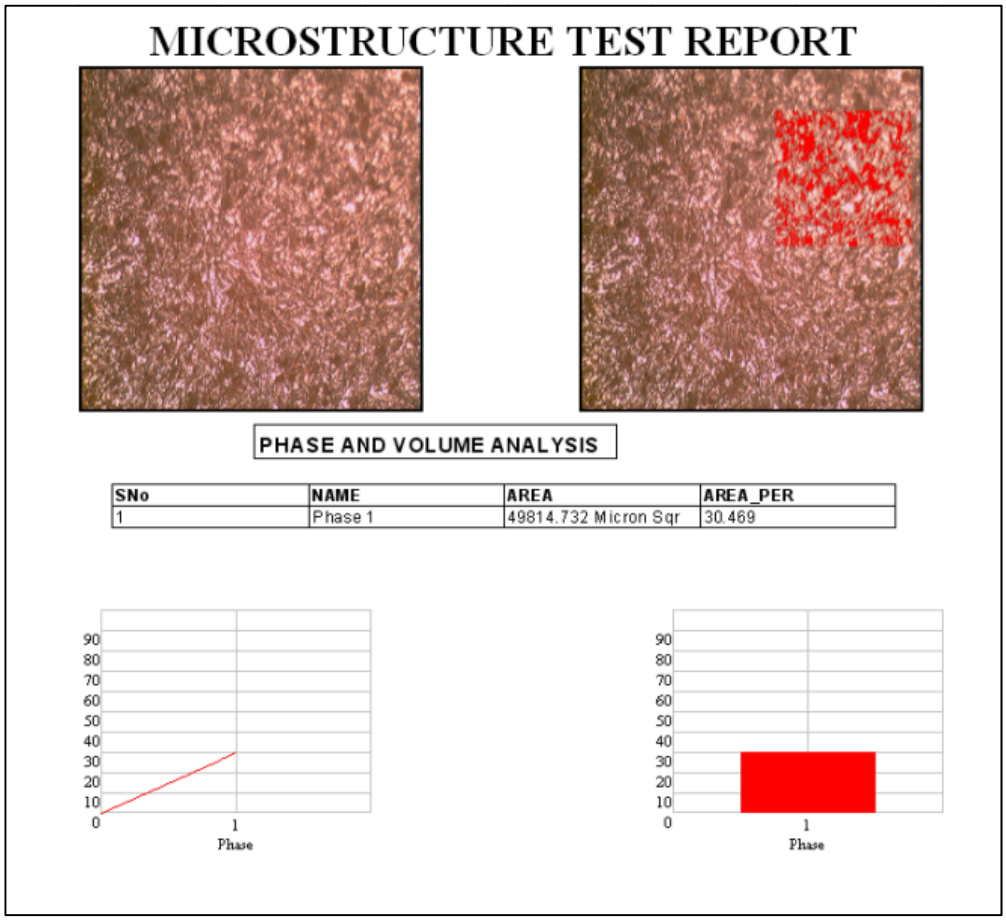

Table C.12 Image analysis result of AlSi7Mg0.8/30 vol% Saffil composite infiltrated at 800 °C from vertical to the fiber orientation

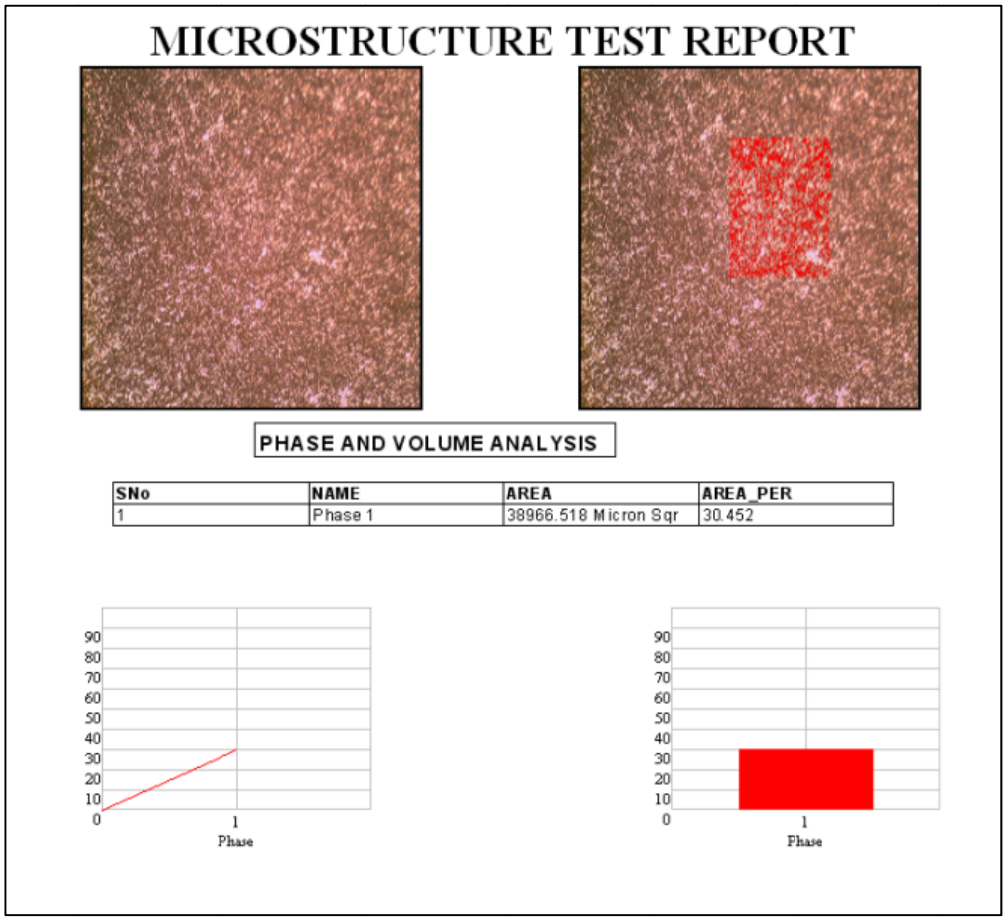

Table C.13 Image analysis result of AlSi10Mg0.8/20vol%Saffil composite infiltrated at 750 °C from parallel to the fiber orientation

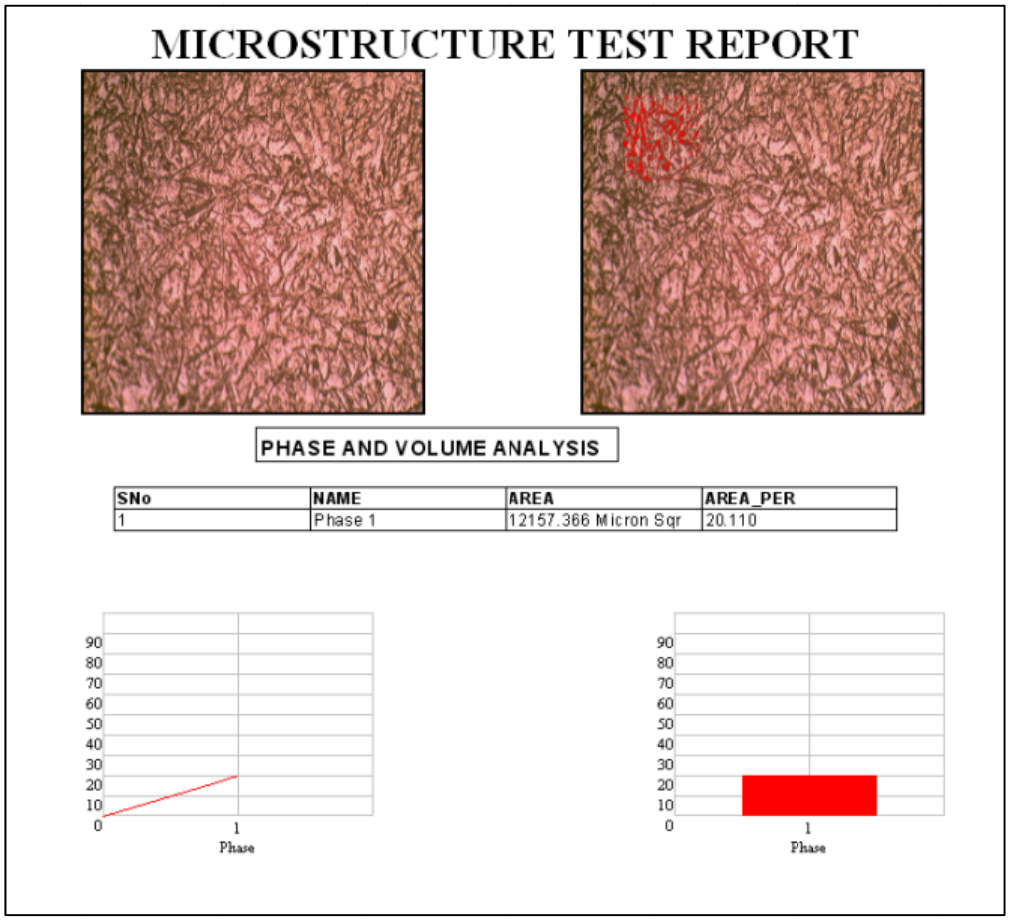

Table C.14 Image analysis result of AlSi10Mg0.8/20vol%Saffil composite infiltrated at 750 °C from vertical to the fiber orientation

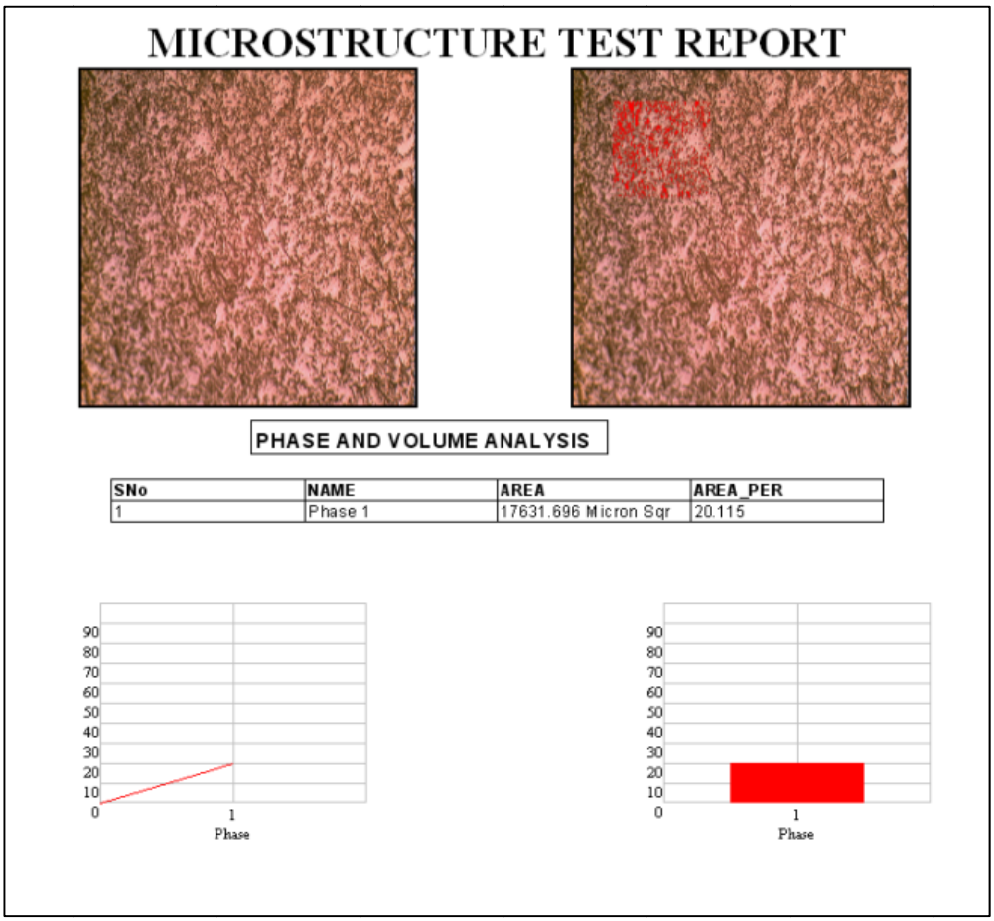

Table C.15 Image analysis result of AlSi10Mg0.8/25vol%Saffil composite infiltrated at 750 °C from parallel to the fiber orientation

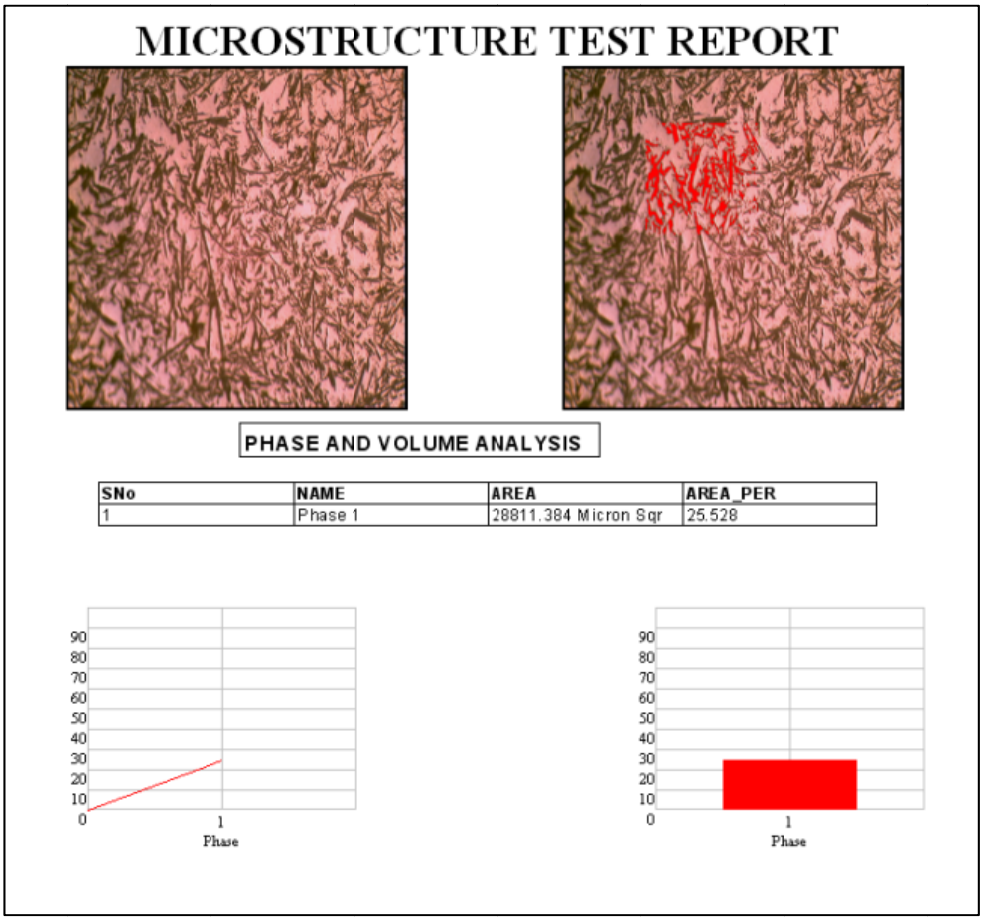

Table C.16 Image analysis result of AlSi10Mg0.8/25vol%Saffil composite infiltrated at 750 °C from vertical to the fiber orientation

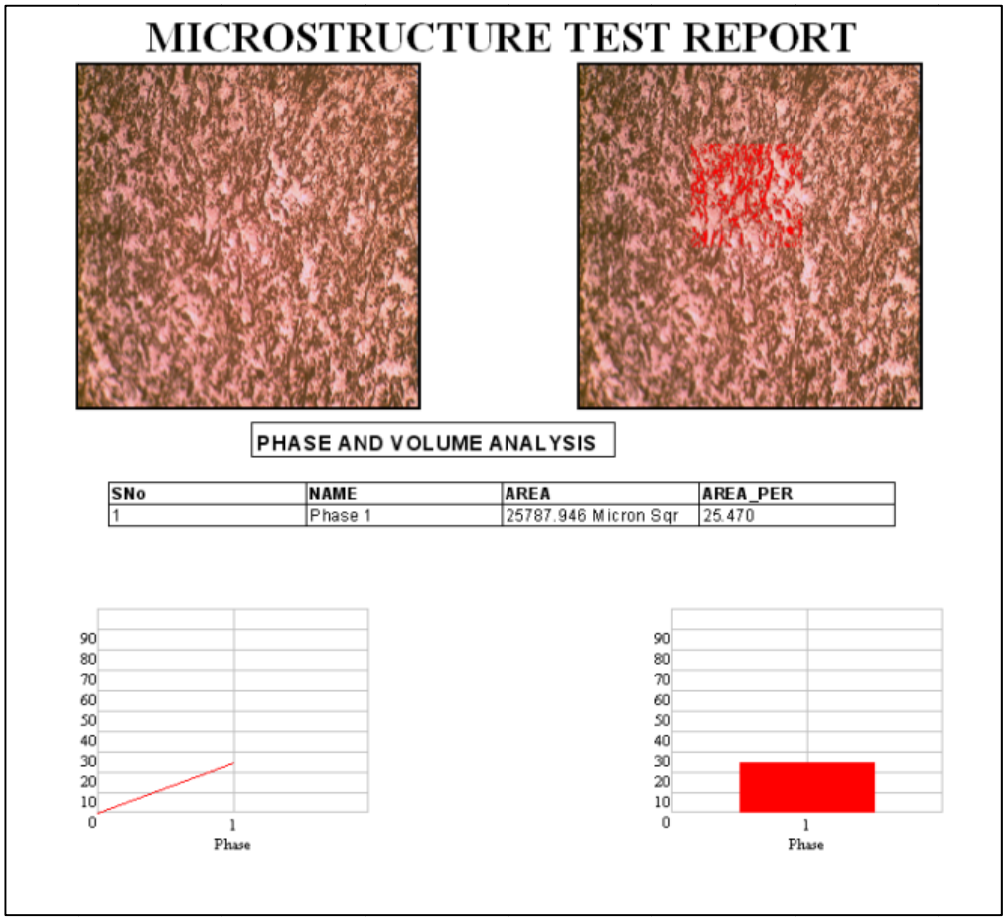

Table C.17 Image analysis result of AlSi10Mg0.8/30vol%Saffil composite infiltrated at 750 °C from parallel to the fiber orientation

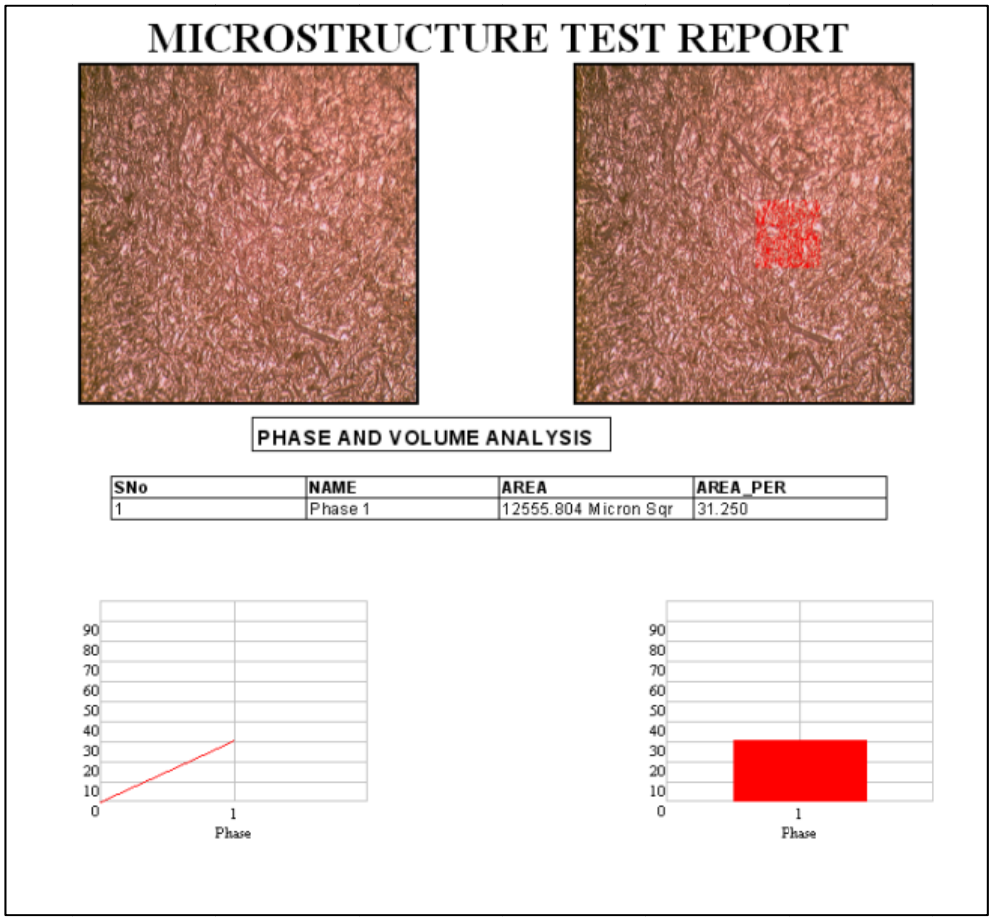

Table C.18 Image analysis result of AlSi10Mg0.8/30vol%Saffil composite infiltrated at 750 °C from vertical to the fiber orientation

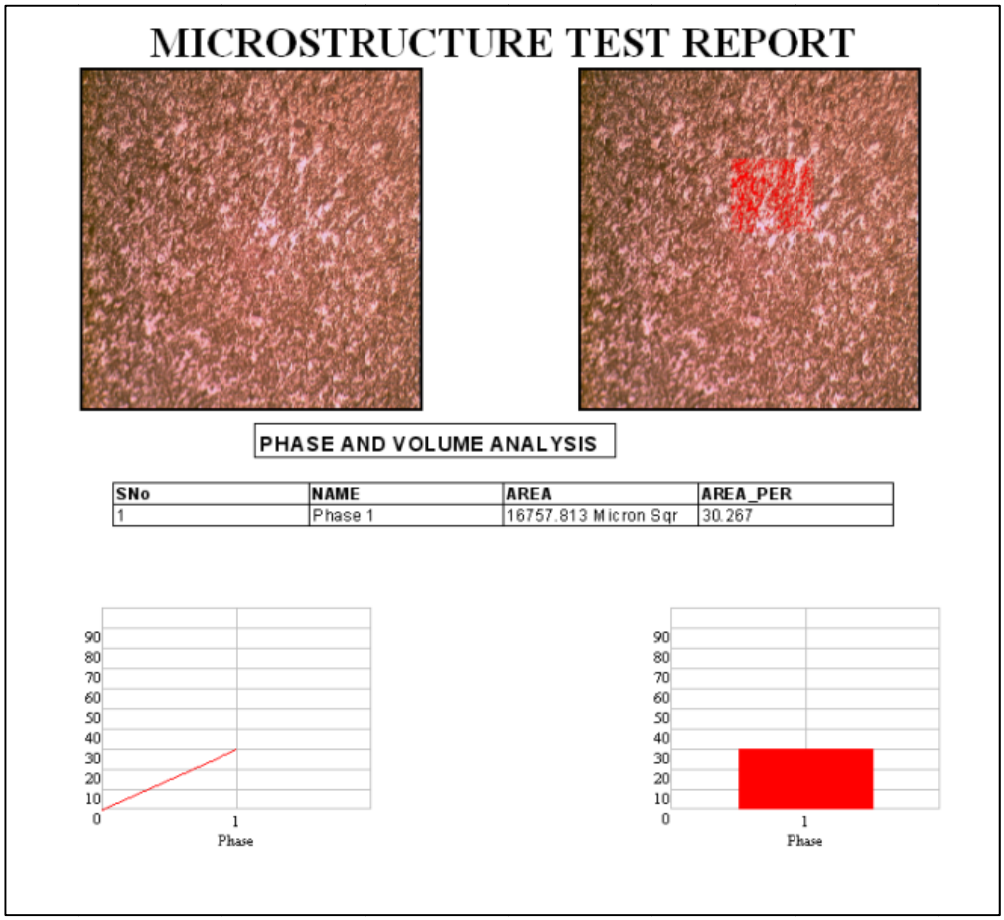

Table C.19 Image analysis result of AlSi10Mg0.8/20vol%Saffil composite infiltrated at 800 °C from parallel to the fiber orientation

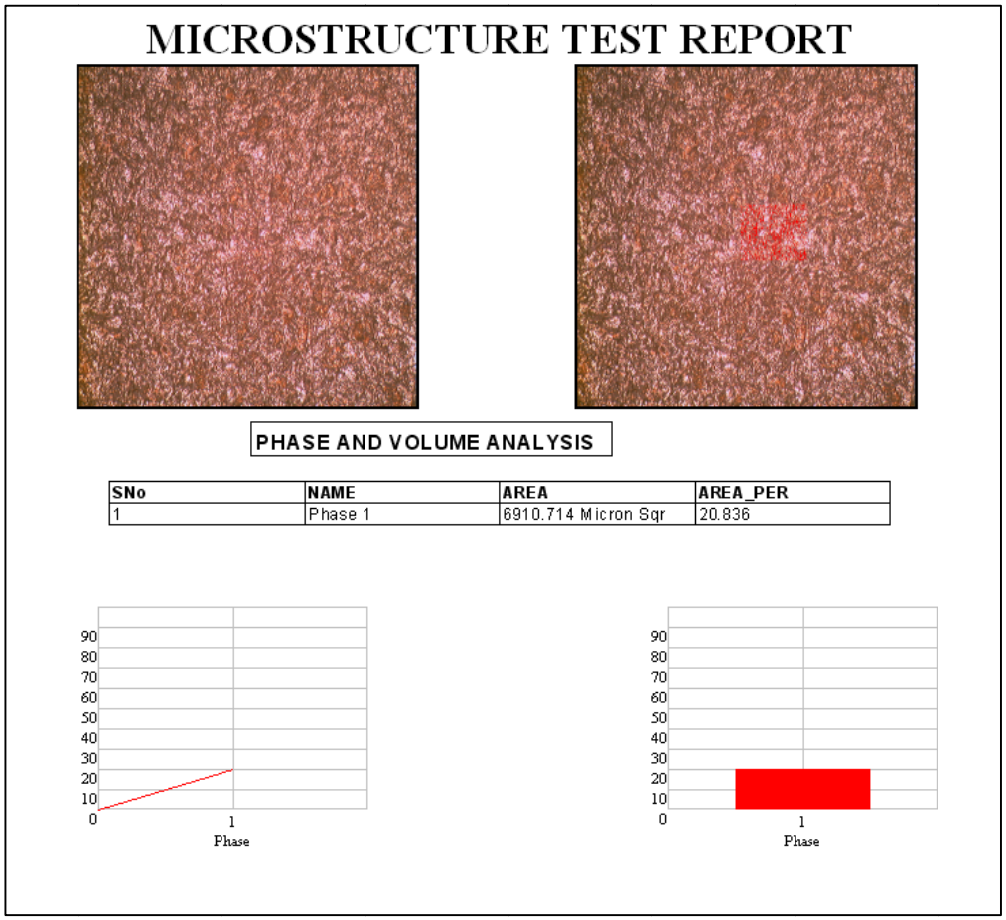

Table C.20 Image analysis result of AlSi10Mg0.8/20vol%Saffil composite infiltrated at 800 °C from vertical to the fiber orientation

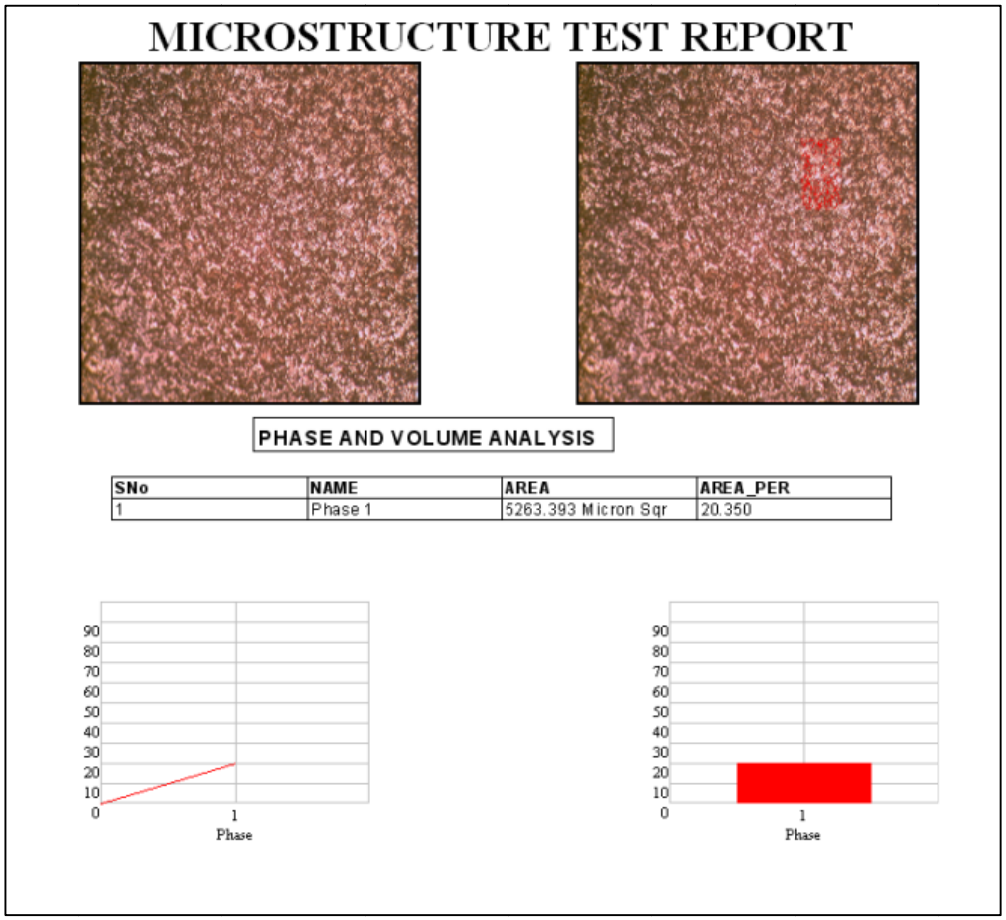

Table C.21 Image analysis result of AlSi10Mg0.8/25vol%Saffil composite infiltrated at 800 °C from parallel to the fiber orientation

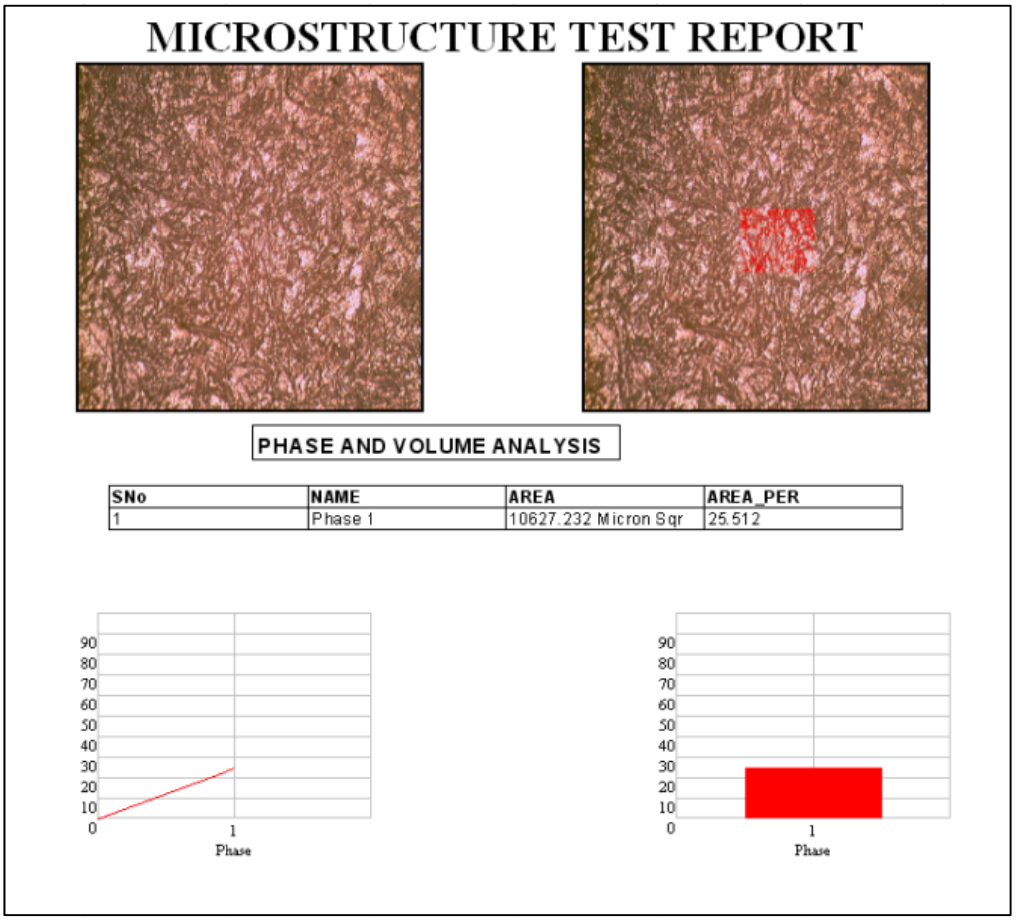

Table C.22 Image analysis result of AlSi10Mg0.8/25vol%Saffil composite infiltrated at 800 °C from vertical to the fiber orientation

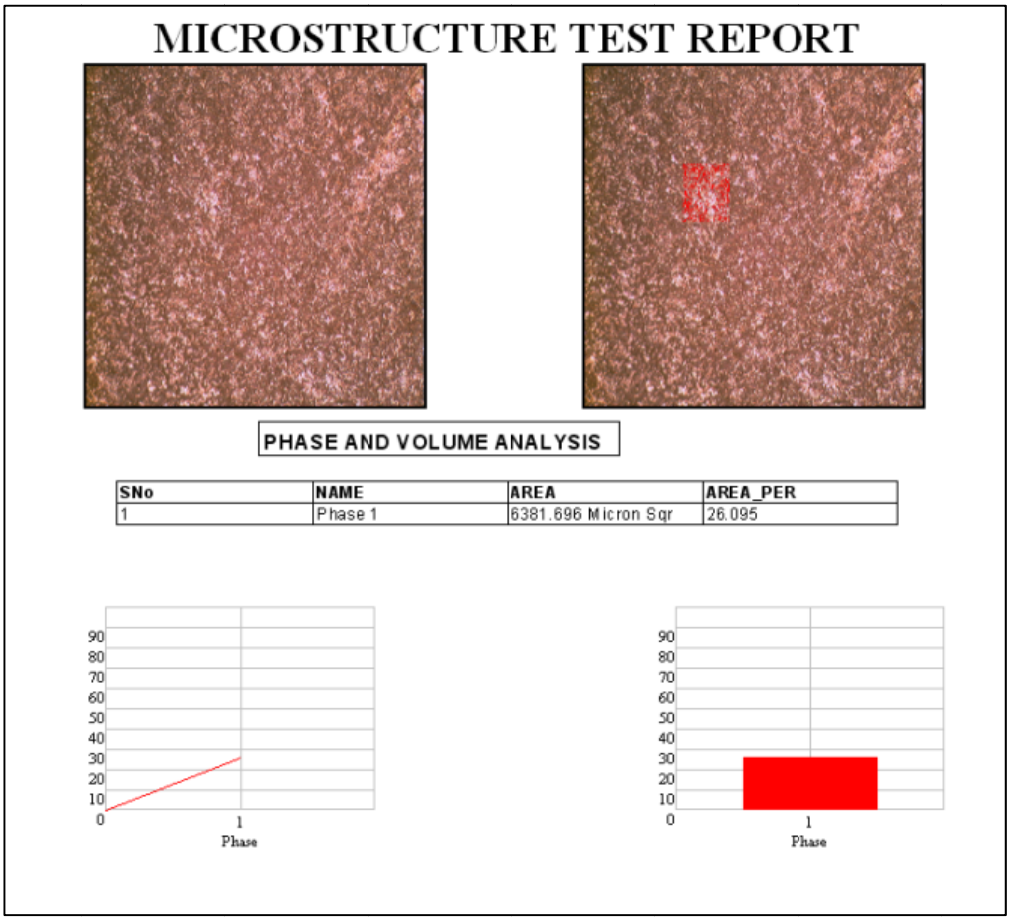

Table C.23 Image analysis result of AlSi10Mg0.8/30vol%Saffil composite infiltrated at 800 °C from parallel to the fiber orientation

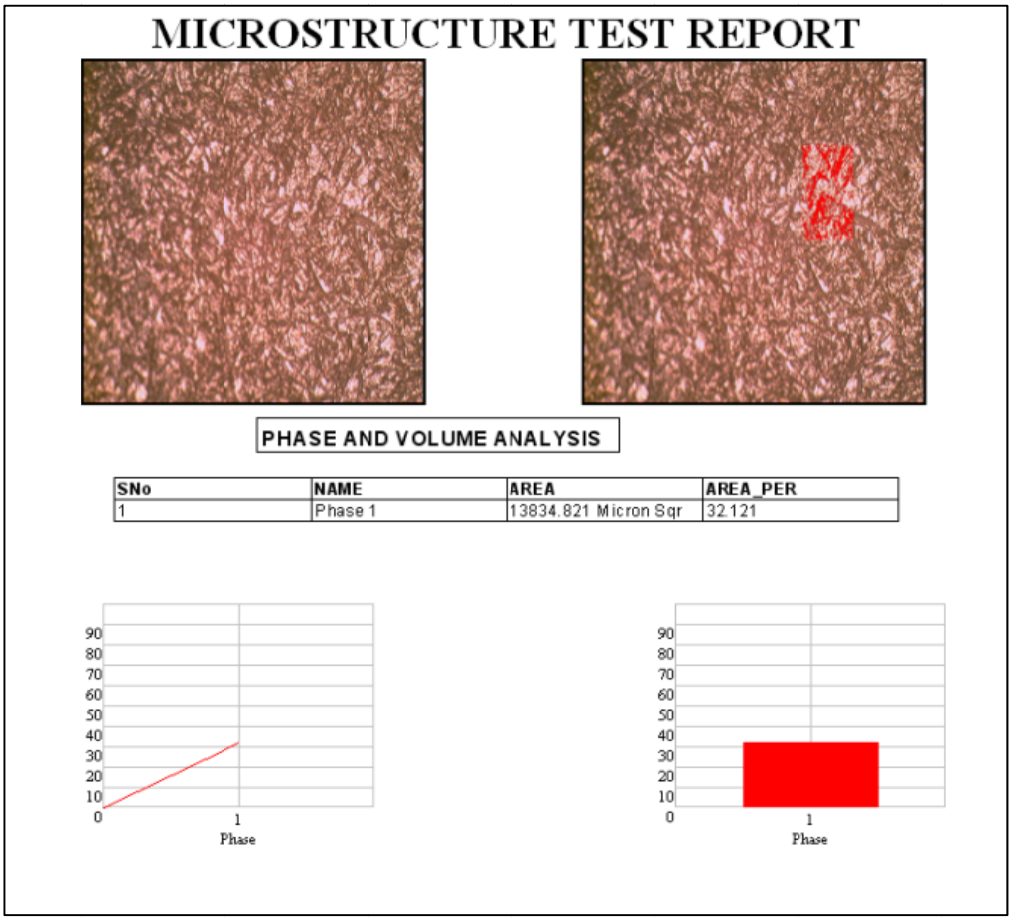

Table C.24 Image analysis result of AlSi10Mg0.8/30vol%Saffil composite infiltrated at 800 °C from vertical to the fiber orientation

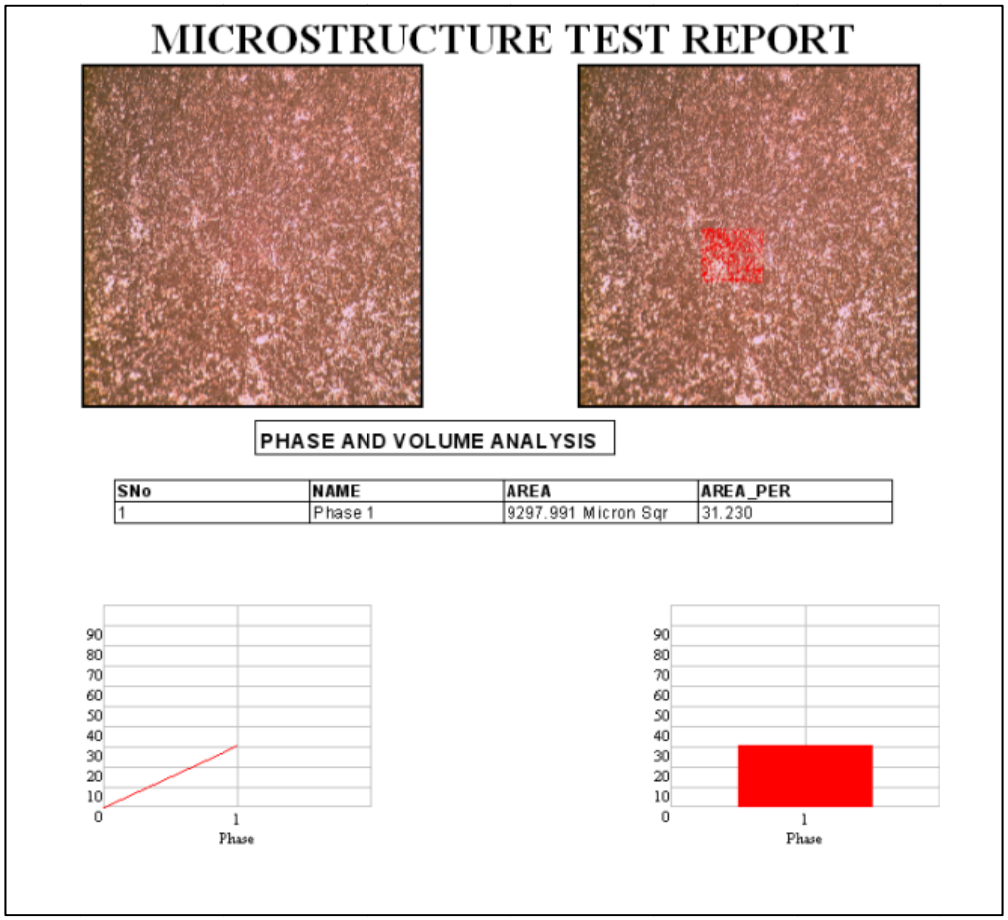

Table C.25 Image analysis result of AlSi10Mg0.8/30vol%Saffil composite insert-component alloy interface at X400 magnification insertion casted at 800 °C

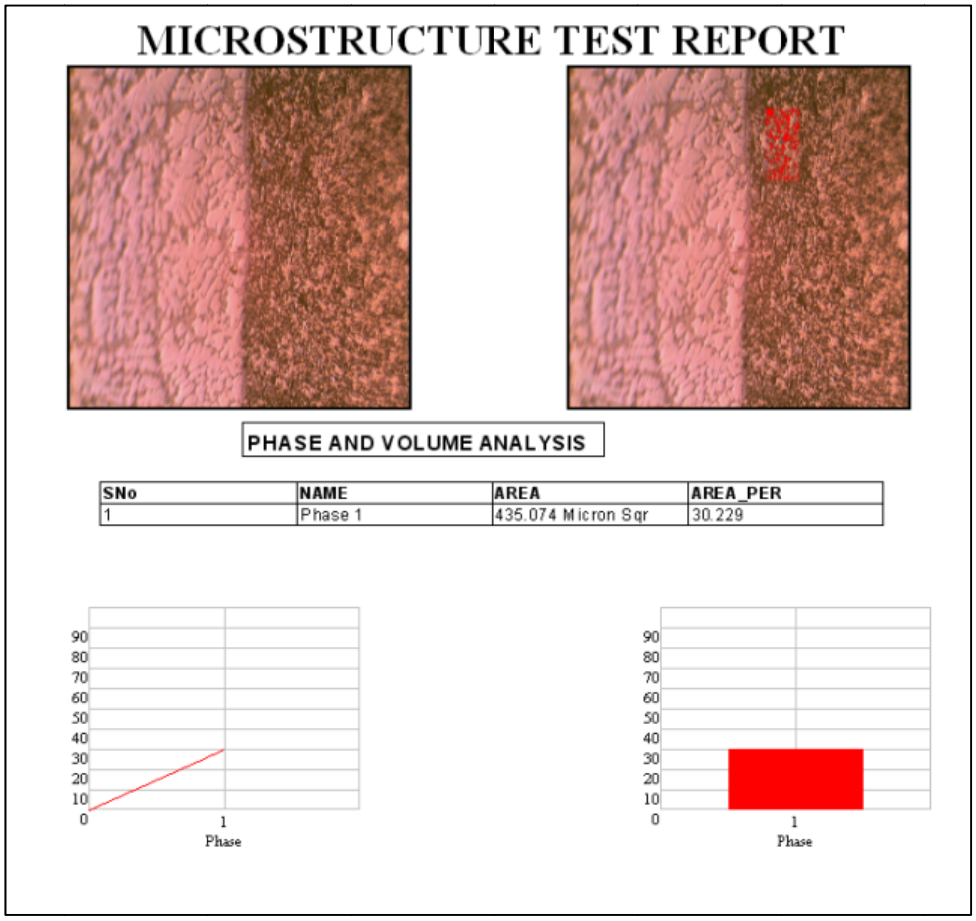

Table C.26 Image analysis result of AlSi10Mg0.8/30vol%Saffil composite insert-component alloy interface at X400 magnification insertion casted at 800 °C

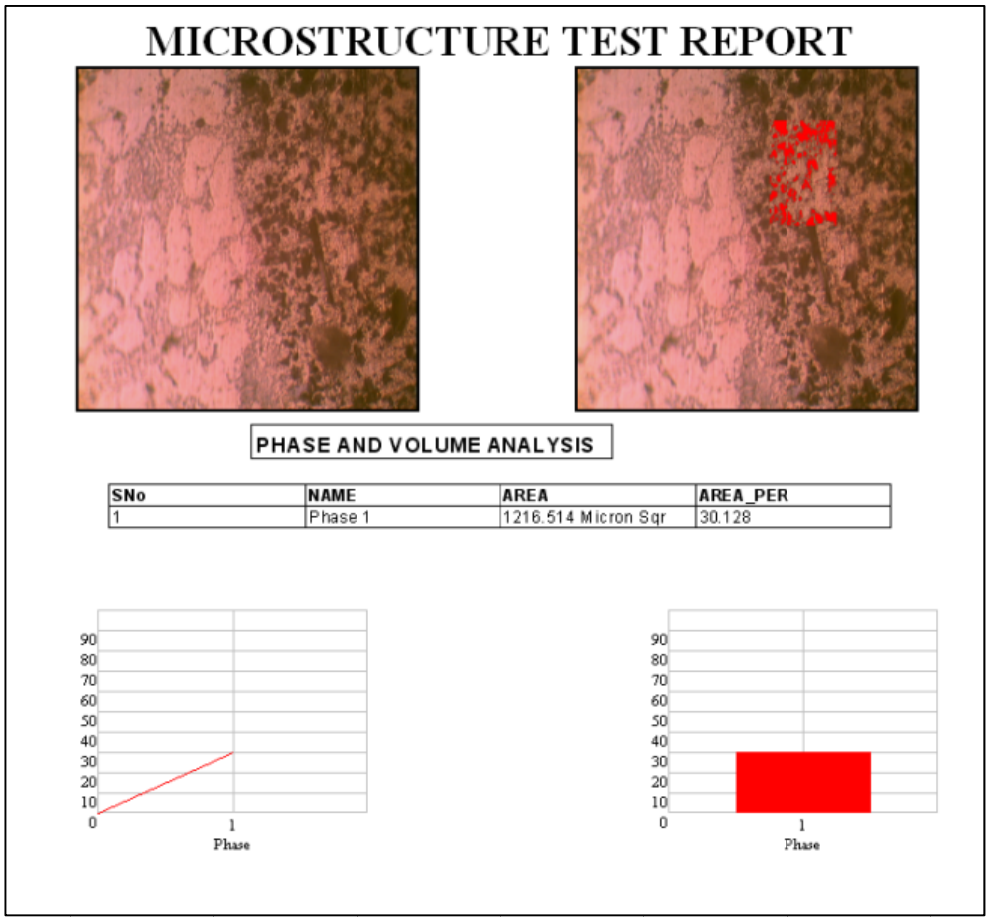

Appendix D: X-Ray Diffraction Cards of Present Phases

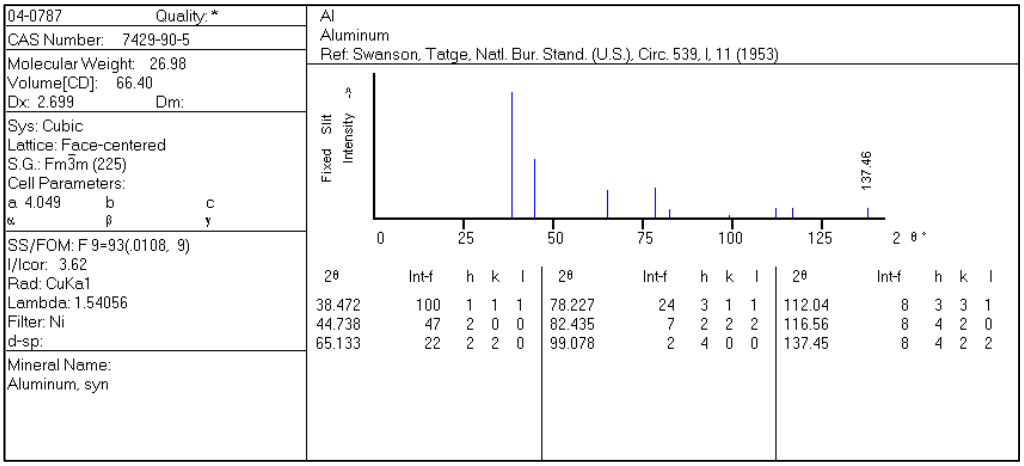

04-0787	Quality: *
CAS Number:	7429-90-5
Molecular Weight:	26.98
Volume[CD]:	66.40
Dx: 2.699	Dm:
Sys: Cubic	
Lattice: Face-centered	
S.G.: Fm3̄m (225)	
Cell Parameters:	
a 4.049	b c
α	β γ
SS/FOM: F 9=93(.0108, 9)	
I/Icor: 3.62	
Rad: CuKa1	
Lambda: 1.54056	
Filter: Ni	
d-sp:	
Mineral Name:	
Aluminum, syn	

Al
Aluminum
Ref: Swanson, Tatge, Natl. Bur. Stand. (U.S.), Circ. 539, I, 11 (1953)

2θ	Int-f	h	k	l	2θ	Int-f	h	k	l	2θ	Int-f	h	k	l
38.472	100	1	1	1	78.227	24	3	1	1	112.04	8	3	3	1
44.738	47	2	0	0	82.435	7	2	2	2	116.56	8	4	2	0
65.133	22	2	2	0	99.078	2	4	0	0	137.45	8	4	2	2

Figure D.1 X-ray details of aluminum

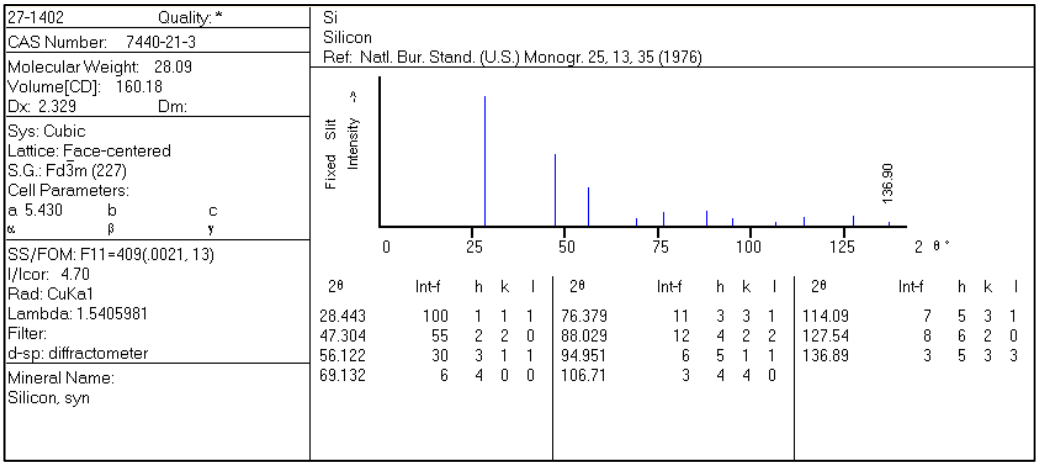

27-1402	Quality: *
CAS Number:	7440-21-3
Molecular Weight:	28.09
Volume[CD]:	160.18
Dx: 2.329	Dm:
Sys: Cubic	
Lattice: Face-centered	
S.G.: Fd3̄m (227)	
Cell Parameters:	
a 5.430	b c
α	β γ
SS/FOM: F11=409(.0021, 13)	
I/Icor: 4.70	
Rad: CuKa1	
Lambda: 1.5405981	
Filter:	
d-sp: diffractometer	
Mineral Name:	
Silicon, syn	

Si
Silicon
Ref: Natl. Bur. Stand. (U.S.) Monogr. 25, 13, 35 (1976)

2θ	Int-f	h	k	l	2θ	Int-f	h	k	l	2θ	Int-f	h	k	l
28.443	100	1	1	1	76.379	11	3	3	1	114.09	7	5	3	1
47.304	55	2	2	0	88.029	12	4	2	2	127.54	8	6	2	0
56.122	30	3	1	1	94.951	6	5	1	1	136.89	3	5	3	3
69.132	6	4	0	0	106.71	3	4	4	0					

Figure D.2 X-ray details of silicon

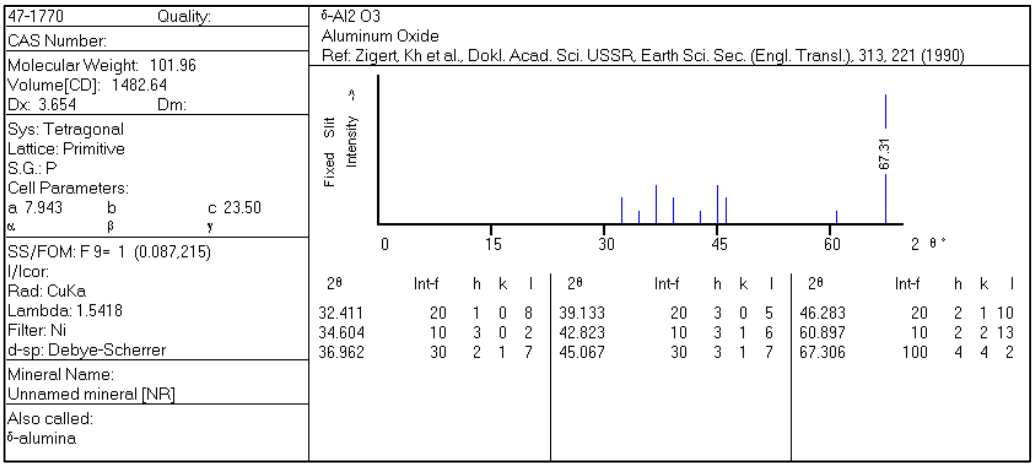

Figure D.3 X-ray details of delta aluminum oxide

Appendix E: Detailed Tabulation of Three Point Bending Test Results

Table E.1 Three point bending test results of AlSi7Mg0.8 matrix composite specimens

Fiber vol%	b (mm)	d (mm)	L (mm)	F (N)	Flexural Strength (MPa)	Av. Flexural Strength	Std. Dev.
0 vol% (@ 750 °C)	9.75	4.91	48.02	2838.00	669.65	570.59	145
0 vol% (@ 750 °C)	9.65	4.81	48.02	2566.00	637.45		
0 vol% (@ 750 °C)	9.65	4.71	48.02	1562.00	404.68		
20 vol% (@ 750 °C)	9.76	4.84	48.02	2343.20	568.42	594.53	59
20 vol% (@ 750 °C)	9.83	4.65	48.02	2119.50	553.07		
20 vol% (@ 750 °C)	9.51	4.57	48.02	2371.00	662.10		
25 vol% (@ 750 °C)	9.71	4.75	48.02	2765.00	699.99	705.89	5
25 vol% (@ 750 °C)	9.81	4.70	48.02	2763.00	707.16		
25 vol% (@ 750 °C)	9.91	4.45	48.02	2514.00	710.52		
30 vol% (@ 750 °C)	9.93	4.65	48.02	3481.00	899.19	740.23	138
30 vol% (@ 750 °C)	9.75	4.57	48.02	2480.00	675.49		
30 vol% (@ 750 °C)	9.86	4.78	48.02	2624.00	646.00		

Table E.1 (Cont'd)

Fiber vol%	b (mm)	d (mm)	L (mm)	F (N)	Flexural Strength (MPa)	Av. Flexural Strength	Std. Dev.
0 vol% (@ 800 °C)	9.67	4.83	48.02	1970.00	484.34	455.15	97
0 vol% (@ 800 °C)	9.65	4.94	48.02	2267.50	534.04		
0 vol% (@ 800 °C)	9.53	4.99	48.02	1485.00	347.09		
20 vol% (@ 800 °C)	9.75	4.98	48.02	2420.00	555.08	566.13	128
20 vol% (@ 800 °C)	9.79	4.88	48.02	2940.00	699.41		
20 vol% (@ 800 °C)	9.76	4.90	48.02	1875.50	443.89		
25 vol% (@ 800 °C)	9.85	4.97	48.02	2892.15	659.29	674.07	93
25 vol% (@ 800 °C)	9.88	4.85	48.02	2468.65	589.15		
25 vol% (@ 800 °C)	9.88	4.77	48.02	3136.15	773.76		
30 vol% (@ 800 °C)	9.74	4.78	48.02	2941.45	733.08	711.62	100
30 vol% (@ 800 °C)	9.71	4.92	48.02	3385.00	798.75		
30 vol% (@ 800 °C)	9.71	4.74	48.02	2372.00	603.04		

Table E.2 Three point bending test results of AlSi10Mg0.8 matrix composite specimens

Fiber vol%	b (mm)	d (mm)	L (mm)	F (N)	Flexural Strength (MPa)	Av. Flexural Strength	Std. Dev.
0 vol% (@ 750 °C)	9.84	4.96	48.02	2764.00	822.42	738.83	73
0 vol% (@ 750 °C)	9.85	4.96	48.02	2383.50	708.48		
0 vol% (@ 750 °C)	9.81	5.02	48.02	2353.00	685.58		
20 vol% (@ 750 °C)	9.83	4.95	48.02	2556.50	764.53	780.23	160
20 vol% (@ 750 °C)	9.87	4.92	48.02	2084.50	628.45		
20 vol% (@ 750 °C)	9.75	4.86	48.02	3030.00	947.72		
25 vol% (@ 750 °C)	9.86	4.76	48.02	2323.40	749.11	865.72	160
25 vol% (@ 750 °C)	9.85	4.82	48.02	3328.00	1047.53		
25 vol% (@ 750 °C)	9.78	4.96	48.02	2674.00	800.52		
30 vol% (@ 750 °C)	9.95	3.81	48.02	2514.00	1253.73	907.64	320
30 vol% (@ 750 °C)	9.85	4.97	48.02	2856.50	845.67		
30 vol% (@ 750 °C)	9.78	4.83	48.02	1975.00	623.52		
0 vol% (@ 800 °C)	9.77	5.01	48.02	2575.00	756.35	649.06	139
0 vol% (@ 800 °C)	9.83	5.08	48.02	2460.50	698.64		
0 vol% (@ 800 °C)	9.89	4.98	48.02	1676.00	492.19		
20 vol% (@ 800 °C)	9.81	4.96	48.02	2163.00	645.56	760.31	171
20 vol% (@ 800 °C)	9.76	4.97	48.02	2271.00	678.53		
20 vol% (@ 800 °C)	9.85	3.89	48.02	1980.00	956.85		

Table E.2 (Cont'd)

Fiber vol%	b (mm)	d (mm)	L (mm)	F (N)	Flexural Strength (MPa)	Av. Flexural Strength	Std. Dev.
25 vol% (@ 800 °C)	9.86	4.89	48.02	3196.00	976.40	858.98	127
25 vol% (@ 800 °C)	9.89	4.68	48.02	2633.10	875.57		
25 vol% (@ 800 °C)	9.76	4.44	48.02	1936.50	724.96		
30 vol% (@ 800 °C)	9.91	4.43	48.02	2674.00	990.36	880.52	155
30 vol% (@ 800 °C)	-	-	-	-	-		
30 vol% (@ 800 °C)	9.76	4.69	48.02	2297.00	770.69		

Appendix F: Detailed Tabulation of Hardness Test Results

Table F.1 Hardness test results of AlSi7Mg0.8 matrix composite specimens obtained from vertical to the fiber orientation

NAME OF THE SPECIMEN	HARDNESS VAUES (HB)					AVERAGE	STD. DEV.
	Measurement No						
	1	2	3	4	5		
0 vol% (@ 750 °C)	92	93	94	93	93	93	1
20 vol% (@ 750 °C)	128	128	131	132	126	129	2
25 vol% (@ 750 °C)	142	150	155	151	147	149	5
30 vol% (@ 750 °C)	142	155	155	153	160	153	7
0 vol% (@ 800 °C)	98	98	101	100	99	99	1
20 vol% (@ 800 °C)	135	138	135	138	134	136	2
25 vol% (@ 800 °C)	138	142	146	144	138	142	4
30 vol% (@ 800 °C)	179	198	179	190	178	185	9

Table F.2 Hardness test results of AlSi7Mg0.8 matrix composite specimens obtained from parallel to the fiber orientation

NAME OF THE SPECIMEN	HARDNESS VAUES (HB)					AVERAGE	STD. DEV.
	Measurement No						
	1	2	3	4	5		
0 vol% (@ 750 °C)	97	95	87	95	91	93	4
20 vol% (@ 750 °C)	121	124	124	125	121	123	2
25 vol% (@ 750 °C)	150	150	142	145	149	147	4
30 vol% (@ 750 °C)	155	142	150	147	151	149	5
0 vol% (@ 800 °C)	102	95	99	104	94	99	4
20 vol% (@ 800 °C)	135	135	135	135	135	135	0
25 vol% (@ 800 °C)	135	135	142	139	135	137	3
30 vol% (@ 800 °C)	174	179	179	174	180	177	3

Table F.3 Hardness test results of AlSi10Mg0.8 matrix composite specimens obtained from vertical to the fiber orientation

NAME OF THE SPECIMEN	HARDNESS VAUES (HB)					AVERAGE	STD. DEV.
	Measurement No						
	1	2	3	4	5		
0 vol% (@ 750 °C)	108	105	112	109	108	108	3
20 vol% (@ 750 °C)	135	135	138	136	135	136	1
25 vol% (@ 750 °C)	150	150	155	145	155	151	4
30 vol% (@ 750 °C)	179	174	169	172	176	174	4
0 vol% (@ 800 °C)	110	112	108	111	115	111	3
20 vol% (@ 800 °C)	135	138	135	137	135	136	1
25 vol% (@ 800 °C)	164	159	155	162	157	159	4
30 vol% (@ 800 °C)	169	169	169	168	172	169	2

Table F.4 Hardness test results of AlSi10Mg0.8 matrix composite specimens obtained from parallel to the fiber orientation

NAME OF THE SPECIMEN	HARDNESS VAUES (HB)					AVERAGE	STD. DEV.
	Measurement No						
	1	2	3	4	5		
0 vol% (@ 750 °C)	110	107	110	110	108	109	1
20 vol% (@ 750 °C)	115	124	131	125	122	123	6
25 vol% (@ 750 °C)	138	150	135	140	142	141	6
30 vol% (@ 750 °C)	150	155	155	147	156	153	4
0 vol% (@ 800 °C)	110	110	115	110	114	112	2
20 vol% (@ 800 °C)	128	128	128	130	126	128	1
25 vol% (@ 800 °C)	164	159	155	162	157	159	4
30 vol% (@ 800 °C)	169	169	169	168	172	169	5

Appendix G: Detailed Results of Density Measurement

Table F.1 Density measurement results of AlSi7Mg0.8 alloy matrix composite specimens

Fiber vol%	Weight in air (g)	Weight in xylene (g)	Volume of the composite (cm^3)	Density of the composite (g/cm^3)	Theoretical density of the composite (g/cm^3)
0 vol% (@ 750 °C)	3.7623	2.5487	1.4046	2.6785	2.6850
20 vol% (@ 750 °C)	4.0457	2.7845	1.4597	2.7716	2.8280
25 vol% (@ 750 °C)	3.6575	2.5378	1.2959	2.8223	2.8638
30 vol% (@ 750 °C)	3.1325	2.1607	1.1248	2.7850	2.8995
0 vol% (@ 800 °C)	3.8067	2.5727	1.4282	2.6653	2.6850
20 vol% (@ 800 °C)	1.1309	0.7783	0.4081	2.7711	2.8280
25 vol% (@ 800 °C)	4.5583	3.1647	1.6130	2.8260	2.8638
30 vol% (@ 800 °C)	4.2073	2.9160	1.4946	2.8151	2.8995

Table F.2 Density measurement results of AlSi10Mg0.8 alloy matrix composite specimens

Fiber vol%	Weight in air (g)	Weight in xylene (g)	Volume of the composite (cm^3)	Density of the composite (g/cm^3)	Theoretical density of the composite (g/cm^3)
0 vol% (@ 750 °C)	3.9827	2.7099	1.4731	2.7035	2.7130
20 vol% (@ 750 °C)	4.1097	2.8165	1.4968	2.7457	2.8504
25 vol% (@ 750 °C)	4.0862	2.8386	1.4440	2.8298	2.8848
30 vol% (@ 750 °C)	4.8796	3.3833	1.7318	2.8176	2.9191
0 vol% (@ 800 °C)	4.2879	2.9160	1.5878	2.7004	2.7130
20 vol% (@ 800 °C)	3.2299	2.2200	1.1689	2.7633	2.8504
25 vol% (@ 800 °C)	5.0366	3.4869	1.7936	2.8080	2.8848
30 vol% (@ 800 °C)	3.0541	2.1112	1.0913	2.7985	2.9191